

### **Reviewer 3#**

The title of this paper is very intriguing that (1) wintertime HONO promotes aerosol formation and (2) >50% of observed HONO is traffic related in Beijing. After reviewing this paper, I think it will be a grave mistake if the editor decides to publish this paper with these two conclusions in any form. The conclusions are pure speculations. I find no evidence to support either of the two claims in this paper.

**Response:** Thank you for your comments. We will answer your questions in the following section point by point.

The discussion for conclusion (1) is in section 3.2. One of the many mistakes in this section is that the authors do not understand that the largest source of OH is from the reaction of HO<sub>2</sub>+NO. Even when OH production from HONO photolysis is larger than from O<sub>3</sub> photolysis, the effect on OH is much smaller than the photolysis rate comparison. Line 301-304 is based on another paper; the data in this paper do not either support or dispute that oxidation by OH promotes aerosol formation. Figure 2D is used at the observation evidence supporting conclusion (1). There are many reasons that HONO/CO correlates with OA/CO. For example, CO is primary in winter in Beijing. If HONO and OA variations are from secondary sources, there will be high correlations as shown. Line 318 states “: : : it was reasonable to mainly ascribe the increase of OA concentration to local secondary formation initiated by OH radical from HONO photolysis.” It is a pure speculation. The observation data in this paper do not support this statement. It is the same with Line 328. The vague statement cannot be supported by the data in this paper. Line 332 is again a speculation. Ammonia is mostly neutralized by sulfate in Beijing. Line 338-400 is another speculative and ambiguous statement. Line 345-345 cites other people’s work but is not supported by the data in this work.

**Response:** Thank you for your instructive comment. The budget of HO<sub>x</sub> or RO<sub>x</sub> radical has been investigated at several locations in China based on field measurements and modelling studies (Tan et al., 2018; Tan et al., 2017; Tan et al., 2019; Tang et al., 2015). Using WRF-Chem model, Tang et al (2015) proposed that HO<sub>2</sub>+NO was the major OH source, followed by HONO photolysis and O<sub>3</sub> photolysis in Beijing, Shanghai and Guangzhou when both primary and secondary OH sources were taken into consideration (Figure R1). As shown in this figure,

however, photolysis of HONO was still an important OH sources and the dominate primary OH source in Beijing. Other studies also confirmed that HONO photolysis is an important OH sources, in particular, dominated the primary OH source at various locations (Figure R2) (Tan et al., 2019;Liu et al., 2019;Tan et al., 2018;Tan et al., 2017).

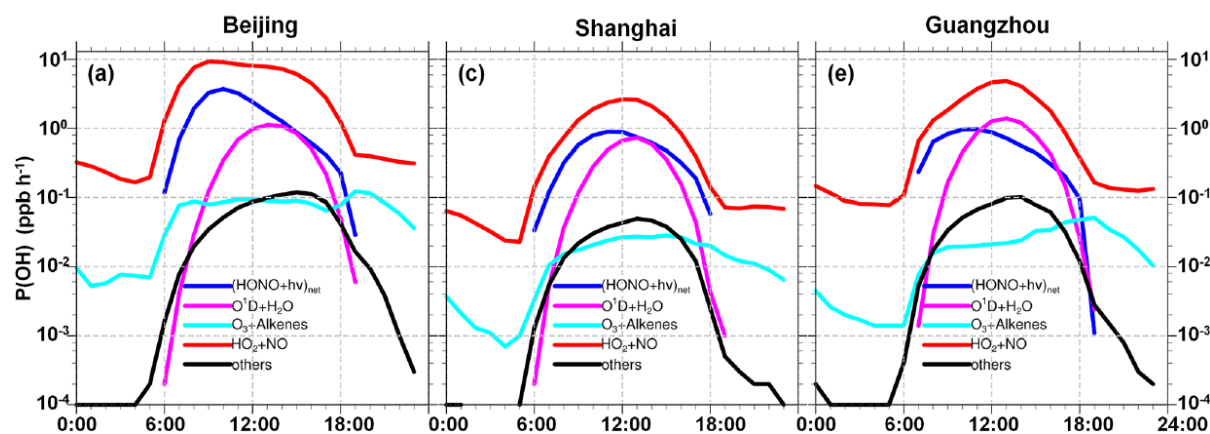


Figure R1. Averaged production rate of OH in Beijing, Shanghai and Guangzhou (Tang et al., 2015).

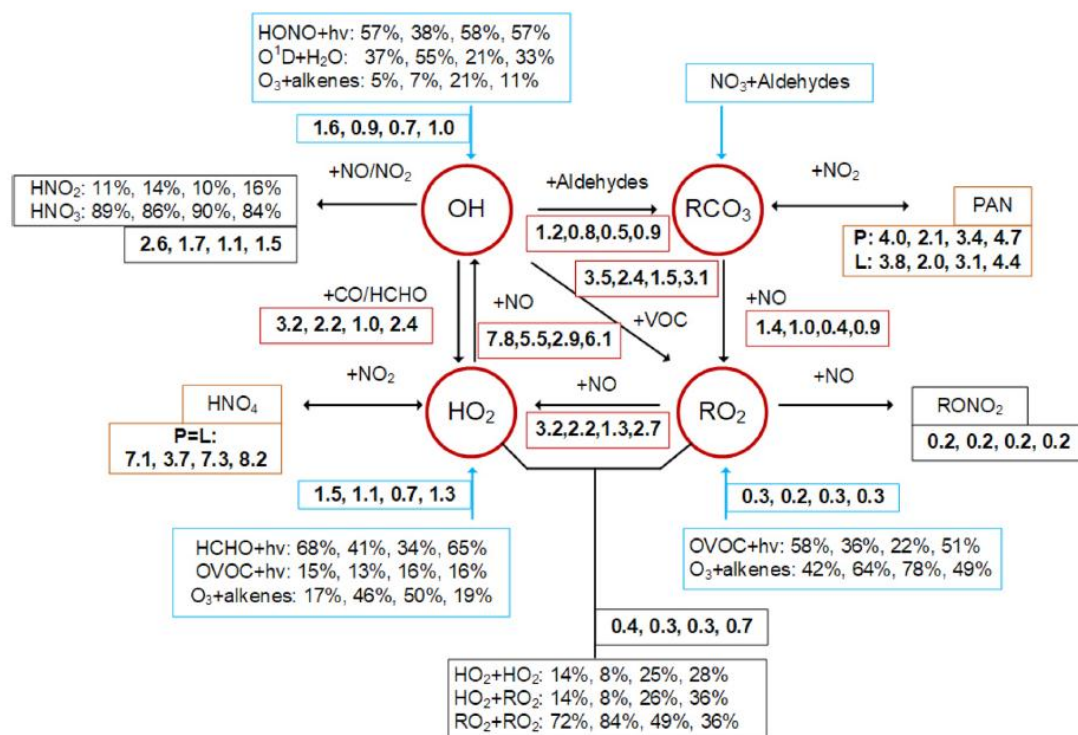


Figure R2. Comparison of the OH–HO<sub>2</sub>–RO<sub>2</sub> radical budget in four cities under daytime conditions (06:00 to 18:00 LT). The numbers are sorted from left to right in the order of Beijing, Shanghai, Guangzhou, and Chongqing. The blue, black, red, and yellow boxes denote the primary radical sources, radical termination, radical propagation, and equilibrium between

radicals and reservoir species, respectively (Tan et al., 2019).

We agree with you that  $\text{HO}_2+\text{NO}$  is the major OH source when both the primary and secondary OH sources are taken into consideration. In section 3.2, we were not going to discuss the budget of OH or  $\text{RO}_x$ . We want to confirm that HONO should play an important role in the initiation of  $\text{RO}_x$  chemistry during our observation. From [line 285 to 289](#), in the original version of the manuscript, we may mislead you because of the improper statements (“This means that the photolysis of HONO dominates the daytime OH production in polluted days in winter, while photolysis of  $\text{O}_3$  behaves as a bigger OH source from April to June. This is consistent with the previous findings that HONO photolysis is the dominant OH source in winter of BTH”). In [lines 324-328](#) in the revised manuscript, we revised it “**These results mean that the photolysis of HONO should play an important role in the initiation of the daytime  $\text{HO}_x$  and  $\text{RO}_x$  chemistry on polluted days in winter, while photolysis of  $\text{O}_3$  becomes more important from April to June.** This is consistent with the previous findings that **HONO photolysis dominates the primary OH source in winter of BTH...**”. At the same time, a sentence has also been added in [lines 305-307](#) in the revised manuscript “**In addition, it has been confirmed that HONO dominates the primary OH source at various locations (Tan et al., 2018;Liu et al., 2019;Tan et al., 2017;Aumont et al., 2003)**”.

We agree that the relationship among different pollutants are very complicated in the atmosphere because many variables are entangled. So, it is difficult to isolate the cause and effect relationship between two variables. In both laboratory and modeling studies, one can change the experiment conditions or the input parameters to test the sensitivity of a target parameter to a given variable. For example, a modeler can change the HONO concentration to simulate the change of aerosol concentration and quantify the influence of HONO on secondary aerosol formation. However, this is impossible for field measurements. Thus, correlation analysis is a common method to reasonably deduce the possible mechanism occurring in the atmosphere based on existing knowledge and reasonable assumptions in field measurements (it does so even in modeling studies and laboratory studies). For example, based on correlation analysis, it has been proposed that amines play a crucial role in new particle formation (Kirkby et al., 2011;Almeida et al., 2013) and  $\text{NH}_3/\text{NO}_2$  can promote sulfate formation in aqueous phase (Wang et al., 2016).

It has been well recognized that secondary organic aerosol is formed via multiple steps oxidation of VOCs (Kroll and Seinfeld, 2008). At the same time, HOx and ROx play very important role in VOCs oxidation (Atkinson et al., 2006). As discussed above, HONO is the important source of primary OH in the atmosphere. It also has been found that HONO is responsible for the initiation of photochemical reactions in chamber studies (Rohrer et al., 2005). In addition, modelling studies have confirmed that HONO can enhance secondary aerosols formation in Beijing-Tianjin-Hebei (BTH) region (Zhang et al., 2019b) and Pearl-River-Delta (PRD) region of China (Zhang et al., 2019a; Xing et al., 2019). Therefore, it is reasonable to deduce that the increase of OA concentration ( $\Delta_{COA}$ ) should be related to the OH from HONO photolysis ( $\Delta_{CHONO}$ ) after normalized to CO as supported by the linear correlation between  $\Delta_{COA/CCO}$  and  $-\Delta_{CHONO/CCO}$  in Figure 2D. CO is a primary pollutant and a stable species in the atmosphere like BC. Thus, it was used to partially alleviate the influence of PBL variation (Cheng et al., 2016). In addition,  $\Delta_{COA/CBC}$  has also been used to characterize SOA formation during air mass transport (Liggio et al., 2016). Therefore, we correlated the  $\Delta_{COA/CCO}$  with the  $-\Delta_{CHONO/CCO}$  rather than the  $COA$  with the  $CHONO$ . This has been pointed out as in lines 291-293 in the revised manuscript “After partially ruling out the possible influence of PBL variation by normalizing the concentrations of all pollutants to CO (Cheng et al., 2016) or BC (Liggio et al., 2016)...”.

It should be noted that the daytime lifetime of HONO is very short due to photolysis. This means regional transport should have little influence on local HONO concentration. However, OA concentration is ready to be affected by regional transport. Thus, we chose these pollution events under stagnant meteorological conditions. Therefore, we pointed out that “As the meteorological condition was stagnant during these cases as indicated by the low wind speed ( $< 1.0 \text{ m s}^{-1}$ , Fig. S5D), it was reasonable to mainly ascribe the increase of OA concentration to local secondary formation initiated by OH radical from HONO photolysis” from line 317 to 319 in the original versions of the manuscript. It has been recognized that oxidation of  $NO_2$  by OH dominates the daytime nitrate formation (Tian et al., 2019). Thus, we can deduce that OH from photolysis of HONO should promote nitrate formation because of the good correlation between the  $\Delta_{C_{nitrate}/CCO}$  and  $-\Delta_{CHONO/CCO}$  in lines 375-377 in the revised manuscript.

In North China Plain,  $NH_3$  is enough to neutralize both sulfate and nitrate due to the

intensive emission of  $\text{NH}_3$ . Figure R3A shows the correlation between the charge of  $\text{NH}_4^+$  and anions (including sulfate, nitrate and chloride) in non-refractory  $\text{PM}_{2.5}$  measured using the ACSM in this work. In general, ammonium can neutralize both nitrate and sulfate. In addition, as shown in Figure R3B, the cations can also neutralize the anions measured using a MARGA in Shijiazhuang from March, 2018 to April, 2019. Therefore, the increase of  $\Delta C_{\text{ammonium}}/C_{\text{CO}}$  and  $-\Delta C_{\text{HONO}}/C_{\text{CO}}$  can be ascribed to the fact that ammonium keeps the pace of nitrate through neutralization. In the revised SI, we added the correlation of the charge between the cations and anions in Fig. S8. In the revised manuscript (lines 368-371), we also pointed out that “We explained the increased ammonium as the result of enhanced neutralization of  $\text{HNO}_3$  by  $\text{NH}_3$  (Wang et al., 2018; Wen et al., 2018; Sun et al., 2018) because  $\text{NH}_4^+$  was adequate to neutralize both sulfate and nitrate as shown in Fig.S8” .

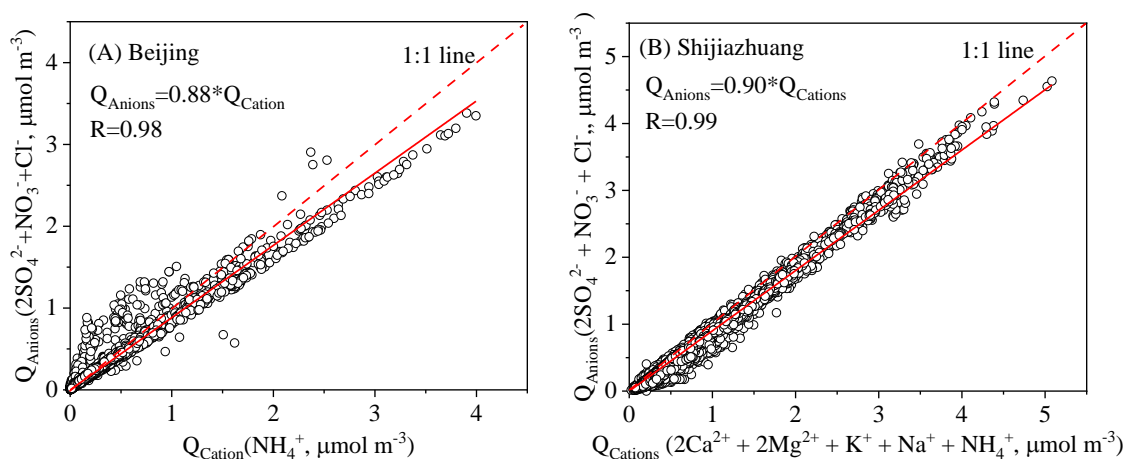


Figure R3. Correlation of the charge between inorganic anions and cations (A) in non-refractory  $\text{PM}_{2.5}$  in Beijing and (B) in soluble  $\text{PM}_{2.5}$  in Shijiazhuang.

From line 338 to 340 in the original manuscript, we concluded that promotion effect of HONO photolysis on nitrate formation could not be excluded. From line 240 to 347, we proposed that HONO photolysis has little influence on sulfate formation based on the correlation between  $\Delta C_{\text{sulfate}}/C_{\text{CO}}$  and  $-\Delta C_{\text{HONO}}/C_{\text{CO}}$  as well as the previous studies, and then made a conclusion that photolysis of HONO could promote aerosol formation during pollution events in winter. From line 348 to 400, we showed the calculation details about HONO emission from vehicle and soil after referring to literatures. From line 345 to 348, we cited the results of modeling studies. We pointed out that “this work well supported the recent modeling results

that HONO could obviously promote the aerosol production in winter (Zhang et al., 2019a; Zhang et al., 2019b; Xing et al., 2019; An et al., 2013) from the point of view of observation”. So, we need to cite these previous work.

Conclusion (2) is based on some calculation that was not described in the paper. Line 376-378 states that the mean emission factor is 1.17% with a lower limit of 0.18% and an upper limit of 1.8%. (Why is the mean so close to the upper limit and 6.6 times larger than the lower limit?) The mean value is similar to previous studies and is not the reason for conclusion (2). Line 381 gives a vehicle HONO emission rate of 0.085 to 0.34 ppbv/h. The unit implies some volume was used in the calculation. No discussion was given on what volume was used and how it varied in a day. Another important factor not considered in this study is the outflow of vehicle HONO and NO<sub>x</sub> by advection at night. It is the largest sink at night but is not included in the budget discussion. The nighttime source of NO<sub>2</sub> from the ground is 38 times less than vehicle emissions. However, no other paper I know of found that HONO concentrations at night cannot be explained mostly by a ground source. It led me to conclude that the vehicle HONO emission source in this paper is overestimated by 10-100 times. The authors should look at previous modeling papers that included vehicle HONO emissions. What they found is that the effect of vehicle HONO emissions is small.

**Response:** Thank you for your comments. As for the contribution of vehicle-related emission to HONO source, the details have been discussed in both [Section 2.2 and 3.3](#). In this work, we used two different methods to estimate the emission ratio of HONO to NO<sub>x</sub> (HONO/NO<sub>x</sub>) from vehicle exhaust. 1.8 % was calculated based on empirical analysis of field data, while 1.17% was obtained by using the low limit correlation of field data. Table R1 and Table S3 summaries the emission ratio from vehicles estimated or measured in China. The lowest value is 0.18% based on chassis dynamometer tests. From [line 376 to 378](#) in the original manuscript we described as “Thus, three levels of vehicle emission factor were considered.  $1.17 \pm 0.05\%$  was taken as the middle value, while 0.18% (Liu et al., 2017) and 1.8 % were the lower limit and the upper limit, respectively”. Here, we used a “middle value” (using the low limit correlation method of filed data) but not a “mean value”. Actually, this value is very close to the mean emission ratio (1.21) if we consider all these reported values in Table R1. In the



revised manuscript, we revised this sentence “Thus, three levels of vehicle emission factor were considered.  $1.17\pm 0.05\%$  was taken as the middle value which was very close to the mean emission ratio (1.21) for all of these reported values in China (Li et al., 2018; Xu et al., 2015; Yang et al., 2014; Liu et al., 2017; Gall et al., 2016; Meng et al., 2019), while 0.18% (Liu et al., 2017) and 1.8 % were the lower limit and the upper limit, respectively” from line 415 to 420 in the revised manuscript.

Table R1. Summary of the measured emission ratio of HONO to NO<sub>x</sub> from vehicles in China.

Time	Place	Methods	$\Delta\text{HONO}/\Delta\text{NO}_x$		Reference
			Range	Mean	
2015/9/1- 2016/8/31	Ji'nan, Shandong	Empirical analysis of field data	0.19%- 0.87%	$0.53\pm 0.20\%$	(Li et al., 2018)
2011/8/3- 2012/5/31	Hongkong	Empirical analysis of field data	0.5%- 1.6%	$1.2\pm 0.4\%$	(Xu et al., 2015)
2015/3/11- 2015/3/21	Hongkong	Tunnel experiment	-	$1.24\pm 0.35\%$	(Liang et al., 2017)
2014	Beijing	Tunnel experiment	-	2.1%	(Yang et al., 2014)
2017	Beijing	Chassis dynamometer test	0.03%- 0.42%	0.18%	(Liu et al., 2017)
2016/12/16 - 2016/12/24	Beijing	Empirical analysis of field data	-	1.3%	(Zhang et al., 2019c)
2016/12/7- 2016/12/13	Beijing	Low limit correlation of field data	-	1.41%	(Meng et al., 2019)
2018/2/1- 2018/6/30	Beijing	Empirical analysis of field data	1.3-2.4%	$1.8\pm 0.5\%$	This study
2018/2/1- 2018/6/30	Beijing	Low limit correlation of field data	-	$1.17\pm 0.05\%$	This study

In Section 2.2, we defined the calculation method for the emission rate of HONO from vehicles “The emission rate ( $E_{\text{HONO}}$ , ppbv h<sup>-1</sup>) was calculated based on the emission flux ( $F_{\text{HONO}}$ , g m<sup>-2</sup> s<sup>-1</sup>) and PBL height ( $H$ , m) according to the following equation,

$$E_{\text{HONO}} = \frac{\alpha \cdot F_{\text{HONO}}}{H} \quad (2)$$

where,  $\alpha$  is the conversion factor ( $\alpha = \frac{1 \times 10^9 \cdot 3600 \cdot R \cdot T}{M \cdot P} = \frac{2.99 \times 10^{13} \cdot T}{M \cdot P}$ ),  $M$  is the molecular weight (g mol<sup>-1</sup>),  $T$  is the temperature (K) and  $P$  is the atmospheric pressure (Pa)” from line 152 to 156

in the original manuscript. The emission flux of HONO was calculated according to the the hourly emission flux of NO<sub>x</sub> from vehicle sector (Yang et al., 2019) and the relative emission ratio of HONO to NO<sub>x</sub> as discussed above. It was pointed out as “The hourly NO<sub>x</sub> emission inventory from vehicles in Beijing, with an annual emission rate of 109.9 Gg yr<sup>-1</sup> (Yang et al., 2019), was used when calculating the  $E_{\text{vehicle}}$  in this work.” from line 379 to 381 in the original manuscript. To make it clearer, we revised this sentence “The  $E_{\text{vehicle}}$  was calculated using the hourly NO<sub>x</sub> emission inventory from vehicles in Beijing (Yang et al., 2019) after converted to emission flux of HONO ( $F_{\text{HONO}}=F_{\text{NO}_x}\times \text{HONO/NO}_x$ ) and the PBL height as described in Section 2.2. Thus, the calculated emission rate reflected the diurnal variation of both the emission inventory and the PBL height” in lines 421-425 in the revised manuscript.

As you suggested, the outflow HONO by advection is an important sink of HONO in the night (Gall et al., 2016;Meng et al., 2019). The the loss of HONO ( $T_{\text{advection}}$ ) via vertical advection can be calculated according to the following equation,

$$T_{\text{vertical}} = -K_h(z, t) \frac{\partial c(z, t)}{\partial z} \frac{1}{h} \quad (\text{R1})$$

where  $K_h(z, t)$  is the eddy diffusivity of heat ( $\text{m}^2 \text{s}^{-1}$ ) at height  $z$  (m) and time  $t$ ,  $h$  is the height of the second layer (Gall et al., 2016). We added two paragraphs to discuss the transport in lines 222-232 “Vertical transport by advection ( $T_{\text{vertical}}$ ), which is an important sink of HONO in the night (Gall et al., 2016;Meng et al., 2019), can be calculated according to equation (12).

$$T_{\text{vertical}} = -K_h(z, t) \frac{\partial c(z, t)}{\partial z} \frac{1}{h} \quad (12)$$

where  $K_h(z, t)$  is the eddy diffusivity of heat ( $\text{m}^2 \text{s}^{-1}$ ) at height  $z$  (m) and time  $t$ ,  $h$  is the height of the second layer (18 m in this study) (Gall et al., 2016). On the other hand, both the vertical and horizontal transport can be estimate according to Eq. (13),

$$T_{\text{vertical}} = k_{\text{dilution}}(c_{\text{HONO}} - c_{\text{HONO,background}}) \quad (13)$$

where  $k_{\text{dilution}}$  is a dilution rate ( $0.23 \text{ h}^{-1}$ , including both vertical and horizontal transport) (Dillon et al., 2002),  $c_{\text{HONO}}$  and  $c_{\text{HONO,background}}$  is the HONO concentration at the observation site and background site, respectively (Dillon et al., 2002)” and lines 574-598 “As pointed in Section 2.2, vertical transport by advection is an important nocturnal sink of HONO (Gall et al., 2016). In this work, the vertical distribution of HONO concentration is unavailable. Recently, Meng et al. (2019) measured the vertical distribution of HONO in Beijing in



December, 2016. The concentration of HONO showed nearly flat profiles from ground level to 240 m in pollution events after sunset, while negative profiles of HONO were observed in pollution events during night (Meng et al., 2019). The nighttime concentration gradient was  $0.0047 \pm 0.0025$  ppb  $m^{-1}$  derived from the nighttime dataset (Meng et al., 2019). In the daytime, we assume a zero concentration gradient. On the other hand, the eddy diffusivity of heat in urban environment was measured in New Delhi, Indian (Yadav et al., 2003). Using their dataset with the wind speed lower than  $2.0$   $m\ s^{-1}$ , we derived the relationship between the  $K_h$  and the wind speed (WS) ( $K_h = 0.9389 \times WS - 0.3374$   $m^2\ s^{-1}$ ). The nighttime  $T_{vertical}$  changed from  $0.15$  to  $0.37$  ppbv  $h^{-1}$  in winter, while it was from  $0.12$  to  $0.68$  ppbv  $h^{-1}$  according to Eq. (12) from April to June. Because the wind speed was usually lower than  $1.0$   $m\ s^{-1}$  in pollution events (Fig. S6), horizontal transport should have little influence on the daytime sources or sinks of HONO because of the short lifetime of HONO. In the night, 79 % of the wind speed was lower than  $1.0$   $m\ s^{-1}$  in winter, thus the air masses from suburban areas should have influence on the sources and sinks of HONO in Beijing. If the HONO concentration at background was zero, the vertical and horizontal transport rate of HONO varied from  $0.17$  to  $0.61$  ppbv  $h^{-1}$  calculated according to Eq. (13) on haze days in winter and from  $0.15$  to  $0.74$  ppbv  $h^{-1}$  in pollution events from April to June. These values are higher than that calculated according to Eq. (12). Because the background HONO concentration was unavailable, we only considered the nighttime transport calculated according to Eq. (12) in the following section". At the same time, the relative contribution of each source in Section 3.3 was updated based on the total sinks.

HONO production from heterogeneous reactions of  $NO_2$  on both aerosol surface and ground surface greatly depend on the uptake coefficient ( $\gamma_{NO_2, BET}$ ) and the surface to volume ratio (S/V). The mean and median surface to volume ratio of aerosols are  $1.33 \times 10^{-3}$  and  $1.36 \times 10^{-3}$   $m^{-1}$  during pollution events. This is comparable with the input parameters in modeling studies (Zhang et al., 2016). However, as discussed from [line 501 to 503](#) in the revised manuscript, the  $\gamma_{NO_2, BET}$  on aerosols varied from  $5 \times 10^{-9}$  to  $9.6 \times 10^{-6}$ . The  $\gamma_{NO_2, BET}$  on pure oxides was usually higher than on composite oxides. The selection of a proper  $\gamma_{NO_2, BET}$  is quite tricky. For example, a fixed  $\gamma_{NO_2, BET}$  was set to  $1 \times 10^{-6}$  in nighttime and  $2 \times 10^{-5}$  in daytime due to photochemical reaction of  $NO_2$  on soot surface in a modelling study (Zhang et al., 2016; Aumont et al., 2003). The nighttime  $\gamma_{NO_2, BET}$  is  $\sim 2$  orders of magnitude higher than ours

( $1.2 \times 10^{-8}$ ) as suggested by Crowley et al. (Crowley et al., 2010). In our previous work, we have measured the  $\gamma_{\text{NO}_2, \text{BET}}$  on kaolin and hematite (Liu et al., 2015) and soot (Han et al., 2013). The initial  $\gamma_{\text{NO}_2, \text{BET}}$  on kaolin is  $4.85 \pm 0.39 \times 10^{-8}$  at 47 % RH. It should be pointed out that the  $\gamma_{\text{NO}_2, \text{BET}}$  decreases significantly with exposure time due to surface saturation. Fig. R4 shows the typical uptake curve of  $\text{NO}_2$  and the  $\gamma_{\text{NO}_2, \text{obs}}$  which is not normalized to the specific surface area. The  $\gamma_{\text{NO}_2, \text{BET}}$  at steady state ( $2.56 \times 10^{-9}$  to  $4.56 \times 10^{-9}$  on kaolin and  $1.23 \times 10^{-8}$  to  $1.50 \times 10^{-8}$  on hematite) is around one order of magnitude lower than the initial  $\gamma_{\text{NO}_2, \text{BET}}$  as shown in Fig. R5. Therefore, we used the recommended value ( $1.2 \times 10^{-8}$ ) (Crowley et al., 2010) as the base case. On the other hand, the  $\gamma_{\text{NO}_2, \text{BET}}$  decreases with RH due to competitive adsorption (Liu et al., 2015). High mass concentration of  $\text{PM}_{2.5}$  usually accompanied with high RH in winter in Beijing. Thus, we calculated the RH dependent  $\gamma_{\text{NO}_2, \text{BET}}$  according to the equation we determined previously (Liu et al., 2015) and the measured ambient RH in this work. This should be more reasonable than a fixed uptake coefficient used in modeling studies.

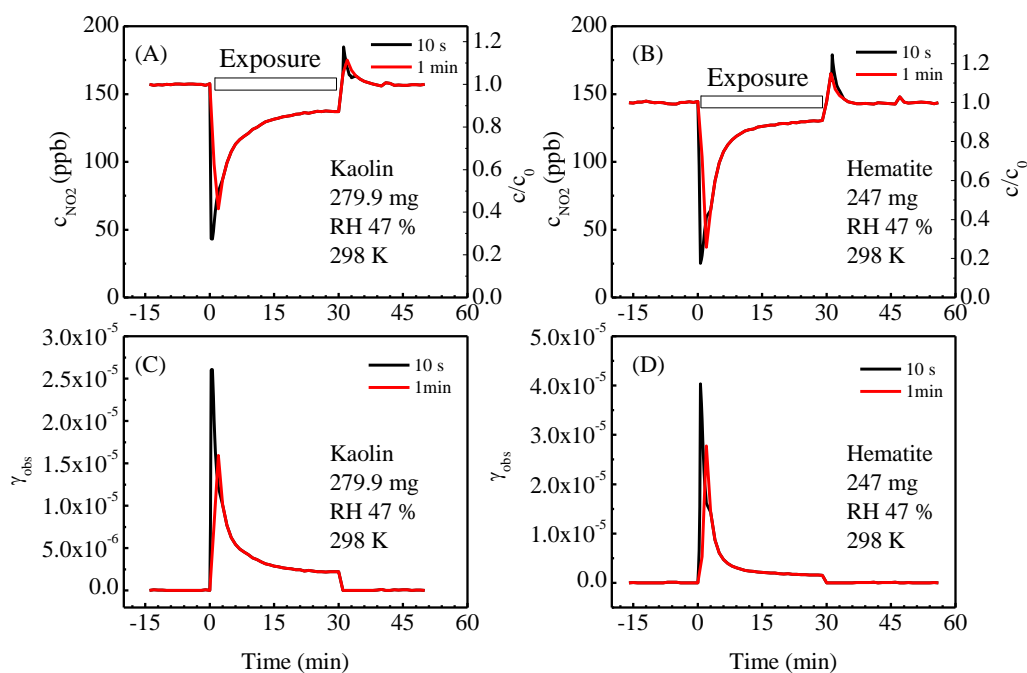


Fig. R4. Uptake curves of  $\text{NO}_2$  on (A) kaolin and (B) hematite; and evolution of the observed uptake coefficient on (C) kaolin and (D) hematite at 298 K and at 47 % of RH (Liu et al., 2015).

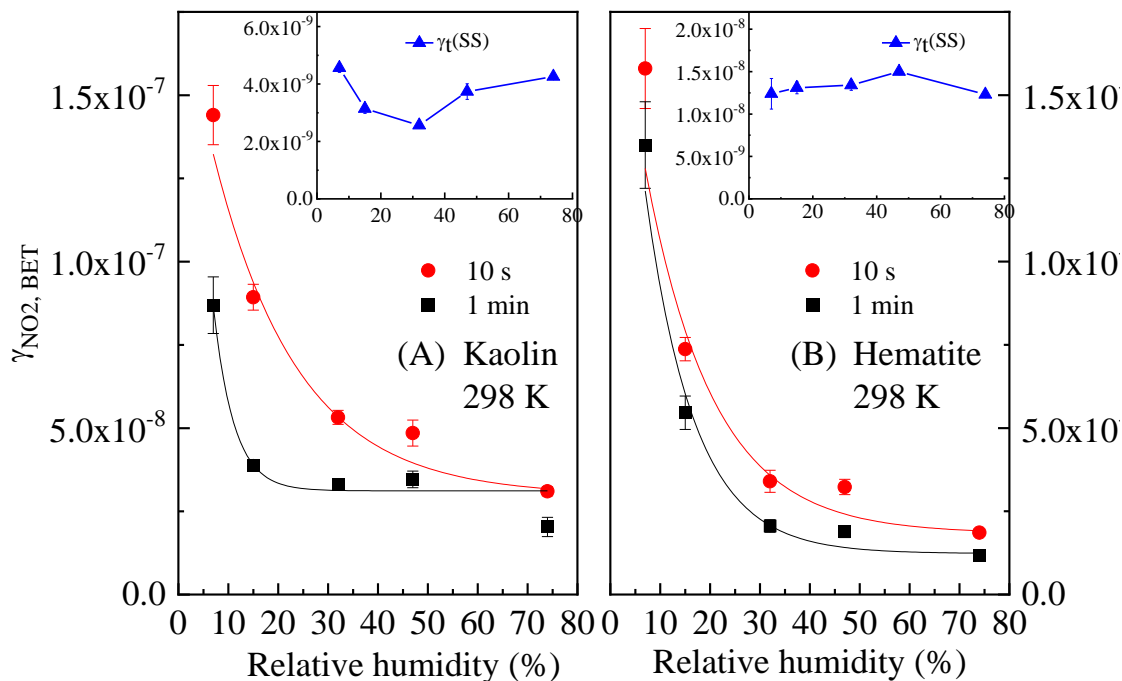


Fig. R2. The dependence of  $\gamma_{\text{NO}_2, \text{BET}}$  on relative humidity (Liu et al., 2015).

In the original version of manuscript, we found a bug when calculating the heterogeneous reaction of  $\text{NO}_2$  on black carbon. A conversion factor of time from second to hour was missed. So, the contribution of heterogeneous reaction to HONO source was underestimated in the original version. Now, the  $P_{\text{aerosol}}$  was  $0.038 \pm 0.030 - 0.088 \pm 0.072$ , which was dominated by the heterogeneous reaction of  $\text{NO}_2$  on black carbon. It was on the same orders as soil emission. However, this was still significantly lower than the contribution of vehicle emission. In the revised manuscript, we updated Figures 3-5 and the corresponding numbers in section 3.3.

As for heterogeneous reaction of  $\text{NO}_2$  on ground surface, we used the same  $\gamma_{\text{NO}_2, \text{BET}}$  on dust aerosol in the night, which is similar to the methodology used in modelling studies (Zhang et al., 2016; Aumont et al., 2003). As pointed out in Section 2.2 from line 197 to 209 in the revised manuscript, the S/V was estimated using the surface roughness calculated in the light of satellite image of Beijing. The calculated surface roughness is 3.85, which is slightly higher than the value (2.2) used by Li et al. (2017). Thus, the calculated S/V varied from 0.0015 to  $0.0385 \text{ m}^{-1}$  (with a mean value of  $0.0125 \text{ m}^{-1}$ ) because of the variation of the PBL height during pollution events. However, a fixed S/V of ground surface was set to  $0.3 \text{ m}^{-1}$  in the modeling studies (Zhang et al., 2016). This corresponds to a surface roughness  $\sim 92$ , which means the

surface area is ~92 times of the projected area of ground. It's too high. If both the  $\gamma_{\text{NO}_2,\text{BET}}$  ( $1 \times 10^{-6}$ ) and surface roughness are increased to the values used in modeling studies, the nighttime production rate of HONO via heterogeneous reaction of  $\text{NO}_2$  on ground surface will be  $2.9 \text{ ppb h}^{-1}$ . This means a large sink missed if this number is reasonable. In lines 558-561 in the revised manuscript, we also revised the sentence “These results mean that heterogeneous reaction might not be a major HONO source. This is consistent with a recent work that found heterogeneous reaction being unimportant when compared with traffic emission during haze events in winter in Beijing (Zhang et al., 2019c)” and in lines 605-607 in the revised manuscript, “Heterogeneous reactions of  $\text{NO}_2$  on aerosol surface and ground surfaces were not the major HONO source during night unlike the modelled results (Zhang et al., 2016; Aumont et al., 2003) ”.

During the Chinese New Year (CNY) and the COVID-19 epidemic in 2020, traffic emission decreased significantly in Beijing. This provides us a unique opportunity to verify the relative importance of each HONO source. We only analyzed the nocturnal data from January 1 to February 29 because the HONO sources related to photochemical reactions could be avoided. The CNY vacation was from January 23 to February 2. These results are in preparation for a separate paper. Fig. R4 shows the relative change of the concentrations of HONO,  $\text{NO}_x$  and non-refractory  $\text{PM}_{2.5}$  (NR- $\text{PM}_{2.5}$ ). The traffic index and the chemical age of the air masses which is defined as  $-\log(\text{NO}_x/\text{NO}_y)$  are also shown in Fig. R4.  $\text{NO}_y$  was measured with a  $\text{NO}_y$  analyzer (Thermo 42i-Y). The concentration of nighttime HONO decreased significantly during the CNY and after the CNY accompanied with the reduction in vehicle emission as supported by both the concentration of  $\text{NO}_x$  and traffic index (Fig. R4B). Interestingly, the NR- $\text{PM}_{2.5}$  concentration during and after the CNY increased obviously when compared with that before the CNY. The effective conversion of  $\text{NO}_2$  aerosol surface was almost constant because both the promotion effect of increased  $\text{PM}_{2.5}$  concentration and the inhibition effect of reduced  $\text{NO}_2$  concentration during and after the CNY as shown in Fig. R4C. On the other hand, we found that the nighttime chemical age of the air masses during and after the CNY was also obviously larger than that before the CNY (Fig. R4D). This means that heterogeneous reaction of  $\text{NO}_2$  on both aerosol surface and ground surface should be more effective due to longer residence of the air masses during and after the CNY than that before the CNY. When the

reduction of  $\text{NO}_2$  concentration was taken into consideration, the product of  $\text{NO}_2$  concentration and  $-\log(\text{NO}_x/\text{NO}_y)$  in different periods increased slightly (Fig. R5). Therefore, the observed HONO concentration should be at least constant in different periods and independent on the reduction of vehicle emission if heterogeneous reaction of  $\text{NO}_2$  on aerosol and ground surfaces dominates nighttime HONO source or if the vehicle emission is a minor HONO source. However, we observed the decrease of HONO along with reduction of vehicle emission (Fig.R4A). This well supports our (and other researchers' (Meng et al., 2019;Zhang et al., 2019c) conclusion that vehicle emission is an important source of HONO in Beijing.

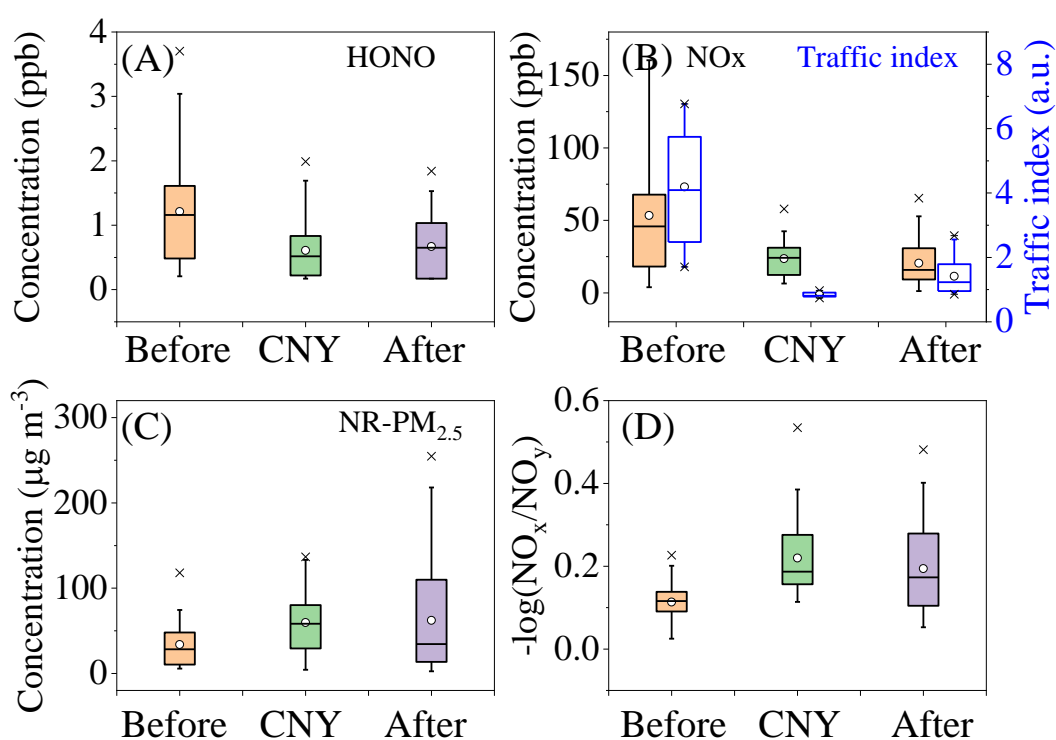


Fig. R4. Relative change of nighttime (A) HONO concentration, (B)  $\text{NO}_x$  concentration and the traffic index, (C) non-refractory  $\text{PM}_{2.5}$  (NR- $\text{PM}_{2.5}$ ) concentration and (D) relative chemical age ( $-\log(\text{NO}_x/\text{NO}_y)$ ) of air masses before Chinese New Year (CNY) (2020.1.1-2020.1.22), during CNY (2020.1.23-2020.2.1) and after CNY (2020.2.2-2020.2.29).

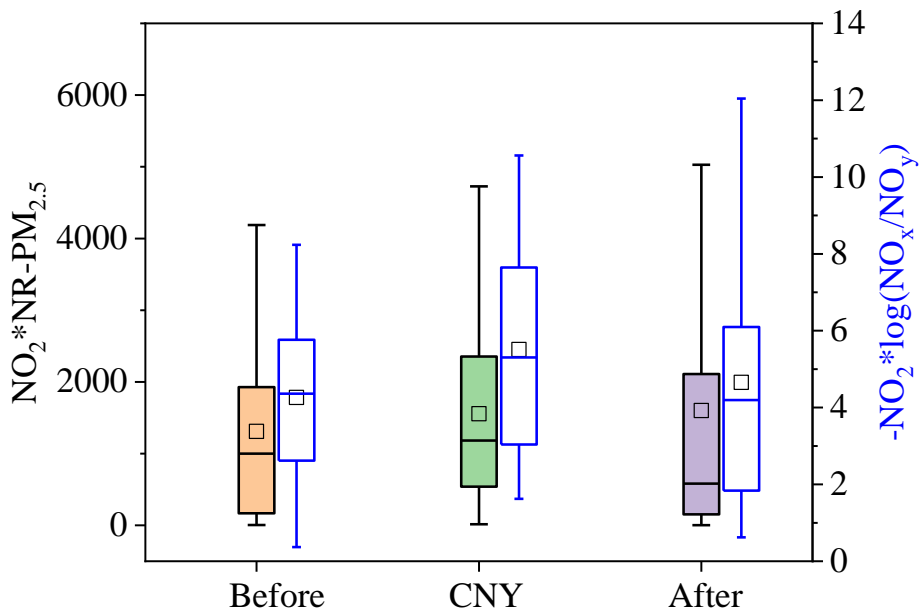


Fig. R5. Relative change of nighttime the product of  $\text{NO}_2$  and  $\text{NR-PM}_{2.5}$  concentration and the product of  $\text{NO}_2$  concentration and  $-\log(\text{NO}_x/\text{NO}_y)$  in different periods.

In lines 523-528 in the revised manuscript, we pointed out “The  $A_s$  of aerosols which was measured using a DMPS varied from  $1 \times 10^{-4}$  to  $4.8 \times 10^{-3} \text{ m}^{-1}$  with a mean value of  $1.4 \pm 0.5 \times 10^{-3} \text{ m}^{-1}$  during pollution events. This value is comparable with that used in modeling studies (Zhang et al., 2016; Aumont et al., 2003). The  $A_s$  of ground surface which was calculated according to Eq. (6) and (7) varied from  $1.5 \times 10^{-3}$  to  $3.85 \times 10^{-2} \text{ m}^{-1}$  with a mean value of  $1.3 \pm 0.9 \times 10^{-2} \text{ m}^{-1}$  during pollution events. The surface roughness was 3.85 calculated according to Eq. (7)”. And from line 544 to 554 in the revised manuscript, we added a paragraph to discuss the reason why we obtained the low production rate of HONO via heterogeneous reaction of  $\text{NO}_2$  on ground and aerosol surfaces as “It should be pointed out that HONO production from heterogeneous reaction of  $\text{NO}_2$  on both aerosol and ground surface greatly depend on the  $\gamma_{\text{NO}_2, \text{BET}}$  and  $A_s$ . The  $A_s$  of aerosols is comparable with the modeling input. However, the small nighttime  $\gamma_{\text{NO}_2, \text{BET}}$  ( $10^{-8} - 10^{-7}$ ) were used in this work rather than the  $\gamma_{\text{NO}_2, \text{BET}}$  ( $1 \times 10^{-6}$ ) used in modelling studies (Zhang et al., 2016; Aumont et al., 2003). This leads to a lower production rate of HONO from heterogeneous reaction of  $\text{NO}_2$  on aerosols. As for heterogeneous reaction of  $\text{NO}_2$  on ground surface, besides the small  $\gamma_{\text{NO}_2, \text{BET}}$  used in this work, the  $A_s$  of ground surface ( $0.0015$  to  $0.0385 \text{ m}^{-1}$ ) calculated using the surface roughness and PBL height was also significantly lower than

the fixed value of  $0.3 \text{ m}^{-1}$  used in modeling studies that might overestimate the contribution of HONO production from heterogeneous reaction of  $\text{NO}_2$  on ground surface”.

In summary, I think that the calculation and reasoning of this paper are either incorrect or ambiguous. It does seem likely that any revision can correct the flaws in the two main conclusions. I suggest that the authors scratch the conclusions and redo the analysis of their observation data.

**Response:** Thank you for your comments again. We have answered your questions above.

### References:

- Almeida, J., Schobesberger, S., Kurten, A., Ortega, I. K., Kupiainen-Maatta, O., Praplan, A. P., Adamov, A., Amorim, A., Bianchi, F., Breitenlechner, M., David, A., Dommen, J., Donahue, N. M., Downard, A., Dunne, E., Duplissy, J., Ehrhart, S., Flagan, R. C., Franchin, A., Guida, R., Hakala, J., Hansel, A., Heinritzi, M., Henschel, H., Jokinen, T., Junninen, H., Kajos, M., Kangasluoma, J., Keskinen, H., Kupc, A., Kurten, T., Kvashin, A. N., Laaksonen, A., Lehtipalo, K., Leiminger, M., Leppa, J., Loukonen, V., Makhmutov, V., Mathot, S., McGrath, M. J., Nieminen, T., Olenius, T., Onnela, A., Petaja, T., Riccobono, F., Riipinen, I., Rissanen, M., Rondo, L., Ruuskanen, T., Santos, F. D., Sarnela, N., Schallhart, S., Schnitzhofer, R., Seinfeld, J. H., Simon, M., Sipila, M., Stozhkov, Y., Stratmann, F., Tome, A., Trostl, J., Tsagkogeorgas, G., Vaattovaara, P., Viisanen, Y., Virtanen, A., Vrtala, A., Wagner, P. E., Weingartner, E., Wex, H., Williamson, C., Wimmer, D., Ye, P., Yli-Juuti, T., Carslaw, K. S., Kulmala, M., Curtius, J., Baltensperger, U., Worsnop, D. R., Vehkamäki, H., and Kirkby, J.: Molecular understanding of sulphuric acid-amine particle nucleation in the atmosphere, *Nature*, 502, 359-363, doi: 10.1038/nature12663, 2013.
- An, J., Li, Y., Chen, Y., Li, J., Qu, Y., and Tang, Y.: Enhancements of major aerosol components due to additional HONO sources in the North China Plain and implications for visibility and haze, *Adv. Atmos. Sci.*, 30, 57-66, 10.1007/s00376-012-2016-9, 2013.
- Atkinson, R., Baulch, D. L., Cox, R. A., Crowley, J. N., Hampson, R. F., Hynes, R. G., Jenkin, M. E., Rossi, M. J., Troe, J., and Subcommittee, I.: Evaluated kinetic and photochemical data for atmospheric chemistry: Volume II - gas phase reactions of organic species, *Atmos. Chem. Phys.*, 6, 3625-4055, doi:10.5194/acp-6-3625-2006, 2006.
- Aumont, B., Chervier, F., and Laval, S.: Contribution of HONO sources to the  $\text{NO}_x/\text{HO}_x/\text{O}_3$  chemistry in the polluted boundary layer, *Atmos. Environ.*, 37, 487-498, [https://doi.org/10.1016/S1352-2310\(02\)00920-2](https://doi.org/10.1016/S1352-2310(02)00920-2), 2003.
- Cheng, Y., Zheng, G., Wei, C., Mu, Q., Zheng, B., Wang, Z., Gao, M., Zhang, Q., He, K., Carmichael, G., Poschl, U., and Su, H.: Reactive nitrogen chemistry in aerosol water as a source of sulfate during haze events in China, *Sci. Adv.*, 2, 10.1126/sciadv.1601530, 2016.
- Dillon, M. B., Lamanna, M. S., Schade, G. W., Goldstein, A. H., and Cohen, R. C.: Chemical evolution of the Sacramento urban plume: Transport and oxidation, *J. Geophys. Res.- Atmos.*, 107, ACH 3-1-ACH 3-15, 10.1029/2001jd000969, 2002.
- Gall, E. T., Griffin, R. J., Steiner, A. L., Dibb, J., Scheuer, E., Gong, L., Rutter, A. P., Cevik, B. K., Kim, S., Lefer, B., and Flynn, J.: Evaluation of nitrous acid sources and sinks in urban outflow, *Atmos. Environ.*, 127, 272-282, <https://doi.org/10.1016/j.atmosenv.2015.12.044>, 2016.
- Kirkby, J., Curtius, J., Almeida, J., Dunne, E., Duplissy, J., Ehrhart, S., Franchin, A., Gagne, S., Ickes, L., Kurten,



A., Kupc, A., Metzger, A., Riccobono, F., Rondo, L., Schobesberger, S., Tsagkogeorgas, G., Wimmer, D., Amorim, A., Bianchi, F., Breitenlechner, M., David, A., Dommen, J., Downard, A., Ehn, M., Flagan, R. C., Haider, S., Hansel, A., Hauser, D., Jud, W., Junninen, H., Kreissl, F., Kvashin, A., Laaksonen, A., Lehtipalo, K., Lima, J., Lovejoy, E. R., Makhmutov, V., Mathot, S., Mikkilä, J., Minginette, P., Mogo, S., Nieminen, T., Onnela, A., Pereira, P., Petaja, T., Schnitzhofer, R., Seinfeld, J. H., Sipila, M., Stozhkov, Y., Stratmann, F., Tome, A., Vanhanen, J., Viisanen, Y., Vrtala, A., Wagner, P. E., Walther, H., Weingartner, E., Wex, H., Winkler, P. M., Carslaw, K. S., Worsnop, D. R., Baltensperger, U., and Kulmala, M.: Role of sulphuric acid, ammonia and galactic cosmic rays in atmospheric aerosol nucleation, *Nature*, 476, 429-433, <http://www.nature.com/nature/journal/v476/n7361/abs/nature10343.html#supplementary-information>, 2011.

Kroll, J. H., and Seinfeld, J. H.: Chemistry of secondary organic aerosol: Formation and evolution of low-volatility organics in the atmosphere, *Atmos. Environ.*, 42, 3593-3624, 2008.

Li, D., Xue, L., Wen, L., Wang, X., Chen, T., Mellouki, A., Chen, J., and Wang, W.: Characteristics and sources of nitrous acid in an urban atmosphere of northern China: Results from 1-yr continuous observations, *Atmos. Environ.*, 182, 296-306, <https://doi.org/10.1016/j.atmosenv.2018.03.033>, 2018.

Liang, Y., Zha, Q., Wang, W., Cui, L., Lui, K. H., Ho, K. F., Wang, Z., Lee, S.-c., and Wang, T.: Revisiting nitrous acid (HONO) emission from on-road vehicles: A tunnel study with a mixed fleet, *J. Air Waste Manage. Assoc.*, 67, 797-805, 10.1080/10962247.2017.1293573, 2017.

Liggio, J., Li, S.-M., Hayden, K., Taha, Y. M., Stroud, C., Darlington, A., Drollette, B. D., Gordon, M., Lee, P., Liu, P., Leithead, A., Moussa, S. G., Wang, D., O'Brien, J., Mittermeier, R. L., Brook, J. R., Lu, G., Staebler, R. M., Han, Y., Tokarek, T. W., Osthoff, H. D., Makar, P. A., Zhang, J., L. Plata, D., and Gentner, D. R.: Oil sands operations as a large source of secondary organic aerosols, *Nature*, 534, 91-94, 10.1038/nature17646 <http://www.nature.com/nature/journal/vaop/ncurrent/abs/nature17646.html#supplementary-information>, 2016.

Liu, Y., Lu, K., Ma, Y., Yang, X., Zhang, W., Wu, Y., Peng, J., Shuai, S., Hu, M., and Zhang, Y.: Direct emission of nitrous acid (HONO) from gasoline cars in China determined by vehicle chassis dynamometer experiments, *Atmos. Environ.*, 169, 89-96, 10.1016/j.atmosenv.2017.07.019, 2017.

Liu, Y. H., Lu, K. D., Li, X., Dong, H. B., Tan, Z. F., Wang, H. C., Zou, Q., Wu, Y. S., Zeng, L. M., Hu, M., Min, K. E., Kecorius, S., Wiedensohler, A., and Zhang, Y. H.: A Comprehensive Model Test of the HONO Sources Constrained to Field Measurements at Rural North China Plain, *Environ. Sci. Technol.*, 53, 3517-3525, 10.1021/acs.est.8b06367, 2019.

Meng, F., Qin, M., Tang, K., Duan, J., Fang, W., Liang, S., Ye, K., Xie, P., Sun, Y., Xie, C., Ye, C., Fu, P., Liu, J., and Liu, W.: High resolution vertical distribution and sources of HONO and NO<sub>2</sub> in the nocturnal boundary layer in urban Beijing, China, *Atmos. Chem. Phys. Discuss.*, 2019, 1-34, 10.5194/acp-2019-613, 2019.

Rohrer, F., Bohn, B., Brauers, T., Bruning, D., Johnen, F. J., Wahner, A., and Kleffmann, J.: Characterisation of the photolytic HONO-source in the atmosphere simulation chamber SAPHIR, *Atmos. Chem. Phys.*, 5, 2189-2201, 10.5194/acp-5-2189-2005, 2005.

Sun, P., Nie, W., Chi, X., Xie, Y., Huang, X., Xu, Z., Qi, X., Xu, Z., Wang, L., Wang, T., Zhang, Q., and Ding, A.: Two years of online measurement of fine particulate nitrate in the western Yangtze River Delta: influences of thermodynamics and N<sub>2</sub>O<sub>5</sub> hydrolysis, *Atmos. Chem. Phys.*, 18, 17177-17190, 10.5194/acp-18-17177-2018, 2018.

Tan, Z., Fuchs, H., Lu, K., Hofzumahaus, A., Bohn, B., Broch, S., Dong, H., Gomm, S., Häsel, R., He, L., Holland, F., Li, X., Liu, Y., Lu, S., Rohrer, F., Shao, M., Wang, B., Wang, M., Wu, Y., Zeng, L., Zhang, Y., Wahner, A., and Zhang, Y.: Radical chemistry at a rural site (Wangdu) in the North China Plain: observation and model calculations of OH, HO<sub>2</sub> and RO<sub>2</sub> radicals, *Atmos. Chem. Phys.*, 17, 663-690, 10.5194/acp-17-663-2017, 2017.

Tan, Z., Rohrer, F., Lu, K., Ma, X., Bohn, B., Broch, S., Dong, H., Fuchs, H., Gkatzelis, G. I., Hofzumahaus, A.,

Holland, F., Li, X., Liu, Y., Liu, Y., Novelli, A., Shao, M., Wang, H., Wu, Y., Zeng, L., Hu, M., Kiendler-Scharr, A., Wahner, A., and Zhang, Y.: Wintertime photochemistry in Beijing: observations of ROx radical concentrations in the North China Plain during the BEST-ONE campaign, *Atmos. Chem. Phys.*, 18, 12391-12411, 10.5194/acp-18-12391-2018, 2018.

Tan, Z. F., Lu, K. D., Jiang, M. Q., Su, R., Wang, H. L., Lou, S. R., Fu, Q. Y., Zhai, C. Z., Tan, Q. W., Yue, D. L., Chen, D. H., Wang, Z. S., Xie, S. D., Zeng, L. M., and Zhang, Y. H.: Daytime atmospheric oxidation capacity in four Chinese megacities during the photochemically polluted season: a case study based on box model simulation, *Atmos. Chem. Phys.*, 19, 3493-3513, 10.5194/acp-19-3493-2019, 2019.

Tang, Y., An, J., Wang, F., Li, Y., Qu, Y., Chen, Y., and Lin, J.: Impacts of an unknown daytime HONO source on the mixing ratio and budget of HONO, and hydroxyl, hydroperoxyl, and organic peroxy radicals, in the coastal regions of China, *Atmos. Chem. Phys.*, 15, 9381-9398, 10.5194/acp-15-9381-2015, 2015.

Tian, M., Liu, Y., Yang, F. M., Zhang, L. M., Peng, C., Chen, Y., Shi, G. M., Wang, H. B., Luo, B., Jiang, C. T., Li, B., Takeda, N., and Koizumi, K.: Increasing importance of nitrate formation for heavy aerosol pollution in two megacities in Sichuan Basin, southwest China, *Environ. Pollut.*, 250, 898-905, 10.1016/j.envpol.2019.04.098, 2019.

Wang, G., Zhang, R., Gomez, M. E., Yang, L., Zamora, M. L., Hu, M., Lin, Y., Peng, J., Guoc, S., Meng, J., Li, J., Cheng, C., Hu, T., Ren, Y., Wang, Y., Gao, J., Cao, J., An, Z., Zhou, W., Li, G., Wang, J., Tian, P., Marrero-Ortiz, W., Secrest, J., Du, Z., Zheng, J., Shang, D., Zeng, L., Shao, M., Wang, W., Huang, Y., Wang, Y., Zhu, Y., Li, Y., Hu, J., Pan, B., Cai, L., Cheng, Y., Ji, Y., Zhang, F., Rosenfeld, D., Liss, P. S., Duce, R. A., Kolb, C. E., and Molina, M. J.: Persistent sulfate formation from London Fog to Chinese haze, *Proc. Natl. Acad. Sci. USA*, 113, 13630-13635, 2016.

Wang, H. C., Lu, K. D., Chen, X. R., Zhu, Q. D., Wu, Z. J., Wu, Y. S., and Sun, K.: Fast particulate nitrate formation via N<sub>2</sub>O<sub>5</sub> uptake aloft in winter in Beijing, *Atmos. Chem. Phys.*, 18, 10483-10495, 10.5194/acp-18-10483-2018, 2018.

Wen, L., Xue, L., Wang, X., Xu, C., Chen, T., Yang, L., Wang, T., Zhang, Q., and Wang, W.: Summertime fine particulate nitrate pollution in the North China Plain: increasing trends, formation mechanisms and implications for control policy, *Atmos. Chem. Phys.*, 18, 11261-11275, 10.5194/acp-18-11261-2018, 2018.

Xing, L., Wu, J., Elser, M., Tong, S., Liu, S., Li, X., Liu, L., Cao, J., Zhou, J., El-Haddad, I., Huang, R., Ge, M., Tie, X., Prévôt, A. S. H., and Li, G.: Wintertime secondary organic aerosol formation in Beijing–Tianjin–Hebei (BTH): contributions of HONO sources and heterogeneous reactions, *Atmos. Chem. Phys.*, 19, 2343-2359, 10.5194/acp-19-2343-2019, 2019.

Xu, Z., Wang, T., Wu, J., Xue, L., Chan, J., Zha, Q., Zhou, S., Louie, P. K. K., and Luk, C. W. Y.: Nitrous acid (HONO) in a polluted subtropical atmosphere: Seasonal variability, direct vehicle emissions and heterogeneous production at ground surface, *Atmos. Environ.*, 106, 100-109, 10.1016/j.atmosenv.2015.01.061, 2015.

Yadav, A. K., Raman, S., and Niyogi, D. D. S.: A note on the estimation of eddy diffusivity and dissipation length in low winds over a tropical urban terrain, *Pure and Applied Geophysics*, 160, 395-404, 10.1007/s00024-003-8785-4, 2003.

Yang, D., Zhang, S., Niu, T., Wang, Y., Xu, H., Zhang, K. M., and Wu, Y.: High-resolution mapping of vehicle emissions of atmospheric pollutants based on large-scale, real-world traffic datasets, *Atmos. Chem. Phys.*, 2019, 8831-8843, 10.5194/acp-2019-32, 2019.

Yang, Q., Su, H., Li, X., Cheng, Y., Lu, K., Cheng, P., Gu, J., Guo, S., Hu, M., Zeng, L., Zhu, T., and Zhang, Y.: Daytime HONO formation in the suburban area of the megacity Beijing, China, *Science China-Chemistry*, 57, 1032-1042, 10.1007/s11426-013-5044-0, 2014.

Zhang, J., An, J., Qu, Y., Liu, X., and Chen, Y.: Impacts of potential HONO sources on the concentrations of

oxidants and secondary organic aerosols in the Beijing-Tianjin-Hebei region of China, *Sci. Total Environ.*, 647, 836-852, <https://doi.org/10.1016/j.scitotenv.2018.08.030>, 2019a.

Zhang, J. W., Chen, J. M., Xue, C. Y., Chen, H., Zhang, Q., Liu, X. G., Mu, Y. J., Guo, Y. T., Wang, D. Y., Chen, Y., Li, J. L., Qu, Y., and An, J. L.: Impacts of six potential HONO sources on HO<sub>x</sub> budgets and SOA formation during a wintertime heavy haze period in the North China Plain, *Sci. Total Environ.*, 681, 110-123, [10.1016/j.scitotenv.2019.05.100](https://doi.org/10.1016/j.scitotenv.2019.05.100), 2019b.

Zhang, L., Wang, T., Zhang, Q., Zheng, J., Xu, Z., and Lv, M.: Potential sources of nitrous acid (HONO) and their impacts on ozone: A WRF-Chem study in a polluted subtropical region, *Journal of Geophysical Research-Atmospheres*, 121, 3645-3662, [10.1002/2015jd024468](https://doi.org/10.1002/2015jd024468), 2016.

Zhang, W., Tong, S., Ge, M., An, J., Shi, Z., Hou, S., Xia, K., Qu, Y., Zhang, H., Chu, B., Sun, Y., and He, H.: Variations and sources of nitrous acid (HONO) during a severe pollution episode in Beijing in winter 2016, *The Science of the total environment*, 648, 253-262, [10.1016/j.scitotenv.2018.08.133](https://doi.org/10.1016/j.scitotenv.2018.08.133), 2019c.

1 **The promotion effect of nitrous acid on aerosol formation in**  
2 **wintertime Beijing: possible contribution of traffic-related**  
3 **emission**

4

5 Yongchun Liu<sup>1\*</sup>, Yusheng Zhang<sup>1</sup>, Chaofan Lian<sup>2,6</sup>, Chao Yan<sup>3</sup>, Zeming Feng<sup>1</sup>, Feixue  
6 Zheng<sup>1</sup>, Xiaolong Fan<sup>1</sup>, Yan Chen<sup>2,6</sup>, Weigang Wang<sup>2,6\*</sup>, Biwu Chu<sup>3,4</sup>, Yonghong Wang<sup>3</sup>,  
7 Jing Cai<sup>3</sup>, Wei Du<sup>3</sup>, Kaspar R. Daellenbach<sup>3</sup>, Juha Kangasluoma<sup>1,3</sup>, Federico Bianchi<sup>1,3</sup>,  
8 Joni Kujansuu<sup>1,3</sup>, Tuukka Petäjä<sup>3</sup>, Xuefei Wang<sup>6</sup>, Bo Hu<sup>5</sup>, Yuesi Wang<sup>5</sup>, Maofa Ge<sup>2</sup>,  
9 Hong He<sup>4</sup> and Markku Kulmala<sup>1,3\*</sup>

10

11 1. Aerosol and Haze Laboratory, Advanced Innovation Center for Soft Matter Science and  
12 Engineering, Beijing University of Chemical Technology, Beijing, 100029, China

13 2. State Key Laboratory for Structural Chemistry of Unstable and Stable Species, Beijing  
14 National Laboratory for Molecular Sciences, Institute of Chemistry, Chinese Academy of  
15 Sciences, Beijing 100190, China

16 3. Institute for Atmospheric and Earth System Research/Physics, Faculty of Science, University  
17 of Helsinki, P.O. Box 64, FI-00014, Finland

18 4. State Key Joint Laboratory of Environment Simulation and Pollution Control, Research  
19 Center for Eco-Environmental Sciences, Chinese Academy of Sciences, Beijing, 100085, China

20 5. State Key Laboratory of Atmospheric Boundary Layer Physics and Atmospheric Chemistry,  
21 Institute of Atmospheric Physics, Chinese Academy of Sciences, Beijing, 100029, China

22 6. University of Chinese Academy of Sciences, Beijing 100049, PR China

23 *Correspondence to:* liuyc@buct.edu.cn, wangwg@iccas.ac.cn or markku.kulmala@helsinki.fi

24

25 **Abstract**

26 Secondary aerosol is a major component of PM<sub>2.5</sub>, yet its formation mechanism in the  
27 ambient atmosphere is still an open question. Based on field measurements in  
28 downtown Beijing, we show that the photolysis of nitrous acid (HONO) could promote  
29 the formation of organic and nitrate aerosol in wintertime Beijing as evidenced by the  
30 growth of the mass concentration of organic and nitrate aerosols linearly increasing as  
31 a function of consumed HONO from early morning to noon. The increased nitrate also  
32 lead to the formation of particulate matter ammonium by enhancing the neutralization  
33 of nitric acid by ammonia. We further illustrate that over 50 % of the ambient HONO  
34 during pollution events in wintertime Beijing might be related to traffic-related  
35 emission including direct emission and formation via the reaction between OH and  
36 vehicle-emitted NO. Overall, our results highlight that the traffic-related HONO plays  
37 an important role in the oxidative capacity and in turn, contribute to the haze formation  
38 in winter Beijing. Mitigation of HONO and NO<sub>x</sub> emission from the vehicles might be  
39 an effective way to reduce secondary aerosol mass formation and severe haze events in  
40 wintertime Beijing.

41

## 42 **1. Introduction**

43 China is one of the most suffering countries from the pollution of fine particulate matter  
44 with diameter less than or equal to 2.5  $\mu\text{m}$  ( $\text{PM}_{2.5}$ ) (Lelieveld et al., 2015). Although  
45 the regional air quality has been continuously improving since the central government  
46 of China issued the Clean Air Act in 2013 (Vu et al., 2019),  $\text{PM}_{2.5}$  concentration is still  
47 significantly higher than that in developed countries (Fu et al., 2014;An et al., 2019).  
48 Nowadays, a consensus has been reached that haze events are driven by local emissions  
49 (An et al., 2019), regional transport (Zheng et al., 2015b) and secondary formation  
50 (Huang et al., 2014;He et al., 2018) of pollutants under unfavorable meteorological  
51 conditions (stagnant atmosphere and high relative humidity) (Zhu et al., 2018;Liu et al.,  
52 2017c). A feedback loop between meteorological parameters and haze formation has  
53 also been found playing an important role in the evolution of haze events (Zhang et al.,  
54 2018).

55 Secondary aerosol can contribute up to ~70 % to the aerosol mass concentration on  
56 polluted days (Huang et al., 2014). Several reaction pathways have been proposed in  
57 the atmospheric chemistry community, such as sulfate formation via heterogeneous  
58 oxidation of  $\text{SO}_2$  promoted by  $\text{H}_2\text{O}_2$  and/or  $\text{NO}_2$  on mineral dust (Huang et al., 2015;He  
59 et al., 2014), aqueous oxidation of  $\text{SO}_2$  promoted by  $\text{NO}_2$  in the presence or absence of  
60  $\text{NH}_3$  in particle-bound water film (He et al., 2014;Wang et al., 2016), catalytic  
61 conversion of  $\text{SO}_2$  to sulfate by black carbon (Zhang et al., 2020), nitrate formation via  
62 efficient hydrolysis of  $\text{N}_2\text{O}_5$  on aerosol surfaces (Wang et al., 2017c;Wang et al.,  
63 2019;Kulmala, 2018;Li et al., 2017), and the haze formation initiated by new particle

64 formation and growth (Guo et al., 2014;Guo et al., 2020). During the past years, strict  
65 control of coal combustion has successfully reduced the SO<sub>2</sub> concentration, resulting in  
66 a reduction of sulfate (SO<sub>4</sub><sup>2-</sup>) component in PM<sub>2.5</sub>; in stark contrast, the contributions  
67 from organic and nitrate become increasingly more significant in China (Lang et al.,  
68 2017).

69 The formation of secondary organic aerosol (SOA) starts from the gas-phase  
70 oxidation of volatile organic compounds (VOCs) leading to various oxidized low-  
71 volatility and semi-volatile products (Bianchi et al., 2019), followed by their  
72 partitioning into the particle phase (Hallquist et al., 2009). Similarly, the formation of  
73 nitrate aerosol in the daytime is largely due to the partitioning of gaseous nitric acid,  
74 which is formed via the oxidation of NO<sub>2</sub> by OH (Seinfeld and Pandis, 2006;Wang et  
75 al., 2019). It is traditionally believed that the wintertime atmospheric oxidation capacity  
76 is weak due to the weak solar radiation, which limits the formation of SOA and nitrate  
77 (Sun et al., 2013). However, it is very recently shown that the peak OH concentration  
78 on polluted days in winter Beijing varies from 2×10<sup>6</sup> to 6×10<sup>6</sup> molecules cm<sup>-3</sup>, which  
79 is 6-10 times higher than what is predicted by the global model (Tan et al., 2018). This  
80 discrepancy can be largely reduced after accounting for other OH production processes  
81 in model simulations, which shows that the photolysis of nitrous acid (HONO)  
82 dominates the initiation of HO<sub>x</sub> (OH and HO<sub>2</sub>) and RO<sub>x</sub> (RO and RO<sub>2</sub>) radical chain in  
83 wintertime Beijing (Tan et al., 2018), and some other cities (Ren et al., 2006;Stutz et  
84 al., 2013).

85 The HONO concentration has been measured with a wide rang from 0.18 to 9.71



86 ppbv at different locations, such as Beijing (Zhang et al., 2019d;Hu et al.,  
87 2002;Hendrick et al., 2014;Wang et al., 2017b), Shanghai (Wang et al., 2013;Zhang et  
88 al., 2019b), Guangdong (Hu et al., 2002;Su et al., 2008a), Hongkong (Xu et al., 2015),  
89 Shandong (Li et al., 2018), Xi'an (Huang et al., 2017b) and so on in China since 2000.  
90 More recently, modelling studies have suggested that nitrous acid (HONO) could  
91 enhance secondary aerosols formation in Beijing-Tianjin-Hebei (BTH) region (Zhang  
92 et al., 2019c), Pearl-River-Delta (PRD) region of China (Zhang et al., 2019a;Xing et al.,  
93 2019) and Houston (Czader et al., 2015). These results imply that the role of HONO in  
94 haze chemistry might be crucial in wintertime Beijing, while the direct evidence from  
95 observation has not been reported, yet. On the other hand, the HONO budget has been  
96 investigated via modelling studies (Liu et al., 2019c;Zhang et al., 2019c) and  
97 photostationary state calculations (Wang et al., 2017b;Li et al., 2018;Huang et al.,  
98 2017b;Lee et al., 2016;Oswald et al., 2015;Zhang et al., 2019d) at different locations.  
99 At the present time, the study of the HONO budget is still far from closed, which would  
100 require a significant effort on both the accurate measurement of HONO and the  
101 determination of related kinetic parameters for its production pathways (Liu et al.,  
102 2019c). For example, photo-enhanced conversion of NO<sub>2</sub> (Su et al., 2008b) and  
103 photolysis of particulate nitrate were found to be the two major mechanisms with large  
104 potential of HONO formation during noontime, but the associated uncertainty may  
105 reduce their importance (Liu et al., 2019c). The heterogeneous reactions of NO<sub>2</sub> on  
106 ground/aerosol surfaces were proposed to be an important HONO source during  
107 nighttime (Wang et al., 2017b;Zhang et al., 2019c) and daytime in Beijing-Tianjin-

108 Hebei (BTH) (Zhang et al., 2019c), but it was unimportant compared with the unknown  
109 sources and the homogeneous reaction between NO and OH in Ji'an (Li et al., 2018) or  
110 compared with the traffic emission on haze days in Beijing (Zhang et al., 2019d). The  
111 traffic emission was found to be an important HONO source during nighttime and a  
112 minor daytime HONO source in BTH (Zhang et al., 2019c). However, it was proposed  
113 that direct emission of HONO from vehicles should contribute about 51.1 % (Meng et  
114 al., 2019) and 52 % of HONO source on haze days in Beijing (Zhang et al., 2019d).  
115 These results mean that more studies are still required on the HONO budget. In  
116 particular, it is meaningful to analyze the HONO budget in polluted events for  
117 understanding the possible influence of HONO sources on secondary pollutants  
118 formation.

119 In this work, we carried out comprehensive measurements at a newly constructed  
120 observation station (Aerosol and Haze Laboratory, Beijing University of Chemical  
121 Technology, AHL/BUCT Station) located in the western campus of Beijing University  
122 of Chemical Technology in downtown Beijing. We show observational evidence that  
123 HONO has a prominent promotion effect on the secondary aerosol mass formation in  
124 winter. Traffic-related emission seems to be a vital contributor to ambient HONO  
125 during the pollution events in winter in Beijing.

## 126 **2. Materials and methods**

127 **2.1 Field measurements.** Field measurements were performed at AHL/BUCT Station  
128 (Lat. 39°56'31" and Lon. 116°17'52") from February 1 to June 30, 2018. The  
129 observation station is on a rooftop of the main building, which is 550 m from the 3<sup>rd</sup>

130 ring road in the East, 130 m from the Zizhuyuan road in the North and 565 m from the  
131 Nandianchang road in the West (Figure S1). The station is surrounded by both traffic  
132 and residential emissions, thus, is a typical urban observation site.

133 Ambient air was sampled from the roof of the main building with five floors (~18  
134 m above the surface). A PM<sub>2.5</sub> inlet (URG) was used to cut off the particles with  
135 diameter larger than 2.5 μm before going to a Nafion dryer (MD-700-24, Perma Pure).  
136 Then a Time-of-Flight Aerosol Chemical Speciation Monitor equipped a PM<sub>2.5</sub>  
137 aerodynamic lens (ToF-ACSM, Aerodyne) and an Aethalometer (AE33, Magee  
138 Scientific) were connected to the manifold of aerosol sampling tube. The Reynolds  
139 number in the aerosol sampling tube was 800 with the total flow rate of 16.7 lpm and  
140 the residence time of 6.5 s. The details about ToF-ACSM measurement was described  
141 in the Supplement information. Ambient air was drawn from the roof using a Teflon  
142 sampling tube (BMET-S, Beijing Saak-Mar Environmental Instrument Ltd.) with the  
143 residence time <10 s for gas phase pollutants measurements. Trace gases including NO<sub>x</sub>,  
144 SO<sub>2</sub>, CO and O<sub>3</sub> were measured with the corresponding analyzer (Thermo Scientific,  
145 42i, 43i, 48i and 49i). Volatile organic compounds (VOCs) was measured using an  
146 online Single Photon Ionization Time-of-flight Mass Spectrometer (SPI-ToF-MS  
147 3000R, Hexin Mass Spectrometry) with unit mass resolution (UMR). The principle and  
148 the configuration of the instrument has been described in detail elsewhere (Gao et al.,  
149 2013) and the Supplement information. HONO concentration was measured using a  
150 home-made Long Path Absorption Photometer (LOPAP) (Tong et al., 2016). The details  
151 are described in the Supplement information. Particle size and number concentration

152 from 1 nm to 10  $\mu\text{m}$  were measured with Scanning Mobility Particle Sizer (SMPS 3936,  
153 TSI), particle size magnifier (PSM, Airmodus) and Neutral Cluster and Air Ion  
154 Spectrometer (NIAS, Airedt Ltd.). Meteorological parameters including temperature,  
155 pressure, relative humidity (RH), wind speed and direction were measured using a  
156 weather station (AWS310, Vaisala). Visibility and planetary boundary layer (PBL)  
157 height were measured using a visibility sensor (PWD22, Vaisala) and a ceilometer  
158 (CL51, Vaisala), respectively

159 **2.2 HONO budget calculation.** Multiple sources of ambient HONO have been  
160 identified, such as emission from soil ( $E_{\text{soil}}$ ) (Oswald et al., 2015; Meusel et al., 2018)  
161 and vehicle exhaust ( $E_{\text{vehicle}}$ ) (Trinh et al., 2017), production through homogeneous  
162 reaction between NO and OH ( $P_{\text{NO-OH}}$ ) in the atmosphere, photolysis of nitrate ( $P_{\text{nitrate}}$ )  
163 (Bao et al., 2018), nitrous acid ( $P_{\text{HNO}_3}$ ) and nitrophenol ( $P_{\text{nitrophenol}}$ ) (Sangwan and  
164 Zhu, 2018), heterogeneous reaction of  $\text{NO}_2$  on aerosol surface ( $P_{\text{aerosol}}$ ) (Liu et al., 2015)  
165 and ground surface ( $P_{\text{ground}}$ ) (Liu et al., 2019c; Li et al., 2018; Wang et al., 2017b).  
166 However, the photolysis of  $\text{HNO}_3$  and nitrophenol were excluded in this work because  
167 they were believed as minor sources (Lee et al., 2016) and their concentrations were  
168 unavailable during our observation. The removal pathways of HONO including  
169 photolysis ( $L_{\text{photolysis}}$ ), the homogeneous reaction with OH radical ( $L_{\text{HONO-OH}}$ ) and dry  
170 deposition ( $L_{\text{deposition}}$ ) (Liu et al., 2019c) were considered.

171 The HONO budget could be calculated by,

$$172 \frac{dc_{\text{HONO}}}{dt} = E_{\text{HONO}} + P_{\text{HONO}} - L_{\text{HONO}} + T_{\text{vertical}} + T_{\text{horizontal}} \quad (1)$$

173 where  $\frac{dc_{\text{HONO}}}{dt}$  is the observed change rate of HONO mixing ratios ( $\text{ppbv h}^{-1}$ );  $E_{\text{HONO}}$

174 represents the emission rate of HONO from different sources (ppbv h<sup>-1</sup>);  $P_{HONO}$  is the  
 175 in-situ production rate of HONO in the troposphere (ppbv h<sup>-1</sup>);  $L_{HONO}$  is the loss rate of  
 176 HONO (ppbv h<sup>-1</sup>) (Li et al., 2018);  $T_{vertical}$  and  $T_{horizontal}$  are the vertical and horizontal  
 177 transport (Soergel et al., 2011), which can mimic source or sink terms depending on the  
 178 HONO mixing ratios of the advected air relative to that of the measurement site and  
 179 height (Soergel et al., 2011).

180 The emission rate ( $E_{HONO}$ , ppbv h<sup>-1</sup>) was calculated based on the emission flux  
 181 ( $F_{HONO}=EI_{HONO}/A$ , g m<sup>-2</sup> s<sup>-1</sup>) and PBL height ( $H$ , m) according to the following equation,

$$182 \quad E_{HONO} = \frac{\alpha \cdot F_{HONO}}{H} \quad (2)$$

183 where,  $EI_{HONO}$ , is the emission inventory of HONO (g s<sup>-1</sup>),  $A$  is the urban area of Beijing  
 184 (m<sup>2</sup>),  $\alpha$  is the conversion factor ( $\alpha = \frac{1 \times 10^9 \cdot 3600 \cdot R \cdot T}{M \cdot P} = \frac{2.99 \times 10^{13} \cdot T}{M \cdot P}$ ),  $M$  is the molecular  
 185 weight (g mol<sup>-1</sup>),  $T$  is the temperature (K) and  $P$  is the atmospheric pressure (Pa).

186 The production rates of HONO ( $P_{HONO}$ , ppbv h<sup>-1</sup>) in the troposphere was calculated  
 187 by,

$$188 \quad P_{HONO} = 3600 \cdot k_1 \cdot c_{precursor} \quad (3)$$

189 where,  $k_1$  is the quasi first-order reaction rate constant (s<sup>-1</sup>),  $c_{precursor}$  is the concentration  
 190 of precursor (ppbv). For homogeneous reaction between NO and OH,

$$191 \quad k_1 = k_2 \cdot c_{OH} \quad (4)$$

192 where,  $k_2$  is the second-order reaction rate constant ( $7.2 \times 10^{-12}$  cm<sup>3</sup> molecule<sup>-1</sup> s<sup>-1</sup>) (Li et  
 193 al., 2012),  $c_{OH}$  is the OH concentration (molecules cm<sup>-3</sup>). For heterogeneous reaction,

$$194 \quad k_1 = \frac{\gamma \cdot A_s \cdot \omega}{4} \cdot Y_{HONO} \quad (5)$$

195 where,  $A_s$  is the surface area concentration of the reactive surface (m<sup>2</sup> m<sup>-3</sup>),  $\omega$  is the

196 molecular mean speed ( $\text{m s}^{-1}$ ),  $\gamma$  is the uptake coefficient of the precursor,  $Y_{\text{HONO}}$  is the  
197 yield of HONO. For ground surface, the surface area concentration is

$$198 \quad A_s = \frac{\delta}{H} \quad (6)$$

199 where  $\delta$  is the surface roughness, which is calculated according to the mean project area,  
200 perimeter and height of the buildings in Beijing.

$$201 \quad \delta = \frac{f_{\text{building}} \cdot (A_{\text{projected}} + h \cdot P_{\text{building}})}{A_{\text{projected}}} + f_{\text{blank}} \quad (7)$$

202 where  $f_{\text{building}}$  (0.31) and  $f_{\text{blank}}$  (0.69) are the fraction of the projected area ( $A_{\text{projected}}$ ) of  
203 buildings and blank space, respectively;  $P_{\text{building}}$  and  $h$  are the perimeter and the height  
204 of the building, respectively. The  $f_{\text{building}}$  and  $P_{\text{building}}$  are measured from ~1000 buildings  
205 randomly selected on the Google Map using ImageJ software. The mean height (44.5  
206 m) of the building in Beijing is linearly extrapolated from the literature data based on  
207 remote measurement using Light Detection and Ranging (LiDAR) sensor from 2004 to  
208 2008 (Cheng et al., 2011). The  $\delta$  in Beijing is calculated to be 3.85, which is slightly  
209 higher than the value (2.2) used by Li et al. (2018).

210 As for photolysis reaction, the first-order reaction rate was

$$211 \quad k_1 = J \quad (8)$$

212 where,  $J$  is the photolysis rate to produce HONO ( $\text{s}^{-1}$ ).

213 The loss rates of HONO by photolysis ( $L_{\text{photolysis}}$ ), homogeneous reaction with  
214 OH radicals ( $L_{\text{HONO-OH}}$ ) and dry deposition ( $L_{\text{deposition}}$ ) (Liu et al., 2019c) were calculated  
215 according to the following equations.

$$216 \quad L_{\text{photolysis}} = 3600 \cdot J_{\text{HONO}} \cdot c_{\text{HONO}} \quad (9)$$

$$217 \quad L_{\text{HONO-OH}} = 3600 \cdot k_{\text{HONO-OH}} \cdot c_{\text{OH}} \cdot c_{\text{HONO}} \quad (10)$$

218  $L_{deposition} = \frac{3600 \cdot v_d \cdot c_{HONO}}{H}$  (11)

219 where,  $J_{HONO}$  is the photolysis rate of HONO ( $s^{-1}$ ),  $k_{HONO-OH}$  is the second-order reaction  
 220 rate constant between HONO and OH ( $6 \times 10^{-12} \text{ cm}^3 \text{ molecule}^{-1} \text{ s}^{-1}$ ) (Atkinson et al.,  
 221 2004), and  $v_d$  is the dry deposition rate of HONO ( $0.001 \text{ m s}^{-1}$ ) (Han et al., 2017).

222 Vertical transport by advection ( $T_{vertical}$ ), which is an important sink of HONO in  
 223 the night (Gall et al., 2016; Meng et al., 2019), can be calculated according to equation  
 224 (12).

225  $T_{vertical} = -K_h(z, t) \frac{\partial c(z, t)}{\partial z} \frac{1}{h}$  (12)

226 where  $K_h(z, t)$  is the eddy diffusivity of heat ( $\text{m}^2 \text{ s}^{-1}$ ) at height  $z$  (m) and time  $t$ ,  $h$  is the  
 227 height of the second layer (18 m in this study) (Gall et al., 2016). On the other hand,  
 228 both the vertical and horizontal transport can be estimate according to Eq. (13),

229  $T_{vertical} = k_{dilution}(c_{HONO} - c_{HONO,background})$  (13)

230 where  $k_{dilution}$  is a dilution rate ( $0.23 \text{ h}^{-1}$ , including both vertical and horizontal transport)  
 231 (Dillon et al., 2002),  $c_{HONO}$  and  $c_{HONO,background}$  is the HONO concentration at the  
 232 observation site and background site, respectively (Dillon et al., 2002).

233 In addition, even though all the current known sources had been considered in  
 234 models, the modelled daytime HONO concentrations were still lower than the observed  
 235 concentration (Tang et al., 2015; Michoud et al., 2014). Therefore, the HONO  
 236 concentration could be described in equation (14).

237  $\frac{dc_{HONO}}{dt} = E_{soil} + E_{vehicle} + P_{NO-OH} + P_{nitrate} + P_{aerosol} + P_{ground} + P_{unknown} -$   
 238  $L_{photolysis} - L_{HONO-OH} - L_{deposition} + T_{vertical} + L_{horizontal}$  (14)

239 **3. Results and discussion**



240 **3.1 Overview of the air pollution.** The mass concentration of non-refractory PM<sub>2.5</sub>  
241 (NR-PM<sub>2.5</sub>) and HONO along with metrological parameters are shown in Fig. 1. The  
242 time series of other pollutants (SO<sub>2</sub>, CO, O<sub>3</sub>, benzene, toluene and black carbon) are  
243 shown in Fig. S2 in the Supplement information.

244 Similar to previous measurements (Guo et al., 2014;Wang et al., 2016), the air  
245 pollution events showed a periodic cycle of 3-5 days during the observation, as  
246 indicated by the concentration of NR-PM<sub>2.5</sub> (Fig. 1A), gaseous pollutants and the  
247 visibility. During the observation period, 20-60% of hourly PM<sub>2.5</sub> concentration was  
248 higher than 75 µg m<sup>-3</sup> (the criterion for pollution according to the national air quality  
249 standards) in each month (Fig. S3A). Both the frequency of severe polluted episodes  
250 and the mean mass concentration of PM<sub>2.5</sub> and NR-PM<sub>2.5</sub> were obviously higher in  
251 March than that in the rest months (Fig. 1 and S3). This can be explained by both the  
252 intensive emission during the heating season as evidenced by the high concentration of  
253 primary pollutants including CO, SO<sub>2</sub> and BC (Table S1) and the stagnant  
254 meteorological conditions supported by the low wind speed (<2 m s<sup>-1</sup>) and the low  
255 planetary boundary layer (PBL) height, in particular, in March (Fig. S4A).

256 OA and nitrate dominated the NR-PM<sub>2.5</sub>, while their relative contribution varied  
257 significantly during the observation (Fig. 1B and Table S1). This is similar to the  
258 previously reported NR-PM<sub>1.0</sub> composition (Sun et al., 2015). The monthly mean  
259 fraction of OA varied from 45.9±10.2 % to 52.6±18.7 %, which was accompanied by a  
260 slight increase of sulfate from 16.0±9.1 % to 18.2±8.0 % (Fig. S4D). At the same time,  
261 the monthly mean fraction of nitrate and chloride decreased from 26.7±8.8 % to

262 16.7±12.8 % and from 7.7±6.1 % to 0.3±0.2 %, respectively. Ammonium showed a  
263 peak value (14.2±2.8 %) in March, then slightly decreased to 12.2±5.2 %. The intensive  
264 emission of chloride from coal combustion during heating season (Cho et al., 2008) and  
265 firework burning (Zhang et al., 2017), which was transported from Tangshan during  
266 Chinese New Year (Fig. S5A and B), led to high fraction of chloride in February and  
267 March. The decrease in nitrate and ammonium fractions from February to June should  
268 be related to **the increase in temperature** (Fig. S2) which was in favor of NH<sub>4</sub>NO<sub>3</sub>  
269 decomposition (Wang et al., 2015). Besides the reduction of the contribution from other  
270 components, secondary formation due to increased UV light (Fig. S4C) might also  
271 favor the increased OA fraction (Huang et al., 2014). This means that chemical  
272 transformation in March should still be vigorous although the UV light intensity in  
273 March is lower than in summer (Fig. S4C). It also implies other factors may compensate  
274 the weak UV light intensity in March.

275 HONO, which has been recognized as the important precursor of **primary** OH  
276 radical (Ren et al., 2006; Alicke et al., 2003), ranged from 0.05 to 10.32 ppbv from  
277 February 1 to June 30, 2018 (Fig. 1C) with the mean value of 1.26±1.06 ppbv. In winter  
278 (February and March), HONO concentration was 1.15±1.10 ppbv and comparable to  
279 the previous results (1.05±0.89 ppbv) measured in the winter of Beijing (Wang et al.,  
280 2017b; Hou et al., 2016), while it was slightly lower than that from April to June  
281 (1.35±1.11 ppbv) in this work and those measured in the summer of Shanghai (2.31  
282 ppbv, in May) (Cui et al., 2018) and Guangzhou (2.8 ppbv, in July) (Qin et al., 2009).  
283 The mean HONO concentration in March (1.53±1.25 ppbv) was higher than that in

284 February and April (Fig. S3D), while was slightly higher or close to that in May and  
285 June. Chamber studies have found that HONO is responsible for the initiation of  
286 photosmog reactions (Rohrer et al., 2005). It is reasonable to postulate that HONO  
287 probably play an important **role** in the secondary chemistry of particle formation in  
288 March.

289 **3.2 Promotion effect of HONO photolysis on aerosol formation in winter.** Oxidation  
290 of precursors by OH radicals is the main mechanism regarding to secondary aerosol  
291 formation in the troposphere. After partially ruling out the possible influence of PBL  
292 variation by normalizing the concentrations of all pollutants to CO (Cheng et al., 2016)  
293 **or BC (Liggio et al., 2016)**, we found all secondary species including sulfate, nitrate  
294 and ammonium show obvious daytime peaks from 7:00 am to 6:00 pm (Figure S5C)  
295 (Cheng et al., 2016). The similar trends were observed after the concentrations of  
296 pollutants were normalized to BC (not shown). This suggests they might connect with  
297 photochemistry.

298 Photolysis of H<sub>2</sub>O<sub>2</sub>, HCHO, O<sub>3</sub> and HONO, and **the reaction between NO and HO<sub>2</sub>**  
299 are known as sources of OH radical in the atmosphere (Alicke et al., 2003; Volkamer et  
300 al., 2010; Tan et al., 2018; Tang et al., 2015). In this work, the concentration of H<sub>2</sub>O<sub>2</sub>,  
301 HCHO and **HO<sub>2</sub>** are unavailable. Thus, their contributions to OH production were not  
302 discussed here. However, it has been well recognized that the photolysis of HONO is  
303 the **dominant** source of OH in the dawn and dusk period (Holland et al., 2003), even  
304 contributes up to 60% of daytime OH source in winter (Spataro et al., 2013; Rohrer et  
305 al., 2005). **In addition, it has been confirmed that HONO dominates the primary OH**

306 source at various locations (Tan et al., 2018;Liu et al., 2019c;Tan et al., 2017;Aumont  
307 et al., 2003). Therefore, it is meaningful to discuss the contribution of HONO to  
308 secondary aerosol formation through OH production. We simply compared the OH  
309 production via photolysis of HONO ( $P_{\text{OH-HONO}}=J_{\text{HONO}}\times C_{\text{HONO}}$ ) and  $\text{O}_3$  ( $P_{\text{OH-}}$   
310  $\text{O}_3=J_{\text{O}_3}\times C_{\text{O}_3}$ ) in Fig. 2 when the  $\text{PM}_{2.5}$  concentration was larger than  $50 \mu\text{g m}^{-3}$  and the  
311 RH was less than 90 % to understand the chemistry in pollution events. Under these  
312 conditions, local chemistry should be more important as 75 % of the wind speed was  
313 less than  $1.0 \text{ m s}^{-1}$  (Fig. S6). The details about the  $J_{\text{HONO}}$  and  $J_{\text{O}_3}$  calculation were  
314 shown in the Supplement information and their time series were shown in Fig. S7. On  
315 polluted days in winter, the daytime  $P_{\text{OH-HONO}}$  was always significantly higher than the  
316  $P_{\text{OH-O}_3}$  in winter and the maximal  $P_{\text{OH-HONO}}$  and  $P_{\text{OH-O}_3}$  were  $1.73\pm 0.86 \times 10^7$  molecules  
317  $\text{cm}^{-3} \text{ s}^{-1}$  ( $2.43\pm 1.21 \text{ ppb h}^{-1}$ ) and  $1.03\pm 1.06 \times 10^7$  molecules  $\text{cm}^{-3} \text{ s}^{-1}$  ( $1.45\pm 1.49 \text{ ppb h}^{-1}$ ),  
318 respectively (Fig. 2A). Owing to the high HONO concentration accumulated  
319 throughout the night, the maximal  $P_{\text{OH-HONO}}$  in winter was as about 2-6 times of that  
320 was observed in the wintertime of Colorado, USA ( $\sim 0.59 \text{ ppb h}^{-1}$ ) (Kim et al., 2014),  
321 New York, USA ( $\sim 0.40 \text{ ppb h}^{-1}$ ) (Kanaya et al., 2007) and Nanjing, China ( $0.90\pm 0.27$   
322  $\text{ppb h}^{-1}$ ) (Liu et al., 2019b). In the period from April to June, the daily maxima of  $P_{\text{OH-}}$   
323  $\text{HONO}$  and  $P_{\text{OH-O}_3}$  were  $2.48\pm 1.42 \times 10^7$  molecules  $\text{cm}^{-3} \text{ s}^{-1}$  ( $3.48\pm 1.99 \text{ ppb h}^{-1}$ ) and  
324  $6.51\pm 4.17 \times 10^7$  molecules  $\text{cm}^{-3} \text{ s}^{-1}$  ( $9.15\pm 5.86 \text{ ppb h}^{-1}$ ), respectively. These results  
325 mean that the photolysis of HONO should play an important role in the initiation of the  
326 daytime  $\text{HO}_x$  and  $\text{RO}_x$  chemistry on polluted days in winter, while photolysis of  $\text{O}_3$   
327 becomes more important from April to June. This is consistent with the previous

328 findings that HONO photolysis dominates the primary OH source in winter of BTH  
329 (Xing et al., 2019; Tan et al., 2018), Colorado and New York City (Ren et al., 2006; Kim  
330 et al., 2014), while photolysis of O<sub>3</sub> and HCHO related reactions usually dominated  
331 primary OH production in summer (Alicke et al., 2003).

332 Oxidation of trace gas pollutants, in particular VOCs, by OH is their main removal  
333 pathway in the troposphere (Atkinson and Arey, 2003), subsequently, contribute to  
334 secondary aerosol formation (Kroll and Seinfeld, 2008). A very recent work has found  
335 that oxidation of VOCs from local traffic emission is still efficient even under pollution  
336 conditions (Guo et al., 2020). We partially ascribe this to the high HONO concentration  
337 in winter Beijing. To confirm this assumption, 12 episodes in winter were chosen (Fig.  
338 1) to uncover the connection between aerosol formation and HONO photolysis. The 1<sup>st</sup>,  
339 3<sup>rd</sup> and 5<sup>th</sup> episodes were clean days and the other 9 episodes were typical haze events  
340 with duration above 2 days. The features of these episodes were summarized in Table  
341 S2. Fig. 2C shows the CO-normalized daytime profiles of OA and HONO in the 7<sup>th</sup> and  
342 12<sup>th</sup> episodes as two examples. In all selected cases, HONO exhibited quick reduction  
343 due to the photolysis after sunrise, and simultaneously, OA concentration started to  
344 increase. This is similar to the evolution of the concentration of pollutants in a typical  
345 smog chamber experiment. We further show the formation of OA ( $\Delta C_{OA}/C_{CO}$ ) as a  
346 function of the consumed HONO ( $-\Delta C_{HONO}/C_{CO}$ ) in Fig. 2D. Except for the 4<sup>th</sup> episode  
347 that was highly affected by firework emission during the Spring Festival,  $\Delta C_{OA}/C_{CO}$   
348 showed a linear dependence on  $-\Delta C_{HONO}/C_{CO}$  in winter, and the correlation coefficient  
349 was 0.75. As the meteorological condition was stagnant during these cases as indicated

350 by the low wind speed ( $< 1.0 \text{ m s}^{-1}$ , Fig. S5D), it was reasonable to ascribe the increase  
351 of OA concentration to local secondary formation initiated by OH radical and  
352 photolysis of HONO should play an important role in initiation the  $\text{HO}_x$  and  $\text{RO}_x$   
353 chemistry. This kind of correlation could not be seen for the pollution events from April  
354 to June because the primary OH production was no longer dominated by HONO  
355 photolysis as indicated by Fig. 2D. It should be noted that oxidation of biogenic alkenes  
356 by  $\text{O}_3$  might also contribute to OA formation. However, anthropogenic VOCs instead  
357 of biogenic VOCs dominated the wintertime VOCs in Beijing (Liu et al., 2017a).  
358 Although vehicles can emit isoprene (Zou et al., 2019), the contribution of isoprene to  
359 the observed increase of OA concentration should be unimportant due to the low  
360 concentration of isoprene in winter (Zou et al., 2019). Therefore, it is reasonable to  
361 conclude that the increase of OA concentration in daytime might be mainly resulted  
362 from oxidation of VOCs by OH.

363 Similar to OA,  $\Delta C_{\text{nitrate}}/C_{\text{CO}}$  in winter also showed good linear correlation with -  
364  $\Delta C_{\text{HONO}}/C_{\text{CO}}$  ( $R=0.67$ , Fig. S5E), suggesting that the increase of particle-phase nitrate  
365 in the daytime should also be promoted by OH radical from HONO photolysis.  
366 Interestingly,  $\Delta C_{\text{ammonium}}/\text{CO}$  also showed a good correlation with  $-\Delta C_{\text{HONO}}/C_{\text{CO}}$   
367 ( $R=0.61$ , Fig. S5E), although particle-phase ammonium should not be directly related  
368 to oxidation of  $\text{NH}_3$  by OH. We explained the increased ammonium as the result of  
369 enhanced neutralization of  $\text{HNO}_3$  by  $\text{NH}_3$  (Wang et al., 2018; Wen et al., 2018; Sun et  
370 al., 2018) because  $\text{NH}_4^+$  was adequate to neutralize both sulfate and nitrate as shown in  
371 Fig.S8. This was consistent with the recent work which observed the important role of

372 photochemical reactions in daytime nitrate formation, while hydrolysis of  $\text{N}_2\text{O}_5$  mainly  
373 contributed to nighttime nitrate (Tian et al., 2019). Although a recent work has found  
374 that daytime hydrolysis of  $\text{N}_2\text{O}_5$  on hygroscopic aerosols is also an important source of  
375 daytime nitrate in winter Beijing (Wang et al., 2017a), the linearly correlation between  
376  $\Delta\text{C}_{\text{nitrate}}/\text{C}_{\text{CO}}$  and  $\Delta\text{C}_{\text{HONO}}/\text{C}_{\text{CO}}$  at least implies that the promotion effect of HONO on  
377 nitrate formation could not be excluded. On the other hand, the correlation between  
378  $\Delta\text{C}_{\text{sulfate}}/\text{C}_{\text{CO}}$  and  $-\Delta\text{C}_{\text{HONO}}/\text{C}_{\text{CO}}$  was much weaker ( $R=0.26$ ), suggesting a weak  
379 connection between particle-phase sulfate and gas-phase  $\text{H}_2\text{SO}_4$ . This was also  
380 consistent with the previous understanding that heterogeneous reactions of  $\text{SO}_2$  were  
381 the **dominant** pathway for sulfate formation (Zheng et al., 2015a;He et al., 2018;Zhang  
382 et al., 2020). Overall, this work well supported the recent modeling results that HONO  
383 could obviously promote the aerosol production in winter (Zhang et al., 2019a;Zhang  
384 et al., 2019c;Xing et al., 2019;An et al., 2013) from the point of view of observation.

385 **3.3 HONO budget in polluted events.** To understand the possible sources of HONO  
386 in polluted events in winter, the HONO budget was calculated for the events when the  
387  $\text{PM}_{2.5}$  concentration was larger than  $50 \mu\text{g m}^{-3}$  and the RH was less than 90 % according  
388 to the method described in Section 2.2.

389 **Vehicle emission.** The  $E_{\text{vehicle}}$  was calculated **according to Eq. (2)** using the relative  
390 emission rate of HONO to  $\text{NO}_x$  and the emission inventory of  $\text{NO}_x$  from vehicles. Firstly,  
391 the ratio of HONO/ $\text{NO}_x$  was calculated according to the method reported by Xu et al.  
392 (Xu et al., 2015) and Li et al. (Li et al., 2018) from the fresh nighttime plumes which  
393 were strictly satisfy the following criteria: 1)  $\text{NO}_x > 45$  ppb (highest 25% of  $\text{NO}_x$  data);



394 2)  $\Delta\text{NO}/\Delta\text{NO}_x > 0.8$ , with good correlation between NO and  $\text{NO}_x$  ( $R > 0.9$ ,  $P < 0.05$ );  
395 3) Good correlation between HONO and  $\text{NO}_x$  ( $R^2 > 0.65$ ,  $P < 0.05$ ); and 4) Dataset from  
396 5:00 am to 8:00 am. The mean emission ratio of HONO to  $\text{NO}_x$  was  $1.8 \pm 0.5\%$  based  
397 on 5 fresh vehicle exhaust plumes during our observation (Table S3). This value is  
398 higher than that in Hongkong ( $1.2 \pm 0.4\%$ ) (Xu et al., 2015), Beijing (1.3%) (Zhang et  
399 al., 2019d) and Jinan ( $0.53 \pm 0.20\%$ ) (Li et al., 2018) using the same method, while is  
400 comparable with the result measured in tunnel experiments (2.1%) carried out in  
401 Beijing (Yang et al., 2014). Secondly, low HONO concentration should be accompanied  
402 with high  $\text{NO}_x$  and high ratio of  $\Delta\text{NO}/\Delta\text{NO}_x$  if direct emission from vehicles was the  
403 major source of HONO and the source from secondary formation was negligible in the  
404 urban atmosphere. Therefore, we further estimated the HONO/ $\text{NO}_x$  ratio using a low  
405 limit correlation method (Li et al., 2012). In the 2D space of HONO versus  $\text{NO}_x$  (Fig.  
406 S8), the lowest margin with  $\Delta\text{NO}/\Delta\text{NO}_x$  larger than 0.8 were chosen for linear  
407 correlation. The ratio of  $\Delta\text{HONO}/\Delta\text{NO}_x$  is  $1.17 \pm 0.05\%$ . This value is lower than that  
408 estimated through empirical method discussed above, while is very close to that  
409 measured in Hongkong ( $1.2 \pm 0.4\%$ ) (Xu et al., 2015) and ( $1.23 \pm 0.35\%$ ) (Liang et al.,  
410 2017), Guangzhou (1.0%) (Li et al., 2012) and Beijing (1.3% and 1.41%) (Zhang et al.,  
411 2019d; Meng et al., 2019). Finally, several studies have measured the direct emission of  
412 HONO from vehicle exhaust. The HONO/ $\text{NO}_x$  was 0.18% from gasoline cars through  
413 chassis dynamometer tests in China (Liu et al., 2017d), while it was 0-0.95% for  
414 gasoline vehicles and 0.16-1.0% for diesel vehicles measured under real-world driving  
415 test cycles in Japan (Trinh et al., 2017). Thus, three levels of vehicle emission factor

416 were considered.  $1.17\pm 0.05\%$  was taken as the middle value which was very close to  
417 the mean emission ratio (1.21) for all of these reported values in China (Li et al.,  
418 2018; Xu et al., 2015; Yang et al., 2014; Liu et al., 2017d; Gall et al., 2016; Meng et al.,  
419 2019), while 0.18% (Liu et al., 2017d) and 1.8 % were the lower limit and the upper  
420 limit, respectively.

421 The  $E_{\text{vehicle}}$  was calculated using the hourly  $\text{NO}_x$  emission inventory from vehicles  
422 in Beijing (Yang et al., 2019) after converted to emission flux of HONO ( $F_{\text{HONO}}=F_{\text{NO}_x}\times$   
423  $\text{HONO}/\text{NO}_x$ ) and the PBL height as described in Section 2.2. Thus, the calculated  
424 emission rate reflected the diurnal variation of both the emission inventory and the PBL  
425 height. The calculated hourly middle value of  $E_{\text{vehicle}}$  using the  $\text{HONO}/\text{NO}_x$  of 1.17%  
426 was from  $0.085\pm 0.038$  to  $0.34\pm 0.15$  ppbv  $\text{h}^{-1}$ , which was slightly higher than the  
427 daytime emission rate of HONO in Xi'an (Huang et al., 2017b). This is reasonable  
428 when the vehicle population in Beijing is taken into consideration. The lower limit of  
429  $E_{\text{vehicle}}$  was  $0.013\pm 0.006-0.053\pm 0.023$  ppbv  $\text{h}^{-1}$ , which was close to the estimated  
430 emission rate of HONO in Jinan (Li et al., 2018). The upper limit was in the range of  
431  $0.13\pm 0.06-0.53\pm 0.23$  ppbv  $\text{h}^{-1}$ .

432 **Soil emission.** The emission flux of HONO from soil depends on the water content, the  
433 nitrogen nutrient content and the temperature of soil (Oswald et al., 2013). Oswald et  
434 al. (2013) measured the emission flux of HONO from 17 soil samples, including  
435 eucalyptus forest, tropical rain forest, coniferous forest, pasture, woody savannah,  
436 grassland, stone desert, maize field, wheat field, jujube field an cotton field etc. Tropical  
437 rain forest, coniferous forest and grassland are the typical plants in downtown Beijing

438 (Huang et al., 2017a). At the same time, their emission fluxes of HONO are comparable  
 439 (Oswald et al., 2013). Thus, we used the emission flux from grassland to calculate the  
 440 emission rate of HONO from soil in Beijing because the temperature and water holding  
 441 content dependent emission flux of HONO was available for grassland soil. Three  
 442 levels of water content including 25-35%, 35-45% and 45-55% were considered. The  
 443 temperature dependence of  $F_{\text{HONO}}$  was calculated using the mean value of the  $F_{\text{HONO}}$   
 444 with different water content, while the low limit and upper limit of  $F_{\text{HONO}}$  were  
 445 calculated using the emission flux from 45-55% of water content and 25-35% of water  
 446 content, respectively. The lower limit, the middle value and the upper limit of the  $E_{\text{soil}}$   
 447 are  $0.0032 \pm 0.0027 - 0.013 \pm 0.014$ ,  $0.0046 \pm 0.0039 - 0.020 \pm 0.20$  and  $0.0057 \pm 0.0047 -$   
 448  $0.025 \pm 0.024$  ppbv h<sup>-1</sup>, respectively, calculated according to Eq. (2).

449 **Homogeneous reaction between NO and OH.** Direct measurement of OH  
 450 concentration was unavailable in this work, while several methods were used to  
 451 estimate the ambient OH concentration. In winter in Beijing, it has been found that the  
 452 OH concentration is linearly correlated with  $J_{\text{O1D}}$ , that's,  $c_{\text{OH}} = J_{\text{O1D}} \times 2 \times 10^{11}$  molecules  
 453 cm<sup>-3</sup> (Tan et al., 2019). However, Tan et al. (2018) reported a larger conversion factor  
 454 ( $4.33 \times 10^{11}$  molecules cm<sup>-3</sup>). Li et al. (2018) estimated the OH radical concentration  
 455 considering both photolysis rate and NO<sub>2</sub> concentration, namely,

$$456 \quad c_{\text{OH}} = \frac{4.1 \times 10^9 \times (J_{\text{O1D}})^{0.83} \times (J_{\text{NO}_2})^{0.19} \times (140c_{\text{NO}_2} + 1)}{0.41c_{\text{NO}_2}^2 + 1.7c_{\text{NO}_2} + 1} \quad (15)$$

457 Overall, the estimated OH concentrations according to Eq. (15) were comparable with  
 458 that estimated by Tan et al. (2019) (Fig. S10C). The method for the photolysis rates  
 459 calculation were shown in the SI and the time series of the photolysis rates were shown

460 in Fig. S7. On polluted days, high concentration of NO<sub>2</sub> resulted into lower OH  
 461 concentrations estimated using the Eq. (15). Therefore, the corresponding P<sub>NO-OH</sub> was  
 462 taken as the low limit for homogeneous reaction between NO and HONO because  
 463 polluted events were discussed in this work, while P<sub>NO-OH</sub> calculated using the OH  
 464 concentration ( $J_{\text{O1D}} \times 4.33 \times 10^{11}$  molecules cm<sup>-3</sup>) (Tan et al., 2018) was taken as the upper  
 465 limit and P<sub>NO-OH</sub> calculated using the OH concentration ( $J_{\text{O1D}} \times 2 \times 10^{11}$  molecules cm<sup>-3</sup>)  
 466 (Tan et al., 2019) was the middle value. In the night, OH concentration usually varied  
 467 from  $1.0 \times 10^5$  molecules cm<sup>-3</sup> (Li et al., 2012; Tan et al., 2018) in winter to  $5 \times 10^5$   
 468 molecules cm<sup>-3</sup> in summer (Tan et al., 2017). The nighttime OH concentration was  
 469 estimated linearly correlated with the product of nighttime O<sub>3</sub> concentration and alkenes  
 470 concentration, namely,

$$471 \quad c_{\text{OH},\text{night}} = 1 \times 10^5 + 4 \times 10^5 \times \frac{(c_{\text{O}_3} \times c_{\text{alkenes}})_{\text{night}} - (c_{\text{O}_3} \times c_{\text{alkenes}})_{\text{night},\text{min}}}{(c_{\text{O}_3} \times c_{\text{alkenes}})_{\text{night},\text{max}} - (c_{\text{O}_3} \times c_{\text{alkenes}})_{\text{night},\text{min}}} \quad (16)$$

472 The time series of OH concentration calculated using different methods was shown in  
 473 Fig. S11. Thus, the lower limit, the middle value and the upper limit of P<sub>NO-OH</sub> were  
 474  $0.007 \pm 0.019$ - $0.43 \pm 0.26$ ,  $0.026 \pm 0.053$ - $0.99 \pm 0.79$  and  $0.028 \pm 0.053$ - $2.14 \pm 1.71$  ppbv h<sup>-1</sup>,  
 475 respectively, calculated according to Eqs. (3) and (4). The calculated middle value of  
 476 P<sub>NO-OH</sub> (with mean daytime value of  $0.49 \pm 0.35$  ppb h<sup>-1</sup>) was comparable with these  
 477 estimated values by Li et al. (2018) ( $0.4$  ppb h<sup>-1</sup>) and Huang et al. (2017b) ( $0.28$  ppb h<sup>-1</sup>).  
 478 It should be noted that measured NO concentration was used to calculate the P<sub>NO-OH</sub>.  
 479 Besides vehicle emission, power plant and industries also contribute NO emission. 40 %  
 480 of NO<sub>x</sub> was from vehicle emission according to the emission inventory of NO<sub>x</sub> in  
 481 Beijing (He et al., 2002).

482 It should be noted that OH concentration was estimated based on  $J_{O1D}$  (Tan et al.,  
483 2019; Tan et al., 2018) or  $J_{O1D}$  and  $J_{NO2}$  (Li et al., 2018). As discussed in Section 3.2,  
484 HONO was an important primary OH source in the daytime. Unfortunately, it could not  
485 be parameterized for calculating OH concentration because the measured or modelled  
486 OH concentration was unavailable in this work. This might underestimate the early  
487 daytime OH concentration, subsequently, the contribution of homogeneous reaction of  
488 NO with OH to HONO source. This need to be further investigated in the future.

489 **Photolysis of nitrate.** A recent work reported the photolysis rate of nitrate ( $J_{nitrate}$ ) in  
490 ambient PM<sub>2.5</sub> at a solar zenith angle of 0° (Bao et al., 2018). The  $J_{nitrate}$  varied from  
491  $1.22 \times 10^{-5}$  to  $4.84 \times 10^{-4} \text{ s}^{-1}$  with the mean value of  $8.24 \times 10^{-5} \text{ s}^{-1}$ . These values were  
492 further normalized according to the zenith angle and UV light at our observation station  
493 to calculate the low limit, the upper limit and the middle  $J_{nitrate}$ . The time series of the  
494 measured nitrate concentration and the middle value of  $J_{nitrate}$  were shown in Fig. 1 and  
495 Fig. S7, respectively. Therefore, the corresponding daytime lower limit, the middle  
496 value and the upper limit of HONO from photolysis of nitrate were  $0.0011 \pm 0.0021$ -  
497  $0.096 \pm 0.092$ ,  $0.0072 \pm 0.0021$ - $0.66 \pm 0.092$  and  $0.042 \pm 0.082$ - $3.86 \pm 0.008 \text{ ppbv h}^{-1}$ ,  
498 respectively, calculated in the light of Eqs. (3) and (8).

499 **Heterogeneous reactions of NO<sub>2</sub> on aerosol and ground surface.** The production of  
500 HONO from heterogeneous reactions of NO<sub>2</sub> on aerosol surface was calculated  
501 according to Eqs. (3) and (5). The aerosol surface concentration was measured with a  
502 SMPS. The uptake coefficient ( $\gamma$ ) of NO<sub>2</sub> on different particles varied from  $5 \times 10^{-9}$  to  
503  $9.6 \times 10^{-6}$  (Ndour et al., 2009; Underwood et al., 2001; Underwood et al., 1999), while it

504 was recommended to be  $1.2 \times 10^{-8}$  (Crowley et al., 2010), which was used to calculate  
505 the  $P_{\text{aerosol}}$  in the base case. It has been found that the  $\gamma$  highly depends on the relative  
506 humidity (RH). The low limit bound of  $P_{\text{aerosol}}$  was calculated based on the RH  
507 dependent uptake coefficient of  $\text{NO}_2$  on kaolinite ( $\gamma_{\text{NO}_2} = 4.47 \times 10^{39} / (1.75 \times 10^{46} + 1.93$   
508  $\times 10^{45} \text{RH})$ ), while the upper limit of  $P_{\text{aerosol}}$  was calculated according to the RH  
509 dependent  $\gamma$  on hematite ( $\gamma_{\text{NO}_2} = 4.46 \times 10^{39} / (6.73 \times 10^{44} + 3.48 \times 10^{44} \text{RH})$ ) (Liu et al.,  
510 2015). Heterogeneous reaction of  $\text{NO}_2$  on black carbon (BC) was also considered in the  
511 night. The surface area concentration of BC was calculated according to its specific  
512 area ( $87 \text{ m}^2 \text{ g}^{-1}$ ) (Su et al., 2018) and the measured mass concentration. The  $\gamma_{\text{NO}_2}$  on BC  
513 is  $1.17 \times 10^{-5}$ , with a HONO yield of 0.8 (Han et al., 2013). The light enhanced uptake  $\gamma$   
514 of  $\text{NO}_2$  ( $1.9 \times 10^{-6}$ ) on mineral dust was further parameterized (Ndour et al., 2008) after  
515 normalized to the solar radiation intensity in Beijing.

516 The contribution of heterogeneous reaction of  $\text{NO}_2$  on ground surface was  
517 calculated similar to that on mineral dust. The same kinetics for heterogeneous reaction  
518 of  $\text{NO}_2$  on aerosol surface were used to calculate the nighttime contribution of ground  
519 surface. A recent work observed a significant enhancement of  $\text{NO}_2$  and HONO  
520 formation by UV light on the real urban grime (Liu et al., 2019a). Thus, RH dependent  
521 kinetic data measured on urban grime ( $\gamma_{\text{NO}_2} = 7.4 \times 10^{-7} + 5.5 \times 10^{-8} \text{RH}$ ) was used to  
522 calculate the daytime upper limit for heterogeneous uptake of  $\text{NO}_2$  on the ground  
523 surface. The  $A_s$  of aerosols varied from  $1 \times 10^{-4}$  to  $4.8 \times 10^{-3} \text{ m}^{-1}$  with a mean value of  
524  $1.4 \pm 0.5 \times 10^{-3} \text{ m}^{-1}$  during pollution events. This value is comparable with that used in  
525 modeling studies (Zhang et al., 2016; Aumont et al., 2003). The  $A_s$  of ground surface

526 which was calculated according to Eq. (6) and (7) varied from  $1.5 \times 10^{-3}$  to  $3.85 \times 10^{-2} \text{ m}^{-1}$   
527  $^1$  with a mean value of  $1.3 \pm 0.9 \times 10^{-2} \text{ m}^{-1}$  during pollution events. The surface roughness  
528 was 3.85 calculated according to Eq. (7). The  $Y_{\text{HONO}}$  was set to 0.5 because of the  
529 hydrolysis reaction of  $\text{NO}_2$  (Liu et al., 2015), while it was 0.8 for light enhanced  
530 reaction (Liu et al., 2019a; Ndour et al., 2008) and on BC (Han et al., 2013).

531 The lower limit, the middle value and the upper limit of  $P_{\text{aerosol}}$  were  $0.038 \pm 0.030$ -  
532  $0.087 \pm 0.072$ ,  $0.038 \pm 0.030$ - $0.088 \pm 0.072$  and  $0.041 \pm 0.032$  -  $0.092 \pm 0.073$  ppbv  $\text{h}^{-1}$ ,  
533 respectively. The corresponding values were  $0.00027 \pm 0.00017$ - $0.0020 \pm 0.0012$ ,  
534  $0.0014 \pm 0.00095$ - $0.0089 \pm 0.006$  and  $0.0025 \pm 0.0023$ - $0.060 \pm 0.032$  ppbv  $\text{h}^{-1}$  for  $P_{\text{ground}}$ .  
535 Although the  $A_s$  of ground surface was higher than that of aerosol, the larger  $\gamma_{\text{NO}_2}$   
536 ( $1.17 \times 10^{-5}$ ) on soot particles than that on other aerosols and ground surface led to a  
537 larger production rate of HONO in this work. The  $P_{\text{aerosol}}$  calculated in this work was  
538 on the same orders as soil emission, while it was lower than the  $P_{\text{aerosol}}$  estimated by  
539 Huang et al. (Huang et al., 2017b) because different calculation methods have been  
540 used. In their work, the production rate of HONO was estimated based on the  
541 conversion rate (Huang et al., 2017b), whilst it was calculated based on the measured  
542 aerosol surface area concentration and uptake coefficient of  $\text{NO}_2$  on different particles  
543 in this work.

544 It should be pointed out that HONO production from heterogeneous reaction of  
545  $\text{NO}_2$  on both aerosol and ground surface greatly depend on the  $\gamma_{\text{NO}_2, \text{BET}}$  and  $A_s$ . The  $A_s$   
546 of aerosols was comparable with the modeling input. However, the small nighttime  $\gamma_{\text{NO}_2, \text{BET}}$   
547 ( $10^{-8}$  -  $10^{-7}$ ) on dust were used in this work rather than the  $\gamma_{\text{NO}_2, \text{BET}}$  ( $1 \times 10^{-6}$ ) used in

548 modelling studies (Zhang et al., 2016; Aumont et al., 2003; Gall et al., 2016). This leads  
549 to a lower production rate of HONO from heterogeneous reaction of NO<sub>2</sub> on aerosols.  
550 As for heterogeneous reaction of NO<sub>2</sub> on ground surface, besides the small  $\gamma_{\text{NO}_2, \text{BET}}$   
551 used in this work, the  $A_s$  of ground surface (0.0015 to 0.0385 m<sup>-1</sup>) calculated using the  
552 surface roughness and PBL height was also significantly lower than the fixed value of  
553 0.3 m<sup>-1</sup> in modeling studies that might overestimate the contribution of HONO  
554 production from heterogeneous reaction of NO<sub>2</sub> on ground surface. It should be noted  
555 that the initial uptake coefficient ( $\gamma_{\text{ini}}$ ) was parameterized in this work. This will  
556 overestimate the contribution of heterogeneous reaction of NO<sub>2</sub> to HONO source  
557 because the steady-state uptake coefficient is usually one order of magnitude lower than  
558  $\gamma_{\text{ini}}$  (Han et al., 2013; Liu et al., 2015). These results mean that heterogeneous reaction  
559 might not be a major HONO source. This is consistent with a recent work that found  
560 heterogeneous reaction being unimportant when compared with traffic emission during  
561 haze events in winter in Beijing (Zhang et al., 2019d).

562 **Sinks of HONO.** The loss rates of HONO by photolysis ( $L_{\text{photolysis}}$ ), homogeneous  
563 reaction with OH radicals ( $L_{\text{HONO-OH}}$ ) and dry deposition were calculated according to  
564 Eqs. (9)-(11). The daytime  $J_{\text{HONO}}$  varied from  $1.71 \times 10^{-5}$  to  $1.13 \times 10^{-3}$  s<sup>-1</sup> on polluted  
565 days in winter, while it was in the range of  $5.89 \times 10^{-5}$  to  $1.53 \times 10^{-3}$  s<sup>-1</sup> from April to June.  
566 These values are comparable to modelling results ( $3.9 \times 10^{-5}$ - $1.8 \times 10^{-3}$  s<sup>-1</sup>) (Gall et al.,  
567 2016). The daytime  $L_{\text{photolysis}}$  were in the range of 0.03-5.23 ppb h<sup>-1</sup> and 0.25-7.10 ppb  
568 h<sup>-1</sup> in winter and the rest months, respectively. It was the major sink of HONO in the  
569 daytime. The  $L_{\text{HONO-OH}}$  varied from 0.0049 to 0.069 ppbv h<sup>-1</sup> in winter using the  $k_{\text{HONO-OH}}$ .



570  $\text{OH}$  of  $6 \times 10^{-12} \text{ cm}^3 \text{ molecule}^{-1} \text{ s}^{-1}$  (Atkinson et al., 2004) and the middle value of  $\text{OH}$   
571 concentrations. It was from 0.0050 to 0.085 ppbv  $\text{h}^{-1}$  from April to June. The  $L_{\text{deposition}}$   
572 was in the range of 0.004-0.056 ppbv  $\text{h}^{-1}$  in winter and 0.004-0.030 ppbv  $\text{h}^{-1}$  from April  
573 to June, calculated according to Eq. (11).

574 As pointed in Section 2.2, vertical transport by advection is an important nocturnal  
575 sink of HONO (Gall et al., 2016). In this work, the vertical distribution of HONO  
576 concentration is unavailable. Recently, Meng et al. (2019) measured the vertical  
577 distribution of HONO in Beijing in December, 2016. The concentration of HONO  
578 showed nearly flat profiles from ground level to 240 m in pollution events after sunset,  
579 while negative profiles of HONO were observed in pollution events during night (Meng  
580 et al., 2019). The nighttime concentration gradient was  $0.0047 \pm 0.0025 \text{ ppb m}^{-1}$  derived  
581 from the nighttime dataset (Meng et al., 2019). In the daytime, we assume a zero  
582 concentration gradient. On the other hand, the eddy diffusivity of heat in urban  
583 environment was measured in New Delhi, Indian (Yadav et al., 2003). Using their  
584 dataset with the wind speed lower than  $2.0 \text{ m s}^{-1}$ , we derived the relationship between  
585 the  $K_h$  and the wind speed (WS) ( $K_h = 0.9389 \times \text{WS} - 0.3374 \text{ m}^2 \text{ s}^{-1}$ ). The nighttime  $T_{\text{vertical}}$   
586 changed from 0.15 to 0.37 ppbv  $\text{h}^{-1}$  in winter, while it was from 0.12 to 0.68 ppbv  $\text{h}^{-1}$   
587 according to Eq. (12) from April to June. Because the wind speed was usually lower  
588 than  $1.0 \text{ m s}^{-1}$  in pollution events (Fig. S6), horizontal transport should have little  
589 influence on the daytime sources or sinks of HONO because of the short lifetime of  
590 HONO (Spataro and Ianniello, 2014). In the night, 79 % of the wind speed was lower  
591 than  $1.0 \text{ m s}^{-1}$  in winter, thus the air masses from suburban areas should have influence

592 on the sources and sinks of HONO in Beijing. If the HONO concentration at  
593 background was zero, the vertical and horizontal transport rate of HONO varied from  
594 0.17 to 0.61 ppbv h<sup>-1</sup> which is calculated in the light of Eq. (13) on haze days in winter  
595 and from 0.15 to 0.74 ppbv h<sup>-1</sup> in pollution events from April to June. These values  
596 were higher than that calculated according to Eq. (12). Because the background HONO  
597 concentration was unavailable, we only considered the nighttime transport calculated  
598 according to Eq. (12) in the following section.

599 **Comparison among different HONO sources.** Fig. 3 summarizes the diurnal patterns  
600 of each sources with different parameterizations during the pollution events from  
601 February to March. The black dots and lines mean the middle values, while the shadow  
602 indicates the corresponding lower bound and upper bound. In the nighttime, vehicle  
603 and soil emission, and homogeneous reaction between NO and OH were the important  
604 sources of HONO. In the daytime, however, photolysis of nitrate and homogeneous  
605 reaction between NO and OH dominated the sources of HONO. Heterogeneous  
606 reactions of NO<sub>2</sub> on aerosol surface and ground surfaces were not the major HONO  
607 source during night unlike the modelled results (Zhang et al., 2016; Aumont et al., 2003).

608 Fig. 4A-F shows the HONO budget estimated using the middle values among these  
609 parameters during the polluted events. The mean production rate of HONO varied in  
610 the range of 0.25 - 1.81 ppbv h<sup>-1</sup> from these identified sources, while the corresponding  
611 loss rate was from 0.21 to 2.34 ppbv h<sup>-1</sup> during the polluted events in winter. The main  
612 loss of HONO was the photolysis during the daytime (1.74± 0.44 ppbv h<sup>-1</sup>), whereas it  
613 was vertical transport in the nighttime (0.28±0.08 ppbv h<sup>-1</sup>). Direct emission from

614 vehicles exhaust was the largest nighttime source of HONO ( $0.23\pm 0.06$  ppbv  $h^{-1}$ ),  
615 followed by heterogeneous reactions of  $NO_2$  on the ground surface ( $0.07\pm 0.01$  ppbv  $h^{-1}$ ),  
616 homogeneous reaction between NO and OH ( $0.04\pm 0.01$  ppbv  $h^{-1}$ ), emission from  
617 soil ( $0.014\pm 0.005$  ppbv  $h^{-1}$ ), and heterogeneous reactions of  $NO_2$  on aerosol surface  
618 ( $0.006\pm 0.002$  ppbv  $h^{-1}$ ).  $P_{NO-OH}$  and  $P_{nitrate}$  dominated the daytime HONO production,  
619 with daytime mean values of  $0.49\pm 0.35$  ppbv  $h^{-1}$  and  $0.34\pm 0.23$  ppbv  $h^{-1}$ , respectively.  
620 As shown in Fig. 4, these six sources still underestimated the daytime sources of HONO.  
621 The  $P_{unknown}$  was  $0.20\pm 0.24$  ppbv  $h^{-1}$  in February and March, while it was  $0.50\pm 0.24$   
622 ppbv  $h^{-1}$  from April to June.

623 The  $E_{vehicle}$  contributed  $57.0\pm 10.0\%$  and  $51.5\pm 20.1\%$  to the nighttime HONO  
624 sources from February to March and the rest months, respectively, even when the  
625  $P_{unknown}$  was taken into consideration. The relative contribution of daytime  $E_{vehicle}$   
626 decreased to  $15.2\pm 15.4\%$  in winter and  $9.7\pm 7.8\%$  from April to June. Thus, the daily  
627 mean fraction of the  $E_{vehicle}$  was  $39.6\pm 24.3\%$  and  $34.0\pm 24.3\%$  from February to March  
628 and from April to June, respectively. This means that the  $E_{vehicle}$  dominates the nighttime  
629 HONO source during the polluted events in Beijing, which is consistent with the  
630 previous result that vehicle emission was the major nighttime or haze day HONO source  
631 ( $51.1\%$  -  $52\%$ ) in Beijing (Zhang et al., 2019c; Meng et al., 2019). As pointed out in  
632 Section 3.3,  $E_{vehicle}$  was calculated based on the  $NO_x$  inventory from vehicle sector. On  
633 the other hand, NO is prone to be quickly converted to  $NO_2$  and  $NO_z$  (including HONO,  
634  $HNO_3$ ,  $N_2O_5$ , PAN and organonitrate etc) by  $O_3$ ,  $HO_2$ ,  $RO_2$  and OH in the atmosphere.  
635 It is reasonable to assume that local traffic emission dominates the ambient NO source

636 in the urban environment. Thus, homogeneous reaction between NO and OH in the  
637 atmosphere could also be related to vehicle exhaust. As shown in Fig.3, although the  
638 diurnal curve of  $P_{\text{NO-OH}}$  coincided well with that of OH concentration (Fig. S10), which  
639 means the  $P_{\text{NO-OH}}$  should be mainly determined by OH concentration, the  $P_{\text{NO-OH}}$  should  
640 still reflect the indirect contribution of traffic related emission to HONO source because  
641 the ambient NO concentration was used to calculate the  $P_{\text{NO-OH}}$ . Traffic-related HONO  
642 sources ( $E_{\text{vehicles}} + P_{\text{NO-OH}}$ ) might contribute  $57.8 \pm 15.8\%$  and  $48.6 \pm 15.9\%$  to the daily  
643 HONO source in winter and the rest months, respectively. Even if 40 % of  $\text{NO}_x$  was  
644 from vehicle exhaust in Beijing (He et al., 2002), traffic-related source ( $E_{\text{vehicles}} +$   
645  $0.4P_{\text{NO-OH}}$ ) might still contribute  $46.9 \pm 20.5\%$  in winter and  $39.9 \pm 20.5\%$  from April to  
646 June to the corresponding daily HONO source. The contribution of traffic-related  
647 source was still an important daytime source of HONO ( $43.9 \pm 10.6\%$  for  $E_{\text{vehicles}} + P_{\text{NO-OH}}$   
648 OH, and  $26.7 \pm 12.4\%$  for  $E_{\text{vehicles}} + 0.4P_{\text{NO-OH}}$ ) on polluted days in winter.

649 As shown in Fig. 3, uncertainties existed when calculating each HONO source. To  
650 further understand the role of traffic emission, we also estimated the lower limit of the  
651 traffic-related contribution as follows: 1) the lower limit of  $E_{\text{vehicle}}$  was obtained by  
652 using the lowest reported emission ratio of HONO/ $\text{NO}_x$  from vehicles (0.18%) (Liu et  
653 al., 2017d) rather than 1.17%, which was the empirical value calculated based on the  
654 field measurement in Fig. S7; 2) the lower limit for homogeneous reaction between NO  
655 and OH radical was calculated according to the method by Li et al. (2018); 3) the upper  
656 limit of the emission rate from soil was estimated using the emission flux of HONO  
657 with low water content (Oswald et al., 2013); 4) the upper limit of HONO production

658 rate from heterogeneous reaction of NO<sub>2</sub> on the aerosol was calculated using the large  
659 RH-dependent uptake coefficient of NO<sub>2</sub> on hematite (Liu et al., 2015) rather the value  
660 recommended by Crowley et al. (Crowley et al., 2010); 5) the upper limit for  
661 heterogeneous reaction on ground surface was calculated using the RH-dependent  
662 kinetic data measured on urban grime (Liu et al., 2019a). As shown in Fig. 5, traffic-  
663 related source ( $E_{\text{vehicles}} + P_{\text{NO-OH}}$ ) contributed  $25.7 \pm 15.8$  % to the **daily HONO sources**  
664 **in winter** if all NO was assumed to be dominated by local traffic emission, while it was  
665  $14.5 \pm 15.8$  % when 40 % of NO was considered as local traffic emission (He et al.,  
666 2002). Under this circumstance, the daytime  $P_{\text{unknown}}$  of HONO in winter increased to  
667  $0.83 \pm 0.36$  ppbv h<sup>-1</sup>, which was corresponding to  $58.1 \pm 8.6$  % of the HONO source. This  
668 means these assumptions might underestimate the contribution of the HONO sources.  
669 In addition,  $P_{\text{ground}}$ ,  $P_{\text{aerosol}}$  and  $P_{\text{nitrate}}$  could be also partially related to traffic emission  
670 of NO<sub>x</sub> (Lee et al., 2016; Tan et al., 2017). These results mean that the contribution of  
671 traffic-related emission might be larger than our estimation in this work. Therefore, our  
672 work at least suggests that traffic related emission should be a very important HONO  
673 source in winter Beijing although more work is required based on comprehensive  
674 modelling studies.

#### 675 **4. Conclusions and atmospheric implications.**

676 In this work, the promotion effect of HONO on aerosol mass formation in polluted  
677 events was observed based on the good correlation between the growth of OA and  
678 nitrate mass concentration and the consumed HONO from early morning to noon during  
679 the polluted days in winter. This promotion effect could be related to OH production

680 from photolysis of HONO on aerosol formation followed by oxidation process of the  
681 corresponding precursors. Our observation supports well the recent modelling studies  
682 that HONO may significantly promote secondary aerosol mass formation (Zhang et al.,  
683 2019a;Zhang et al., 2019c;Xing et al., 2019;An et al., 2013). Based on **budget analysis**  
684 calculations, traffic-related sources (direction emission and conversion of NO from  
685 vehicle emission) was found to be an important contributor to HONO source during  
686 polluted days in winter in Beijing. This means that HONO from the traffic-related  
687 sources can have an important role in aerosol mass formation in the atmosphere.

688       Vehicle population in China is increasing very quickly (Liu et al., 2017b;Wang et  
689 al., 2011). Thus, the negative influences of the vehicle emission on air quality will  
690 increase especially in populous metropolitan areas (Yang et al., 2019;Guo et al., 2020),  
691 such as Beijing and Shanghai, if targeted pollution control technologies are not applied.  
692 It has been estimated that the vehicles emission accounted for over 40% of total urban  
693 NO<sub>x</sub> emissions in Beijing (He et al., 2002). In the atmosphere, NO<sub>x</sub> involves very  
694 complicated reaction network, from which finally leads to aerosol mass formation and  
695 production of ozone in VOC limited environment. At the same time, reactions of NO<sub>x</sub>  
696 also leads to some reactive NO<sub>z</sub> species (Seinfeld and Pandis, 2006). In particular,  
697 HONO is an important precursor of OH, which governs the conversion of primary  
698 pollutants to secondary pollutants in the atmosphere. Besides **indirect production** of  
699 HONO from NO, the vehicles also directly emits HONO as discussed in this work.  
700 Even if the low limit of emission factor was used to calculating the HONO source from  
701 the vehicles, the traffic-related emission can still be an important source of HONO in

702 winter Beijing. Therefore, this work implies that mitigation of HONO and NO<sub>x</sub>  
703 emission from vehicles might be an effective way to reduce secondary aerosol mass  
704 formation and can have a positive effect on severe haze events in wintertime Beijing.

705 It should be pointed out that we only considered O<sub>3</sub> and HONO when discussing  
706 the sources of OH. Other sources such as HO<sub>2</sub> (and RO<sub>2</sub>) with NO, ozonolysis of  
707 alkenes and photolysis of OVOCs might also contribute to OH radicals in the  
708 atmosphere (Tan et al., 2018). In the future it will be vital to comprehensively analyze  
709 OH sources and to quantify the role of HONO in secondary aerosol mass formation  
710 although photolysis of HONO is the major OH source in winter. On the other hand, as  
711 discussed in Section 3.3, uncertainties about the HONO budget might originate from  
712 the emission factors, OH concentration, and reaction kinetics and so on. **The source of**  
713 **HONO from vehicles was calculated based on the emission inventories, which should**  
714 **have a significant bias (Squires et al., 2020). For example, the emission flux of NO<sub>x</sub>**  
715 **calculated using the emission inventory from Yang et al. (2019) is as 2.4±0.5 times as**  
716 **the reported emission flux reported by Squires et al. (2020).** To take the next step, it is  
717 required to measure the emission factors from vehicle exhaust under real road  
718 conditions in the future. When calculating the OH concentration, the factor between  
719 OH concentration and  $J_{\text{O}1\text{D}}$  might vary over locations and seasons due to different  
720 NO<sub>x</sub>/VOCs ratio (Holland et al., 2003). Direct measurements of OH concentration  
721 would be helpful for decreasing the uncertainty of both OH sources and HONO budget  
722 analysis. Finally, it is necessary to quantify the contribution of traffic-related source of  
723 HONO on secondary aerosol formation based on modelling studies in the future.

724

725 *Data availability.* The experimental data are available upon request to the  
726 corresponding authors.

727

728 *Supplement.* The supplement related to this article is available online at:

729

### 730 **Author information**

731 *Author contributions.* YL, WW and MK designed the experiments. YL wrote the paper  
732 and performed HONO budget analysis. YZ, CL, WW, YC, MG and XW carried out  
733 HONO measurement. ZF, FZ, JC, WD and KD did aerosol composition measurements.  
734 BC and JK did particle size measurements. YW, BH and YW analyzed meteorological  
735 data analysis. CY, FB, JK, TP, HH, MG and MK revised the manuscript.

736

### 737 **Acknowledgements:**

738 This research was financially supported by the National Natural Science Foundation of  
739 China (41877306), the Ministry of Science and Technology of the People's Republic of  
740 China (2019YFC0214701), Academy of Finland via Center of Excellence in  
741 Atmospheric Sciences (272041, 316114, and 315203) and European Research Council  
742 vShandong University via ATM-GTP 266 (742206), the Strategic Priority Research  
743 Program of Chinese Academy of Sciences and Beijing University of Chemical  
744 Technology.

745



746 **References:**

- 747 Alicke, B., Geyer, A., Hofzumahaus, A., Holland, F., Konrad, S., Patz, H. W., Schafer, J., Stutz, J., Volz-  
748 Thomas, A., and Platt, U.: OH formation by HONO photolysis during the BERLIOZ experiment, *Journal*  
749 *of Geophysical Research-Atmospheres*, 108, 17, 10.1029/2001jd000579, 2003.
- 750 An, J., Li, Y., Chen, Y., Li, J., Qu, Y., and Tang, Y.: Enhancements of major aerosol components due to  
751 additional HONO sources in the North China Plain and implications for visibility and haze, *Adv. Atmos.*  
752 *Sci.*, 30, 57-66, 10.1007/s00376-012-2016-9, 2013.
- 753 An, Z., Huang, R.-J., Zhang, R., Tie, X., Li, G., Cao, J., Zhou, W., Shi, Z., Han, Y., Gu, Z., and Ji, Y.:  
754 Severe haze in northern China: A synergy of anthropogenic emissions and atmospheric processes, *Proc.*  
755 *Natl. Acad. Sci. USA*, 116, 8657-8666, 10.1073/pnas.1900125116, 2019.
- 756 Atkinson, R., and Arey, J.: Atmospheric Degradation of Volatile Organic Compounds, *Chem. Rev.*, 103,  
757 4605-4638, doi: 10.1021/cr0206420, 2003.
- 758 Atkinson, R., Baulch, D. L., Cox, R. A., Crowley, J. N., Hampson, R. F., Hynes, R. G., Jenkin, M. E.,  
759 Rossi, M. J., and Troe, J.: Evaluated kinetic and photochemical data for atmospheric chemistry: Volume  
760 I - gas phase reactions of Ox, HOx, NOx and SOx species, *Atmos. Chem. Phys.*, 4, 1461-1738,  
761 10.5194/acp-4-1461-2004, 2004.
- 762 Aumont, B., Chervier, F., and Laval, S.: Contribution of HONO sources to the NOx/HOx/O3 chemistry  
763 in the polluted boundary layer, *Atmos. Environ.*, 37, 487-498, [https://doi.org/10.1016/S1352-](https://doi.org/10.1016/S1352-2310(02)00920-2)  
764 [2310\(02\)00920-2](https://doi.org/10.1016/S1352-2310(02)00920-2), 2003.
- 765 Bao, F., Li, M., Zhang, Y., Chen, C., and Zhao, J.: Photochemical Aging of Beijing Urban PM2.5: HONO  
766 Production, *Environ. Sci. Technol.*, 52, 6309-6316, 10.1021/acs.est.8b00538, 2018.
- 767 Bianchi, F., Kurtén, T., Riva, M., Mohr, C., Rissanen, M. P., Roldin, P., Berndt, T., Crouse, J. D.,  
768 Wennberg, P. O., Mentel, T. F., Wildt, J., Junninen, H., Jokinen, T., Kulmala, M., Worsnop, D. R.,  
769 Thornton, J. A., Donahue, N., Kjaergaard, H. G., and Ehn, M.: Highly Oxygenated Organic Molecules  
770 (HOM) from Gas-Phase Autoxidation Involving Peroxy Radicals: A Key Contributor to Atmospheric  
771 Aerosol, *Chemical Reviews*, 119, 3472-3509, 10.1021/acs.chemrev.8b00395, 2019.
- 772 Cheng, F., Wang, C., Wang, J., Tang, F., and Xi, X.: Trend analysis of building height and total floor  
773 space in Beijing, China using ICESat/GLAS data, *International Journal of Remote Sensing.*, 32, 8823-  
774 8835, 2011.
- 775 Cheng, Y., Zheng, G., Wei, C., Mu, Q., Zheng, B., Wang, Z., Gao, M., Zhang, Q., He, K., Carmichael,  
776 G., Poschl, U., and Su, H.: Reactive nitrogen chemistry in aerosol water as a source of sulfate during  
777 haze events in China, *Sci. Adv.*, 2, 10.1126/sciadv.1601530, 2016.
- 778 Cho, M.-H., Niles, A., uili Huang, Inglese, J., Austin, C. P., Riss, T., and Xia, M.: A bioluminescent  
779 cytotoxicity assay for assessment of membrane integrity using a proteolytic biomarker, *Toxicol. In Vitro.*,  
780 22, 1099-1106, 2008.
- 781 Crowley, J. N., Ammann, M., Cox, R. A., Hynes, R. G., Jenkin, M. E., Mellouki, A., Rossi, M. J., Troe,  
782 J., and Wallington, T. J.: Evaluated kinetic and photochemical data for atmospheric chemistry: Volume  
783 V – heterogeneous reactions on solid substrates, *Atmos. Chem. Phys.*, 10, 9059-9223, doi: 10.5194/acp-  
784 10-9059-2010, 2010.
- 785 Cui, L., Li, R., Zhang, Y., Meng, Y., Fu, H., and Chen, J.: An observational study of nitrous acid (HONO)  
786 in Shanghai, China: The aerosol impact on HONO formation during the haze episodes, *Sci. Total*  
787 *Environ.*, 630, 1057-1070, 10.1016/j.scitotenv.2018.02.063, 2018.
- 788 Czader, B. H., Choi, Y., Li, X., Alvarez, S., and Lefer, B.: Impact of updated traffic emissions on HONO

789 mixing ratios simulated for urban site in Houston, Texas, *Atmos. Chem. Phys.*, 15, 1253-1263,  
790 10.5194/acp-15-1253-2015, 2015.

791 Dillon, M. B., Lamanna, M. S., Schade, G. W., Goldstein, A. H., and Cohen, R. C.: Chemical evolution  
792 of the Sacramento urban plume: Transport and oxidation, *J. Geophys. Res.- Atmos.*, 107, ACH 3-1-ACH  
793 3-15, 10.1029/2001jd000969, 2002.

794 Fu, G. Q., Xu, W. Y., Yang, R. F., Li, J. B., and Zhao, C. S.: The distribution and trends of fog and haze  
795 in the North China Plain over the past 30 years, *Atmos. Chem. Phys.*, 14, 11949-11958, 10.5194/acp-14-  
796 11949-2014, 2014.

797 Gall, E. T., Griffin, R. J., Steiner, A. L., Dibb, J., Scheuer, E., Gong, L., Rutter, A. P., Cevik, B. K., Kim,  
798 S., Lefer, B., and Flynn, J.: Evaluation of nitrous acid sources and sinks in urban outflow, *Atmos.*  
799 *Environ.*, 127, 272-282, <https://doi.org/10.1016/j.atmosenv.2015.12.044>, 2016.

800 Gao, W., Tan, G., Hong, Y., Li, M., Nian, H., Guo, C., Huang, Z., Fu, Z., Dong, J., Xu, X., Cheng, P., and  
801 Zhou, Z.: Development of portable single photon ionization time-of-flight mass spectrometer combined  
802 with membrane inlet, *International Journal of Mass Spectrometry*, 334, 8-12,  
803 <https://doi.org/10.1016/j.ijms.2012.09.003>, 2013.

804 Guo, S., Hu, M., Zamora, M. L., Peng, J., Shang, D., Zheng, J., Du, Z., Wu, Z., Shao, M., Zeng, L.,  
805 Molina, M. J., and Zhang, R.: Elucidating severe urban haze formation in China, *Proc. Natl. Acad. Sci.*  
806 *USA*, 111, 17373-17378, 10.1073/pnas.1419604111, 2014.

807 Guo, S., Hu, M., Peng, J., Wu, Z., Zamora, M. L., Shang, D., Du, Z., Zheng, J., Fang, X., Tang, R., Wu,  
808 Y., Zeng, L., Shuai, S., Zhang, W., Wang, Y., Ji, Y., Li, Y., Zhang, A. L., Wang, W., Zhang, F., Zhao, J.,  
809 Gong, X., Wang, C., Molina, M. J., and Zhang, R.: Remarkable nucleation and growth of ultrafine  
810 particles from vehicular exhaust, *Proc. Natl. Acad. Sci. USA*, 117 3427-3432, 10.1073/pnas.1916366117,  
811 2020.

812 Hallquist, M., Wenger, J. C., Baltensperger, U., Rudich, Y., Simpson, D., Claeys, M., Dommen, J.,  
813 Donahue, N. M., George, C., Goldstein, A. H., Hamilton, J. F., Herrmann, H., Hoffmann, T., Iinuma, Y.,  
814 Jang, M., Jenkin, M. E., Jimenez, J. L., Kiendler-Scharr, A., Maenhaut, W., McFiggans, G., Mentel, T.  
815 F., Monod, A., Prévôt, A. S. H., Seinfeld, J. H., Surratt, J. D., Szmigielski, R., and Wildt, J.: The formation,  
816 properties and impact of secondary organic aerosol: current and emerging issues, *Atmos. Chem. Phys.*,  
817 9, 5155-5236, 10.5194/acp-9-5155-2009, 2009.

818 Han, C., Liu, Y., and He, H.: Role of Organic Carbon in Heterogeneous Reaction of NO<sub>2</sub> with Soot,  
819 *Environ. Sci Technol.*, 47, 3174-3181, 10.1021/es304468n, 2013.

820 Han, X., Zhang, M. G., Skorokhod, A., and Kou, X. X.: Modeling dry deposition of reactive nitrogen in  
821 China with RAMS-CMAQ, *Atmos. Environ.*, 166, 47-61, 10.1016/j.atmosenv.2017.07.015, 2017.

822 He, H., Wang, Y., Ma, Q., Ma, J., Chu, B., Ji, D., Tang, G., Liu, C., Zhang, H., and Hao, J.: Mineral dust  
823 and NO<sub>x</sub> promote the conversion of SO<sub>2</sub> to sulfate in heavy pollution days, *Sci. Rep.*, 4,  
824 10.1038/srep04172, 2014.

825 He, K., Huo, H., and Zhang, Q.: Urban air pollution in China: current status, characteristics, and progress,  
826 *Annual Review of Energy Environment* 27, 397-431, 2002.

827 He, P. Z., Alexander, B., Geng, L., Chi, X. Y., Fan, S. D., Zhan, H. C., Kang, H., Zheng, G. J., Cheng, Y.  
828 F., Su, H., Liu, C., and Xie, Z. Q.: Isotopic constraints on heterogeneous sulfate production in Beijing  
829 haze, *Atmos. Chem. Phys.*, 18, 5515-5528, 10.5194/acp-18-5515-2018, 2018.

830 Hendrick, F., Muller, J. F., Clemer, K., Wang, P., De Maziere, M., Fayt, C., Gielen, C., Hermans, C., Ma,  
831 J. Z., Pinardi, G., Stavrou, T., Vlemmix, T., and Van Roozendaal, M.: Four years of ground-based  
832 MAX-DOAS observations of HONO and NO<sub>2</sub> in the Beijing area, *Atmos. Chem. Phys.*, 14, 765-781,

833 10.5194/acp-14-765-2014, 2014.

834 Holland, F., Hofzumahaus, A., Schafer, R., Kraus, A., and Patz, H. W.: Measurements of OH and HO<sub>2</sub>

835 radical concentrations and photolysis frequencies during BERLIOZ, *Journal of Geophysical Research-*

836 *Atmospheres*, 108, 22, 10.1029/2001jd001393, 2003.

837 Hou, S., Tong, S., Ge, M., and An, J.: Comparison of atmospheric nitrous acid during severe haze and

838 clean periods in Beijing, China, *Atmos. Environ.*, 124, 199-206,

839 <https://doi.org/10.1016/j.atmosenv.2015.06.023>, 2016.

840 Hu, M., Zhou, F., Shao, K., Zhang, Y., Tang, X., and Slanina, J.: Diurnal variations of aerosol chemical

841 compositions and related gaseous pollutants in Beijing and Guangzhou, *Journal of Environmental*

842 *Science and Health, Part A*, 37, 479-488, 10.1081/ESE-120003229, 2002.

843 Huang, H., Chen, Y., Clinton, N., Wang, J., Wang, X., Liu, C., Gong, P., Yang, J., Bai, Y., Zheng, Y., and

844 Zhu, Z.: Mapping major land cover dynamics in Beijing using all Landsat images in Google Earth Engine,

845 *Remote Sensing of Environment*, 202, 166-176, <https://doi.org/10.1016/j.rse.2017.02.021>, 2017a.

846 Huang, L., Zhao, Y., Li, H., and Chen, Z.: Kinetics of Heterogeneous Reaction of Sulfur Dioxide on

847 Authentic Mineral Dust: Effects of Relative Humidity and Hydrogen Peroxide, *Environ. Sci. Technol.*,

848 49, 10797-10805, 10.1021/acs.est.5b03930, 2015.

849 Huang, R.-J., Zhang, Y., Bozzetti, C., Ho, K.-F., Cao, J.-J., Han, Y., Daellenbach, K. R., Slowik, J. G.,

850 Platt, S. M., Canonaco, F., Zotter, P., Wolf, R., Pieber, S. M., Bruns, E. A., Crippa, M., Ciarelli, G.,

851 Piazzalunga, A., Schwikowski, M., Abbaszade, G., Schnelle-Kreis, J., Zimmermann, R., An, Z., Szidat,

852 S., Baltensperger, U., Haddad, I. E., and Prevot, A. S. H.: High secondary aerosol contribution to

853 particulate pollution during haze events in China, *Nature*, 514(7521), 218-222, 10.1038/nature13774,

854 2014.

855 Huang, R.-J., Yang, L., Cao, J., Wang, Q., Tie, X., Ho, K.-F., Shen, Z., Zhang, R., Li, G., Zhu, C., Zhang,

856 N., Dai, W., Zhou, J., Liu, S., Chen, Y., Chen, J., and O'Dowd, C. D.: Concentration and sources of

857 atmospheric nitrous acid (HONO) at an urban site in Western China, *Sci. Total Environ.*, 593, 165-172,

858 10.1016/j.scitotenv.2017.02.166, 2017b.

859 Kanaya, Y., Cao, R., Akimoto, H., Fukuda, M., Komazaki, Y., Yokouchi, Y., Koike, M., Tanimoto, H.,

860 Takegawa, N., and Kondo, a. Y.: Urban photochemistry in central Tokyo: 1. Observed and modeled OH

861 and HO<sub>2</sub> radical concentrations during the winter and summer of 2004, *J. Geophys. Res.- Atmos.*, 112,

862 10.1029/2007JD008670, 2007.

863 Kim, S., VandenBoer, T. C., Young, C. J., Riedel, T. P., Thornton, J. A., Swarthout, B., Sive, B., Lerner,

864 B., Gilman, J. B., Warneke, C., Roberts, J. M., Guenther, A., Wagner, N. L., Dubé, W. P., Williams, E.,

865 and Brown, S. S.: The primary and recycling sources of OH during the NACHTT-2011 campaign: HONO

866 as an important OH primary source in the wintertime, *J. Geophys. Res.- Atmos.*, 119, 6886-6896,

867 [doi:10.1002/2013JD019784](https://doi.org/10.1002/2013JD019784), 2014.

868 Kroll, J. H., and Seinfeld, J. H.: Chemistry of secondary organic aerosol: Formation and evolution of

869 low-volatility organics in the atmosphere, *Atmos. Environ.*, 42, 3593-3624, 2008.

870 Kulmala, M.: Build a global Earth observatory, *Nature*, 553, 21-23, 10.1038/d41586-017-08967-y, 2018.

871 Lang, J., Zhang, Y., Zhou, Y., Cheng, S., Chen, D., Guo, X., Chen, S., Li, X., Xing, X., and Wang, H.: Trends of PM<sub>2.5</sub> and Chemical Composition in Beijing, 2000-2015, *Aerosol Air Qual. Res.*, 17, 412-

872 425, 10.4209/aaqr.2016.07.0307, 2017.

874 Lee, J. D., Whalley, L. K., Heard, D. E., Stone, D., Dunmore, R. E., Hamilton, J. F., Young, D. E., Allan,

875 J. D., Laufs, S., and Kleffmann, J.: Detailed budget analysis of HONO in central London reveals a

876 missing daytime source, *Atmos. Chem. Phys.*, 16, 2747-2764, 10.5194/acp-16-2747-2016, 2016.

877 Lelieveld, J., Evans, J. S., Fnais, M., Giannadaki, D., and Pozzer, A.: The contribution of outdoor air  
878 pollution sources to premature mortality on a global scale, *Nature*, 525, 367-371, 10.1038/nature15371,  
879 2015.

880 Li, D., Xue, L., Wen, L., Wang, X., Chen, T., Mellouki, A., Chen, J., and Wang, W.: Characteristics and  
881 sources of nitrous acid in an urban atmosphere of northern China: Results from 1-yr continuous  
882 observations, *Atmos. Environ.*, 182, 296-306, <https://doi.org/10.1016/j.atmosenv.2018.03.033>, 2018.

883 Li, X., Brauers, T., H'aseler, R., Bohn, B., Fuchs, H., Hofzumahaus, A., Holland, F., Lou, S., Lu, K. D.,  
884 Rohrer, F., Hu, M., Zeng, L. M., Zhang, Y. H., Garland, R. M., Su, H., Nowak, A., Wiedensohler, A.,  
885 Takegawa, N., Shao, M., and Wahner, A.: Exploring the atmospheric chemistry of nitrous acid (HONO)  
886 at a rural site in Southern China, *Atmos. Chem. Phys.*, 12, 1497-1513, 2012.

887 Li, Z. Q., Guo, J. P., Ding, A. J., Liao, H., Liu, J. J., Sun, Y. L., Wang, T. J., Xue, H. W., Zhang, H. S.,  
888 and Zhu, B.: Aerosol and boundary-layer interactions and impact on air quality, *Natl. Sci. Rev.*, 4, 810-  
889 833, 10.1093/nsr/nwx117, 2017.

890 Liang, Y., Zha, Q., Wang, W., Cui, L., Lui, K. H., Ho, K. F., Wang, Z., Lee, S.-c., and Wang, T.: Revisiting  
891 nitrous acid (HONO) emission from on-road vehicles: A tunnel study with a mixed fleet, *J. Air Waste  
892 Manage. Assoc.*, 67, 797-805, 10.1080/10962247.2017.1293573, 2017.

893 Liggio, J., Li, S.-M., Hayden, K., Taha, Y. M., Stroud, C., Darlington, A., Drollette, B. D., Gordon, M.,  
894 Lee, P., Liu, P., Leithead, A., Moussa, S. G., Wang, D., O'Brien, J., Mittermeier, R. L., Brook, J. R., Lu,  
895 G., Staebler, R. M., Han, Y., Tokarek, T. W., Osthoff, H. D., Makar, P. A., Zhang, J., L. Plata, D., and  
896 Gentner, D. R.: Oil sands operations as a large source of secondary organic aerosols, *Nature*, 534, 91-94,  
897 10.1038/nature17646  
898 <http://www.nature.com/nature/journal/vaop/ncurrent/abs/nature17646.html#supplementary-information>,  
899 2016.

900 Liu, C., Ma, Z., Mu, Y., Liu, J., Zhang, C., Zhang, Y., Liu, P., and Zhang, H.: The levels, variation  
901 characteristics, and sources of atmospheric non-methane hydrocarbon compounds during wintertime in  
902 Beijing, China, *Atmos. Chem. Phys.*, 17, 10633-10649, 10.5194/acp-17-10633-2017, 2017a.

903 Liu, F., Beirle, S., Zhang, Q., van der A, R. J., Zheng, B., Tong, D., and He, K.: NO<sub>x</sub> emission trends  
904 over Chinese cities estimated from OMI observations during 2005 to 2015, *Atmos. Chem. Phys.*, 17,  
905 9261-9275, 10.5194/acp-17-9261-2017, 2017b.

906 Liu, J., Li, S., Mekic, M., Jiang, H., Zhou, W., Loisel, G., Song, W., Wang, X., and Gligorovski, S.:  
907 Photoenhanced Uptake of NO<sub>2</sub> and HONO Formation on Real Urban Grime, *Environmental Science &  
908 Technology Letters*, 6, 413-417, 10.1021/acs.estlett.9b00308, 2019a.

909 Liu, T., Gong, S., He, J., Yu, M., Wang, Q., Li, H., Liu, W., Zhang, J., Li, L., Wang, X., Li, S., Lu, Y., Du,  
910 H., Wang, Y., Zhou, C., Liu, H., and Zhao, Q.: Attributions of meteorological and emission factors to the  
911 2015 winter severe haze pollution episodes in China's Jing-Jin-Ji area, *Atmos. Chem. Phys.*, 17, 2971-  
912 2980, 10.5194/acp-17-2971-2017, 2017c.

913 Liu, Y., Han, C., Ma, J., Bao, X., and He, H.: Influence of relative humidity on heterogeneous kinetics of  
914 NO<sub>2</sub> on kaolin and hematite, *Phys. Chem. Chem. Phys.*, 17, 19424-19431, doi: 10.1039/C5CP02223A,  
915 2015.

916 Liu, Y., Lu, K., Ma, Y., Yang, X., Zhang, W., Wu, Y., Peng, J., Shuai, S., Hu, M., and Zhang, Y.: Direct  
917 emission of nitrous acid (HONO) from gasoline cars in China determined by vehicle chassis  
918 dynamometer experiments, *Atmos. Environ.*, 169, 89-96, 10.1016/j.atmosenv.2017.07.019, 2017d.

919 Liu, Y., Nie, W., Xu, Z., Wang, T., Wang, R., Li, Y., Wang, L., Chi, X., and Ding, A.: Contributions of  
920 different sources to nitrous acid (HONO) at the SORPES station in eastern China: results from one-year

921 continuous observation, *Atmos. Chem. Phys. Discuss.*, 2019, 1-47, 10.5194/acp-2019-219, 2019b.

922 Liu, Y. H., Lu, K. D., Li, X., Dong, H. B., Tan, Z. F., Wang, H. C., Zou, Q., Wu, Y. S., Zeng, L. M., Hu,  
923 M., Min, K. E., Kecorius, S., Wiedensohler, A., and Zhang, Y. H.: A Comprehensive Model Test of the  
924 HONO Sources Constrained to Field Measurements at Rural North China Plain, *Environ. Sci. Technol.*,  
925 53, 3517-3525, 10.1021/acs.est.8b06367, 2019c.

926 Meng, F., Qin, M., Tang, K., Duan, J., Fang, W., Liang, S., Ye, K., Xie, P., Sun, Y., Xie, C., Ye, C., Fu,  
927 P., Liu, J., and Liu, W.: High resolution vertical distribution and sources of HONO and NO<sub>2</sub> in the  
928 nocturnal boundary layer in urban Beijing, China, *Atmos. Chem. Phys. Discuss.*, 2019, 1-34,  
929 10.5194/acp-2019-613, 2019.

930 Meusel, H., Tamm, A., Kuhn, U., Wu, D., Leifke, A. L., Fiedler, S., Ruckteschler, N., Yordanova, P.,  
931 Lang-Yona, N., Pöhlker, M., Lelieveld, J., Hoffmann, T., Poeschl, U., Su, H., Weber, B., and Cheng, Y.:  
932 Emission of nitrous acid from soil and biological soil crusts represents an important source of HONO in  
933 the remote atmosphere in Cyprus, *Atmos. Chem. Phys.*, 18, 799-813, 10.5194/acp-18-799-2018, 2018.

934 Michoud, V., Colomb, A., Borbon, A., Miet, K., Beekmann, M., Camredon, M., Aumont, B., Perrier, S.,  
935 Zapf, P., Siour, G., Ait-Helal, W., Afif, C., Kukui, A., Furger, M., Dupont, J. C., Haeffelin, M., and  
936 Doussin, J. F.: Study of the unknown HONO daytime source at a European suburban site during the  
937 MEGAPOLI summer and winter field campaigns, *Atmos. Chem. Phys.*, 14, 2805-2822, 10.5194/acp-14-  
938 2805-2014, 2014.

939 Ndour, M., D'Anna, B., George, C., Ka, O., Balkanski, Y., K., J., S., and K., A., M.: Photoenhanced  
940 uptake of NO<sub>2</sub> on mineral dust: Laboratory experiments and model simulations, *Geophys. Res. Lett.*, 35,  
941 L05812. doi:05810.01029/02007GL032006, 2008.

942 Ndour, M., Nicolas, M., D'Anna, B., Ka, O., and George, C.: Photoreactivity of NO<sub>2</sub> on mineral dusts  
943 originating from different locations of the Sahara desert, *Phys. Chem. Chem. Phys.*, 11, 1312-1319, 2009.

944 Oswald, R., Behrendt, T., Ermel, M., Wu, D., Su, H., Cheng, Y., Breuninger, C., Moravek, A., Mougín,  
945 E., Delon, C., Loubet, B., Pommerening-Röser, A., Sörgel, M., Pöschl, U., Hoffmann, T., Andreae, M.  
946 O., Meixner, F. X., and Trebs, I.: HONO Emissions from Soil Bacteria as a Major Source of Atmospheric  
947 Reactive Nitrogen, *Science*, 341, 1233-1235, 10.1126/science.1242266, 2013.

948 Oswald, R., Ermel, M., Hens, K., Novelli, A., Ouwersloot, H. G., Paasonen, P., Petäjä, T., Sipilä, M.,  
949 Kerönen, P., Bäck, J., Königstedt, R., Hosaynali Beygi, Z., Fischer, H., Bohn, B., Kubistin, D., Harder,  
950 H., Martinez, M., Williams, J., Hoffmann, T., Trebs, I., and Sörgel, M.: A comparison of HONO budgets  
951 for two measurement heights at a field station within the boreal forest in Finland, *Atmos. Chem. Phys.*,  
952 15, 799-813, 10.5194/acp-15-799-2015, 2015.

953 Qin, M., Xie, P., Su, H., Gu, J., Peng, F., Li, S., Zeng, L., Liu, J., Liu, W., and Zhang, Y.: An observational  
954 study of the HONO-NO<sub>2</sub> coupling at an urban site in Guangzhou City, South China, *Atmos. Environ.*,  
955 43, 5731-5742, 10.1016/j.atmosenv.2009.08.017, 2009.

956 Ren, X., Brune, W. H., Mao, J., Mitchell, M. J., Leshner, R. L., Simpas, J. B., Metcalf, A. R., Schwab, J.  
957 J., Cai, C., Li, Y., Demerjian, K. L., Felton, H. D., Boynton, G., Adams, A., Perry, J., He, Y., Zhou, X.,  
958 and Hou, J.: Behavior of OH and HO<sub>2</sub> in the winter atmosphere in New York City, *Atmos. Environ.*, 40,  
959 252-263, <https://doi.org/10.1016/j.atmosenv.2005.11.073>, 2006.

960 Rohrer, F., Bohn, B., Brauers, T., Brüning, D., Johnen, F. J., Wahner, A., and Kleffmann, J.:  
961 Characterisation of the photolytic HONO-source in the atmosphere simulation chamber SAPHIR, *Atmos.*  
962 *Chem. Phys.*, 5, 2189-2201, 10.5194/acp-5-2189-2005, 2005.

963 Sangwan, M., and Zhu, L.: Role of Methyl-2-nitrophenol Photolysis as a Potential Source of OH Radicals  
964 in the Polluted Atmosphere: Implications from Laboratory Investigation, *J. Phys. Chem. A*, 122, 1861-

965 1872, 10.1021/acs.jpca.7b11235, 2018.  
 966 Seinfeld, J. H., and Pandis, S. N.: Atmospheric chemistry and physics: From air pollution to climate  
 967 change, Second ed., John Wiley and Sons, New Jersey, 2006.  
 968 Soergel, M., Regelin, E., Bozem, H., Diesch, J. M., Drewnick, F., Fischer, H., Harder, H., Held, A.,  
 969 Hosaynali-Beygi, Z., Martinez, M., and Zetzsch, C.: Quantification of the unknown HONO daytime  
 970 source and its relation to NO<sub>2</sub>, *Atmos. Chem. Phys.*, 11, 10433-10447, 10.5194/acp-11-10433-2011,  
 971 2011.  
 972 Spataro, F., Ianniello, A., Esposito, G., Allegrini, I., Zhu, T., and Hu, M.: Occurrence of atmospheric  
 973 nitrous acid in the urban area of Beijing (China), *Sci. Total Environ.*, 447, 210-224,  
 974 <https://doi.org/10.1016/j.scitotenv.2012.12.065>, 2013.  
 975 Spataro, F., and Ianniello, A.: Sources of atmospheric nitrous acid: State of the science, current research  
 976 needs, and future prospects, *J. Air Waste Manage. Assoc.*, 64, 1232-1250,  
 977 10.1080/10962247.2014.952846, 2014.  
 978 Squires, F. A., Nemitz, E., Langford, B., Wild, O., Drysdale, W. S., Acton, W. J. F., Fu, P., Grimmond, C.  
 979 S. B., Hamilton, J. F., Hewitt, C. N., Holloway, M., Kotthaus, S., Lee, J., Metzger, S., Pingingtha-Durden,  
 980 N., Shaw, M., Vaughan, A. R., Wang, X., Wu, R., Zhang, Q., and Zhang, Y.: Measurements of traffic  
 981 dominated pollutant emissions in a Chinese megacity, *Atmos. Chem. Phys. Discuss.*, 2020, 1-33,  
 982 10.5194/acp-2019-1105, 2020.  
 983 Stutz, J., Wong, K. W., and Tsai, C.: Field Observations of Daytime HONO Chemistry and Its Impact on  
 984 the OH Radical Budget, in: *Disposal of Dangerous Chemicals in Urban Areas and Mega Cities*,  
 985 Dordrecht, 2013, 1-14.  
 986 Su, H., Cheng, Y. F., Cheng, P., Zhang, Y. H., Dong, S., Zeng, L. M., Wang, X., Slanina, J., Shao, M.,  
 987 and Wiedensohler, A.: Observation of nighttime nitrous acid (HONO) formation at a non-urban site  
 988 during PRIDE-PRD2004 in China, *Atmos. Environ.*, 42, 6219-6232, 10.1016/j.atmosenv.2008.04.006,  
 989 2008a.  
 990 Su, H., Cheng, Y. F., Shao, M., Gao, D. F., Yu, Z. Y., Zeng, L. M., Slanina, J., Zhang, Y. H., and  
 991 Wiedensohler, A.: Nitrous acid (HONO) and its daytime sources at a rural site during the 2004 PRIDE-  
 992 PRD experiment in China, *Journal of Geophysical Research-Atmospheres*, 113, 10.1029/2007jd009060,  
 993 2008b.  
 994 Su, P. H., Kuo, D. T. F., Shih, Y. H., and Chen, C. Y.: Sorption of organic compounds to two diesel soot  
 995 black carbons in water evaluated by liquid chromatography and polyparameter linear solvation energy  
 996 relationship, *Water Res.*, 144, 709-718, 10.1016/j.watres.2018.07.064, 2018.  
 997 Sun, P., Nie, W., Chi, X., Xie, Y., Huang, X., Xu, Z., Qi, X., Xu, Z., Wang, L., Wang, T., Zhang, Q., and  
 998 Ding, A.: Two years of online measurement of fine particulate nitrate in the western Yangtze River Delta:  
 999 influences of thermodynamics and N<sub>2</sub>O<sub>5</sub> hydrolysis, *Atmos. Chem. Phys.*, 18, 17177-17190,  
 1000 10.5194/acp-18-17177-2018, 2018.  
 1001 Sun, Y. L., Wang, Z. F., Fu, P. Q., Yang, T., Jiang, Q., Dong, H. B., Li, J., and Jia, J. J.: Aerosol  
 1002 composition, sources and processes during wintertime in Beijing, China, *Atmos. Chem. Phys.*, 13, 4577-  
 1003 4592, 10.5194/acp-13-4577-2013, 2013.  
 1004 Sun, Y. L., Wang, Z. F., Du, W., Zhang, Q., Wang, Q. Q., Fu, P. Q., Pan, X. L., Li, J., Jayne, J., and  
 1005 Worsnop, D. R.: Long-term real-time measurements of aerosol particle composition in Beijing, China:  
 1006 seasonal variations, meteorological effects, and source analysis, *Atmos. Chem. Phys.*, 15, 10149-10165,  
 1007 10.5194/acp-15-10149-2015, 2015.  
 1008 Tan, Z., Fuchs, H., Lu, K., Hofzumahaus, A., Bohn, B., Broch, S., Dong, H., Gomm, S., Häsel, R., He,

1009 L., Holland, F., Li, X., Liu, Y., Lu, S., Rohrer, F., Shao, M., Wang, B., Wang, M., Wu, Y., Zeng, L., Zhang,  
1010 Y., Wahner, A., and Zhang, Y.: Radical chemistry at a rural site (Wangdu) in the North China Plain:  
1011 observation and model calculations of OH, HO<sub>2</sub> and RO<sub>2</sub> radicals, *Atmos. Chem. Phys.*, 17, 663-690,  
1012 10.5194/acp-17-663-2017, 2017.

1013 Tan, Z., Rohrer, F., Lu, K., Ma, X., Bohn, B., Broch, S., Dong, H., Fuchs, H., Gkatzelis, G. I.,  
1014 Hofzumahaus, A., Holland, F., Li, X., Liu, Y., Liu, Y., Novelli, A., Shao, M., Wang, H., Wu, Y., Zeng, L.,  
1015 Hu, M., Kiendler-Scharr, A., Wahner, A., and Zhang, Y.: Wintertime photochemistry in Beijing:  
1016 observations of RO<sub>x</sub> radical concentrations in the North China Plain during the BEST-ONE campaign,  
1017 *Atmos. Chem. Phys.*, 18, 12391-12411, 10.5194/acp-18-12391-2018, 2018.

1018 Tan, Z. F., Lu, K. D., Jiang, M. Q., Su, R., Wang, H. L., Lou, S. R., Fu, Q. Y., Zhai, C. Z., Tan, Q. W.,  
1019 Yue, D. L., Chen, D. H., Wang, Z. S., Xie, S. D., Zeng, L. M., and Zhang, Y. H.: Daytime atmospheric  
1020 oxidation capacity in four Chinese megacities during the photochemically polluted season: a case study  
1021 based on box model simulation, *Atmos. Chem. Phys.*, 19, 3493-3513, 10.5194/acp-19-3493-2019, 2019.

1022 Tang, Y., An, J., Wang, F., Li, Y., Qu, Y., Chen, Y., and Lin, J.: Impacts of an unknown daytime HONO  
1023 source on the mixing ratio and budget of HONO, and hydroxyl, hydroperoxyl, and organic peroxy  
1024 radicals, in the coastal regions of China, *Atmos. Chem. Phys.*, 15, 9381-9398, 10.5194/acp-15-9381-  
1025 2015, 2015.

1026 Tian, M., Liu, Y., Yang, F. M., Zhang, L. M., Peng, C., Chen, Y., Shi, G. M., Wang, H. B., Luo, B., Jiang,  
1027 C. T., Li, B., Takeda, N., and Koizumi, K.: Increasing importance of nitrate formation for heavy aerosol  
1028 pollution in two megacities in Sichuan Basin, southwest China, *Environ. Pollut.*, 250, 898-905,  
1029 10.1016/j.envpol.2019.04.098, 2019.

1030 Tong, S., Hou, S., Zhang, Y., Chu, B., Liu, Y., He, H., Zhao, P., and Ge, M.: Exploring the nitrous acid  
1031 (HONO) formation mechanism in winter Beijing: direct emissions and heterogeneous production in  
1032 urban and suburban areas, *Faraday Discuss.*, 189, 213-230, 10.1039/c5fd00163c, 2016.

1033 Trinh, H. T., Imanishi, K., Morikawa, T., Hagino, H., and Takenaka, N.: Gaseous nitrous acid (HONO)  
1034 and nitrogen oxides (NO<sub>x</sub>) emission from gasoline and diesel vehicles under real-world driving test  
1035 cycles, *J. Air Waste Manage. Assoc.*, 67, 412-420, 10.1080/10962247.2016.1240726, 2017.

1036 Underwood, G. M., Miller, T. M., and Grassian, V. H.: Transmission FT-IR and Knudsen Cell Study of  
1037 the Heterogeneous Reactivity of Gaseous Nitrogen Dioxide on Mineral Oxide Particles, *J. Phys. Chem.*  
1038 *A*, 103 6184-6190, 1999.

1039 Underwood, G. M., Song, C. H., Phadnis, M., Carmichael, G. R., and Grassian, V. H.: Heterogeneous  
1040 reactions of NO<sub>2</sub> and HNO<sub>3</sub> on oxides and mineral dust: A combined laboratory and modeling study, *J.*  
1041 *Geophys. Res.- Atmos.*, 106, 18055-18066, 10.1029/2000jd900552, 2001.

1042 Volkamer, R., Sheehy, P., Molina, L. T., and Molina, M. J.: Oxidative capacity of the Mexico City  
1043 atmosphere – Part 1: A radical source perspective, *Atmos. Chem. Phys.*, 10, 6969-6991, 10.5194/acp-10-  
1044 6969-2010, 2010.

1045 Vu, T. V., Shi, Z., Cheng, J., Zhang, Q., He, K., Wang, S., and Harrison, R. M.: Assessing the impact of  
1046 Clean Air Action Plan on Air Quality Trends in Beijing Megacity using a machine learning technique,  
1047 *Atmos. Chem. Phys. Discuss.*, 2019, 1-18, 10.5194/acp-2019-173, 2019.

1048 Wang, G., Zhang, R., Gomez, M. E., Yang, L., Zamora, M. L., Hu, M., Lin, Y., Peng, J., Guoc, S., Meng,  
1049 J., Li, J., Cheng, C., Hu, T., Ren, Y., Wang, Y., Gao, J., Cao, J., An, Z., Zhou, W., Li, G., Wang, J., Tian,  
1050 P., Marrero-Ortiz, W., Secret, J., Du, Z., Zheng, J., Shang, D., Zeng, L., Shao, M., Wang, W., Huang, Y.,  
1051 Wang, Y., Zhu, Y., Li, Y., Hu, J., Pan, B., Cai, L., Cheng, Y., Ji, Y., Zhang, F., Rosenfeld, D., Liss, P. S.,  
1052 Duce, R. A., Kolb, C. E., and Molina, M. J.: Persistent sulfate formation from London Fog to Chinese

1053 haze, *Proc. Natl. Acad. Sci. USA*, 113, 13630-13635, 2016.

1054 Wang, H., Lu, K., Chen, X., Zhu, Q., Chen, Q., Guo, S., Jiang, M., Li, X., Shang, D., Tan, Z., Wu, Y.,  
1055 Wu, Z., Zou, Q., Zheng, Y., Zeng, L., Zhu, T., Hu, M., and Zhang, Y.: High N<sub>2</sub>O<sub>5</sub> Concentrations  
1056 Observed in Urban Beijing: Implications of a Large Nitrate Formation Pathway, *Environmental Science  
1057 & Technology Letters*, 4, 416-420, 10.1021/acs.estlett.7b00341, 2017a.

1058 Wang, H. C., Lu, K. D., Chen, X. R., Zhu, Q. D., Wu, Z. J., Wu, Y. S., and Sun, K.: Fast particulate nitrate  
1059 formation via N<sub>2</sub>O<sub>5</sub> uptake aloft in winter in Beijing, *Atmos. Chem. Phys.*, 18, 10483-10495,  
1060 10.5194/acp-18-10483-2018, 2018.

1061 Wang, J., Zhang, X., Guo, J., Wang, Z., and Zhang, M.: Observation of nitrous acid (HONO) in Beijing,  
1062 China: Seasonal variation, nocturnal formation and daytime budget, *Sci. Total Environ.*, 587, 350-359,  
1063 10.1016/j.scitotenv.2017.02.159, 2017b.

1064 Wang, S., Zhou, R., Zhao, H., Wang, Z., Chen, L., and Zhou, B.: Long-term observation of atmospheric  
1065 nitrous acid (HONO) and its implication to local NO<sub>2</sub> levels in Shanghai, China, *Atmos. Environ.*, 77,  
1066 718-724, 10.1016/j.atmosenv.2013.05.071, 2013.

1067 Wang, S., Nan, J., Shi, C., Fu, Q., Gao, S., Wang, D., Cui, H., Saiz-Lopez, A., and Zhou, B.: Atmospheric  
1068 ammonia and its impacts on regional air quality over the megacity of Shanghai, China, *Sci. Rep.*, 5,  
1069 15842-15842, 10.1038/srep15842, 2015.

1070 Wang, Y. L., Song, W., Yang, W., Sun, X. C., Tong, Y. D., Wang, X. M., Liu, C. Q., Bai, Z. P., and Liu,  
1071 X. Y.: Influences of Atmospheric Pollution on the Contributions of Major Oxidation Pathways to PM<sub>2.5</sub>  
1072 Nitrate Formation in Beijing, *Journal of Geophysical Research-Atmospheres*, 124, 4174-4185,  
1073 10.1029/2019jd030284, 2019.

1074 Wang, Y. S., Teter, J., and Sperling, D.: China's soaring vehicle population: Even greater than forecasted?,  
1075 *Energy Policy*, 39, 3296-3306, 10.1016/j.enpol.2011.03.020, 2011.

1076 Wang, Z., Wang, W., Tham, Y. J., Li, Q., Wang, H., Wen, L., Wang, X., and Wang, T.: Fast heterogeneous  
1077 N<sub>2</sub>O<sub>5</sub> uptake and ClNO<sub>2</sub> production in power plant and industrial plumes observed in the nocturnal  
1078 residual layer over the North China Plain, *Atmos. Chem. Phys.*, 17, 12361-12378, 10.5194/acp-17-  
1079 12361-2017, 2017c.

1080 Wen, L., Xue, L., Wang, X., Xu, C., Chen, T., Yang, L., Wang, T., Zhang, Q., and Wang, W.: Summertime  
1081 fine particulate nitrate pollution in the North China Plain: increasing trends, formation mechanisms and  
1082 implications for control policy, *Atmos. Chem. Phys.*, 18, 11261-11275, 10.5194/acp-18-11261-2018,  
1083 2018.

1084 Xing, L., Wu, J., Elser, M., Tong, S., Liu, S., Li, X., Liu, L., Cao, J., Zhou, J., El-Haddad, I., Huang, R.,  
1085 Ge, M., Tie, X., Prévôt, A. S. H., and Li, G.: Wintertime secondary organic aerosol formation in Beijing–  
1086 Tianjin–Hebei (BTH): contributions of HONO sources and heterogeneous reactions, *Atmos. Chem.  
1087 Phys.*, 19, 2343-2359, 10.5194/acp-19-2343-2019, 2019.

1088 Xu, Z., Wang, T., Wu, J., Xue, L., Chan, J., Zha, Q., Zhou, S., Louie, P. K. K., and Luk, C. W. Y.: Nitrous  
1089 acid (HONO) in a polluted subtropical atmosphere: Seasonal variability, direct vehicle emissions and  
1090 heterogeneous production at ground surface, *Atmos. Environ.*, 106, 100-109,  
1091 10.1016/j.atmosenv.2015.01.061, 2015.

1092 Yadav, A. K., Raman, S., and Niyogi, D. D. S.: A note on the estimation of eddy diffusivity and  
1093 dissipation length in low winds over a tropical urban terrain, *Pure and Applied Geophysics*, 160, 395-  
1094 404, 10.1007/s00024-003-8785-4, 2003.

1095 Yang, D., Zhang, S., Niu, T., Wang, Y., Xu, H., Zhang, K. M., and Wu, Y.: High-resolution mapping of  
1096 vehicle emissions of atmospheric pollutants based on large-scale, real-world traffic datasets, *Atmos.*



1097 Chem. Phys., 2019, 8831–8843, 10.5194/acp-2019-32, 2019.

1098 Yang, Q., Su, H., Li, X., Cheng, Y., Lu, K., Cheng, P., Gu, J., Guo, S., Hu, M., Zeng, L., Zhu, T., and  
1099 Zhang, Y.: Daytime HONO formation in the suburban area of the megacity Beijing, China, Science  
1100 China-Chemistry, 57, 1032-1042, 10.1007/s11426-013-5044-0, 2014.

1101 Zhang, F., Wang, Y., Peng, J., Chen, L., Sun, Y., Duan, L., Ge, X., Li, Y., Zhao, J., Liu, C., Zhang, X.,  
1102 Zhang, G., Pan, Y., Wang, Y., Zhang, A. L., Ji, Y., Wang, G., Hu, M., Molina, M. J., and Zhang, R.: An  
1103 unexpected catalyst dominates formation and radiative forcing of regional haze, Proc. Natl. Acad. Sci.  
1104 USA, 117, 10.1073/pnas.1919343117, 2020.

1105 Zhang, J., An, J., Qu, Y., Liu, X., and Chen, Y.: Impacts of potential HONO sources on the concentrations  
1106 of oxidants and secondary organic aerosols in the Beijing-Tianjin-Hebei region of China, Sci. Total  
1107 Environ., 647, 836-852, <https://doi.org/10.1016/j.scitotenv.2018.08.030>, 2019a.

1108 Zhang, J., Chen, J., Xue, C., Chen, H., Zhang, Q., Liu, X., Mu, Y., Guo, Y., Wang, D., Chen, Y., Li, J.,  
1109 Qu, Y., and An, J.: Impacts of six potential HONO sources on HOx budgets and SOA formation during  
1110 a wintertime heavy haze period in the North China Plain, Sci. Total Environ., 681, 110-123,  
1111 <https://doi.org/10.1016/j.scitotenv.2019.05.100>, 2019b.

1112 Zhang, J. M., Yang, L. X., Chen, J. M., Mellouki, A., Jiang, P., Gao, Y., Li, Y. Y., Yang, Y. M., and Wang,  
1113 W. X.: Influence of fireworks displays on the chemical characteristics of PM<sub>2.5</sub> in rural and suburban  
1114 areas in Central and East China, Sci. Total Environ., 578, 476-484, 10.1016/j.scitotenv.2016.10.212,  
1115 2017.

1116 Zhang, J. W., Chen, J. M., Xue, C. Y., Chen, H., Zhang, Q., Liu, X. G., Mu, Y. J., Guo, Y. T., Wang, D.  
1117 Y., Chen, Y., Li, J. L., Qu, Y., and An, J. L.: Impacts of six potential HONO sources on HOx budgets and  
1118 SOA formation during a wintertime heavy haze period in the North China Plain, Sci. Total Environ., 681,  
1119 110-123, 10.1016/j.scitotenv.2019.05.100, 2019c.

1120 Zhang, L., Wang, T., Zhang, Q., Zheng, J., Xu, Z., and Lv, M.: Potential sources of nitrous acid (HONO)  
1121 and their impacts on ozone: A WRF-Chem study in a polluted subtropical region, Journal of Geophysical  
1122 Research-Atmospheres, 121, 3645-3662, 10.1002/2015jd024468, 2016.

1123 Zhang, W., Tong, S., Ge, M., An, J., Shi, Z., Hou, S., Xia, K., Qu, Y., Zhang, H., Chu, B., Sun, Y., and  
1124 He, H.: Variations and sources of nitrous acid (HONO) during a severe pollution episode in Beijing in  
1125 winter 2016, The Science of the total environment, 648, 253-262, 10.1016/j.scitotenv.2018.08.133,  
1126 2019d.

1127 Zhang, X. Y., Zhong, J. T., Wang, J. Z., Wang, Y. Q., and Liu, Y. J.: The interdecadal worsening of  
1128 weather conditions affecting aerosol pollution in the Beijing area in relation to climate warming, Atmos.  
1129 Chem. Phys., 18, 5991-5999, 10.5194/acp-18-5991-2018, 2018.

1130 Zheng, B., Zhang, Q., Zhang, Y., He, K. B., Wang, K., Zheng, G. J., Duan, F. K., Ma, Y. L., and Kimoto,  
1131 T.: Heterogeneous chemistry: a mechanism missing in current models to explain secondary inorganic  
1132 aerosol formation during the January 2013 haze episode in North China, Atmos. Chem. Phys., 15, 2031-  
1133 2049, doi: 10.5194/acp-15-2031-2015, 2015a.

1134 Zheng, G. J., Duan, F. K., Su, H., Ma, Y. L., Cheng, Y., Zheng, B., Zhang, Q., Huang, T., Kimoto, T.,  
1135 Chang, D., Pöschl, U., Cheng, Y. F., and He, K. B.: Exploring the severe winter haze in Beijing: the  
1136 impact of synoptic weather, regional transport and heterogeneous reactions, Atmos. Chem. Phys., 15,  
1137 2969-2983, 10.5194/acp-15-2969-2015, 2015b.

1138 Zhu, W. H., Xu, X. D., Zheng, J., Yan, P., Wang, Y. J., and Cai, W. Y.: The characteristics of abnormal  
1139 wintertime pollution events in the Jing-Jin-Ji region and its relationships with meteorological factors, Sci.  
1140 Total Environ., 626, 887-898, 10.1016/j.scitotenv.2018.01.083, 2018.

1141 Zou, Y., Deng, X. J., Deng, T., Yin, C. Q., and Li, F.: One-Year Characterization and Reactivity of  
1142 Isoprene and Its Impact on Surface Ozone Formation at A Suburban Site in Guangzhou, China,  
1143 *Atmosphere*, 10, 10.3390/atmos10040201, 2019.  
1144  
1145

1146 **Figure captions**

1147 Fig. 1. An overviewed measurement of non-refractory-PM<sub>2.5</sub> (NR-PM<sub>2.5</sub>), HONO, NO<sub>x</sub>,  
1148 PM<sub>2.5</sub> and meteorological parameters from Feb. 1 to July 1, 2018. (A) the mass  
1149 concentration of different components of PM<sub>2.5</sub>, (B) the mass fraction of individual  
1150 component, (C) HONO and NO<sub>x</sub> concentration, (D) temperature and RH, (E) wind  
1151 speed and wind direction, (F) UVB and PBL height and (G) visibility and PM<sub>2.5</sub>  
1152 concentration during observation. We consider the period before Apr. 1 as winter.  
1153 During the winter period, 12 cases are selected and numbered, including three clean  
1154 cases (1, 3, and 5, marked in yellow) and the rest 9 pollution episodes (marked in blue).

1155 **Fig. 2.** Contribution of HONO to OH production and correlation between OA and  
1156 HONO concentration. Diurnal production rates of OH from photolysis of HONO and  
1157 O<sub>3</sub> on polluted days with PM<sub>2.5</sub> concentration larger than 50 μg m<sup>-3</sup> and RH less than  
1158 90 % (A) from Feb 1 to Mar 31, (B) from Apr 1 to Jun 30; (C) Daytime variation of  
1159 OA/CO and HONO/CO concentration for the 7<sup>th</sup> and 12<sup>th</sup> episodes and (D) correlation  
1160 of the daytime OA/CO increased and consumed HONO/CO.

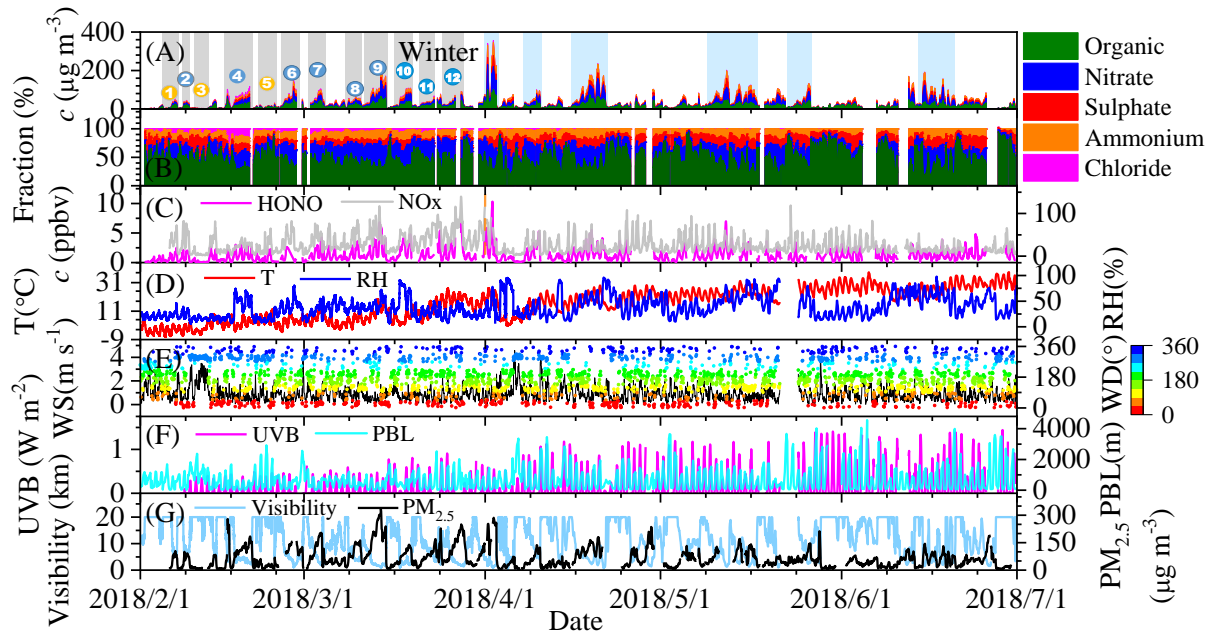
1161 **Fig. 3.** Diurnal pattern of HONO sources calculated with different parameterizations.  
1162 The low bound, the middle value, and upper bound of (A) soil emission calculated  
1163 based on 45-55%, 35-45% and 25-35% of water content, (B) vehicle emission with  
1164 relative emission factor to NO<sub>x</sub> of 0.18%, 1.17±0.05% and 1.8 %, (C) production from  
1165 reaction between NO and OH, whose concentration estimated using Xu (Xu et al.,  
1166 2015), (Tan et al., 2019)

1167 **Fig. 4.** The budget of HONO (A) and (B) Diurnal production rates of HONO, (C) and

1168 (D) loss rates of HONO, (E) and (F) relative contribution of each source on polluted  
1169 days with  $\text{PM}_{2.5}$  concentrations higher than  $50 \mu\text{g m}^{-3}$  and RH less than 90 %. The left  
1170 column shows the data from February 1 to March 31) and the right one shows the data  
1171 from April 1 to June 30.

1172 **Fig. 5.** (A)-(B) Diurnal production rates and (C)-(D) diurnal loss rates of HONO; (E)-  
1173 (F) relative contribution of HONO sources on polluted days with  $\text{PM}_{2.5}$  concentrations  
1174 higher than  $50 \mu\text{g m}^{-3}$  and RH less than 90 %. The  $E_{\text{vehicle}}$  is calculated using the low  
1175 limit of HONO/NO<sub>x</sub> from vehicles (0.18%) (Liu et al., 2017d) and the  $P_{\text{NO-OH}}$  is  
1176 calculated using the low limit of OH concentration, while the upper limit of  $E_{\text{soil}}$ ,  $P_{\text{aerosol}}$   
1177 and  $P_{\text{ground}}$  are used as described in the text.

1178 **Figures**

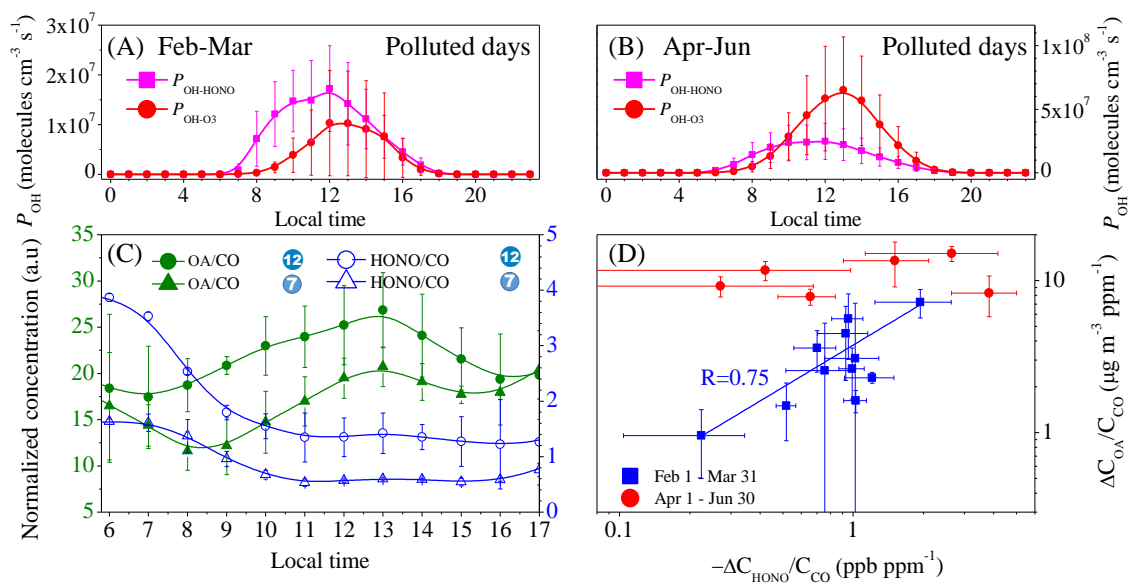


1179

1180

1181

**Fig. 1.**

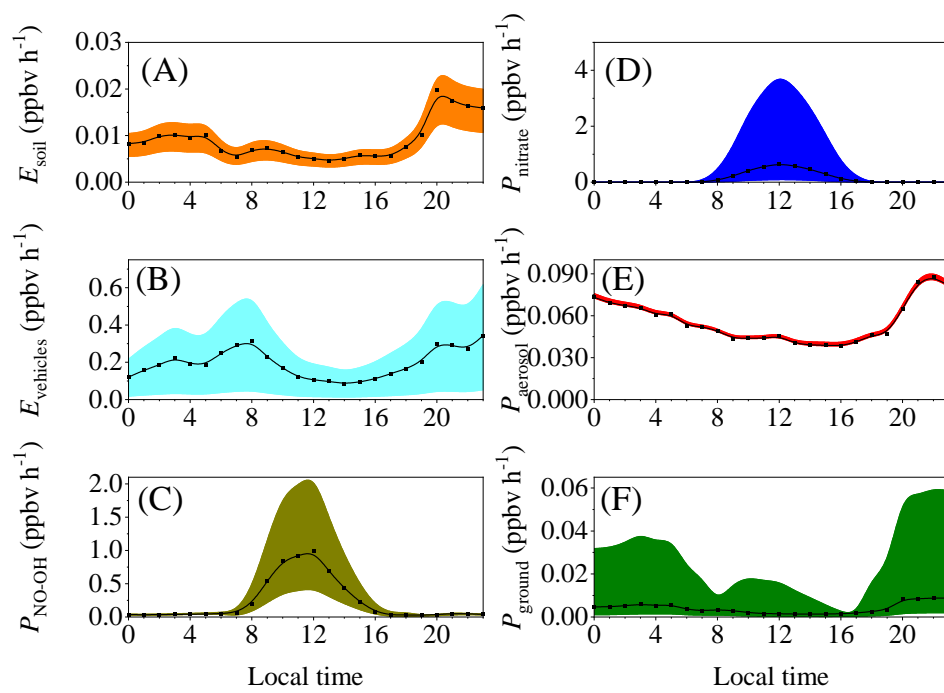


1182

1183

1184

Fig. 2.

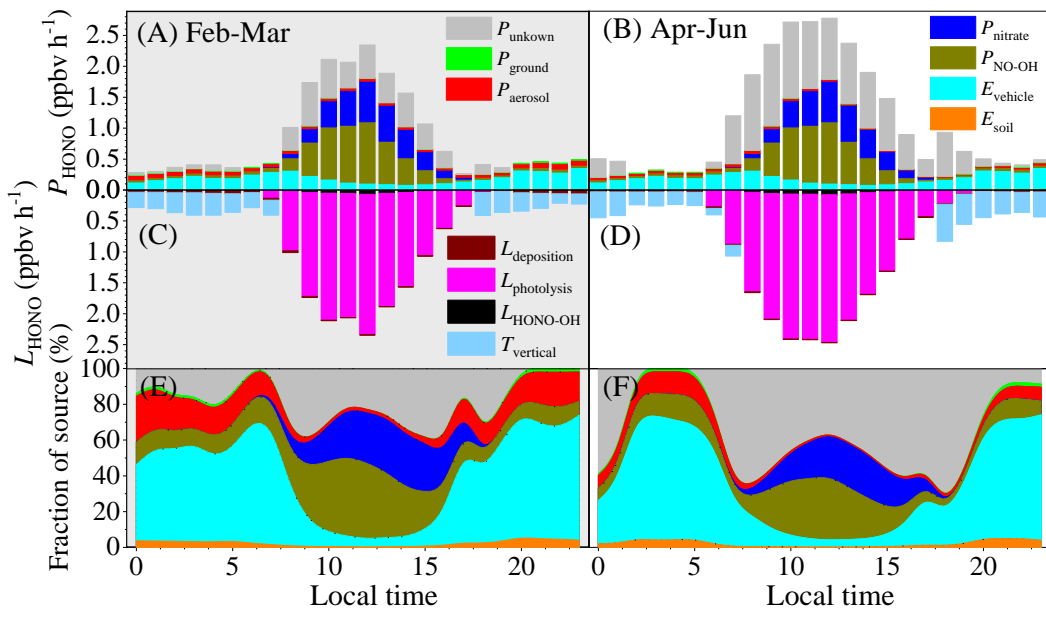


1185

1186

1187

**Fig. 3**



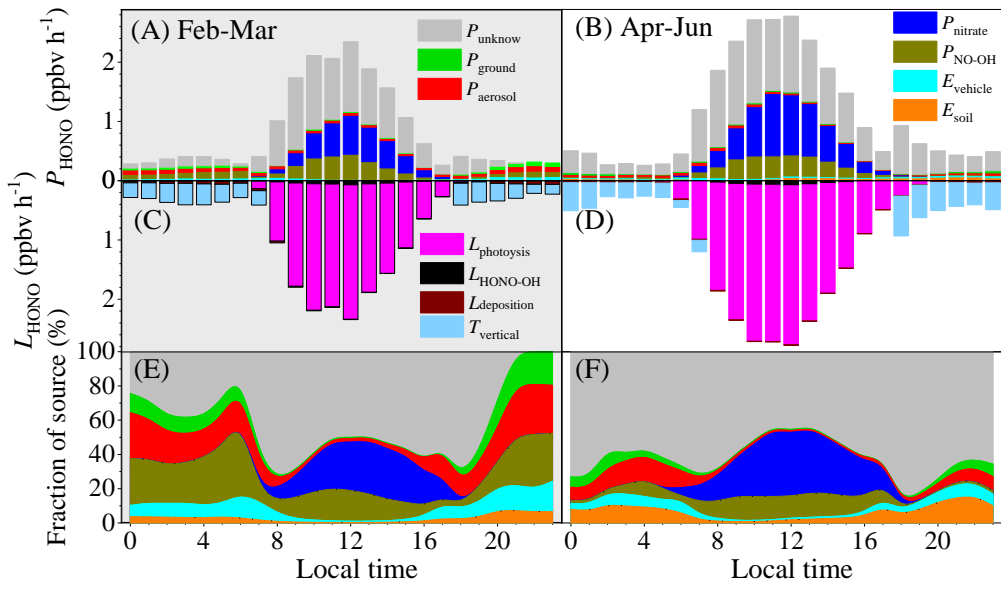
1188

1189

1190

**Fig. 4.**





1191

1192

Fig. 5.

1 **The promotion effect of nitrous acid on aerosol formation in**  
2 **wintertime Beijing: possible contribution of traffic-related**  
3 **emission**

4

5 Yongchun Liu<sup>1\*</sup>, Yusheng Zhang<sup>1</sup>, Chaofan Lian<sup>2,6</sup>, Chao Yan<sup>3</sup>, Zeming Feng<sup>1</sup>, Feixue  
6 Zheng<sup>1</sup>, Xiaolong Fan<sup>1</sup>, Yan Chen<sup>2,6</sup>, Weigang Wang<sup>2,6\*</sup>, Biwu Chu<sup>3,4</sup>, Yonghong Wang<sup>3</sup>,  
7 Jing Cai<sup>3</sup>, Wei Du<sup>3</sup>, Kaspar R. Daellenbach<sup>3</sup>, Juha Kangasluoma<sup>1,3</sup>, Federico Bianchi<sup>1,3</sup>,  
8 Joni Kujansuu<sup>1,3</sup>, Tuukka Petäjä<sup>3</sup>, Xuefei Wang<sup>6</sup>, Bo Hu<sup>5</sup>, Yuesi Wang<sup>5</sup>, Maofa Ge<sup>2</sup>,  
9 Hong He<sup>4</sup> and Markku Kulmala<sup>1,3\*</sup>

10

11 1. Aerosol and Haze Laboratory, Advanced Innovation Center for Soft Matter Science and  
12 Engineering, Beijing University of Chemical Technology, Beijing, 100029, China

13 2. State Key Laboratory for Structural Chemistry of Unstable and Stable Species, Beijing  
14 National Laboratory for Molecular Sciences, Institute of Chemistry, Chinese Academy of  
15 Sciences, Beijing 100190, China

16 3. Institute for Atmospheric and Earth System Research/Physics, Faculty of Science, University  
17 of Helsinki, P.O. Box 64, FI-00014, Finland

18 4. State Key Joint Laboratory of Environment Simulation and Pollution Control, Research  
19 Center for Eco-Environmental Sciences, Chinese Academy of Sciences, Beijing, 100085, China

20 5. State Key Laboratory of Atmospheric Boundary Layer Physics and Atmospheric Chemistry,  
21 Institute of Atmospheric Physics, Chinese Academy of Sciences, Beijing, 100029, China

22 6. University of Chinese Academy of Sciences, Beijing 100049, PR China

23

24

25 **Supplement information**

26 **Non-refractory PM<sub>2.5</sub> (NR-PM<sub>2.5</sub>) measurement.** Concentration of NR-PM<sub>2.5</sub> was  
27 measured with a ToF-ACSM (Aerodyne Co. Ltd., USA). The operation protocol and  
28 the configuration of ToF-ACSM has been described well in previous work (Fröhlich et  
29 al., 2013). Namely, PM<sub>2.5</sub> particles from the inlet were focused by a PM<sub>2.5</sub> aerodynamic  
30 lens (Williams et al., 2013), and then vaporized by a standard vaporizer heated at 600  
31 °C followed by electronic ionization (EI, 70 eV). The non-refractory components  
32 including chloride, nitrate, sulfate, ammonia and organics were measured using a time-  
33 of-flight mass spectrometer with unit mass resolution (UMR). The concentrations of  
34 the above species were calculated based on the measured fragments signals, the signal  
35 ions (SI), the fragment table, the measured ionization efficiency (IE) of nitrate and the  
36 corresponding relative ionization efficiency (RIE) for sulfate, chloride, ammonia and  
37 organics. IE calibration of nitrate was performed using 300 nm dry NH<sub>4</sub>NO<sub>3</sub> every  
38 month during this observation study.

39 **VOCs measurement.** VOCs were measured using a Single Photo Ionization Time-of-  
40 flight Mass spectrometer (SPI-ToF-MS 3000R, Hexin Mass Spectrometry). 0.8 L min<sup>-1</sup>  
41 of filtered air was sucked from the whole sampling tube and heated to 80 °C in the  
42 inlet. VOCs were selectively enriched continuously through a polydimethylsiloxane  
43 (PDMS) membrane, and then ionized by VUV light (10.5 eV) with a deuterium lamp.  
44 The concentration of VOCs was determined with the time-of-flight mass spectrometer  
45 (ToF-MS) based upon external standard curves of PAMS and TO-15 standard gases  
46 (Linde Electronics & Specialty Gases, USA). VOCs with m/z from 40 to 300 were

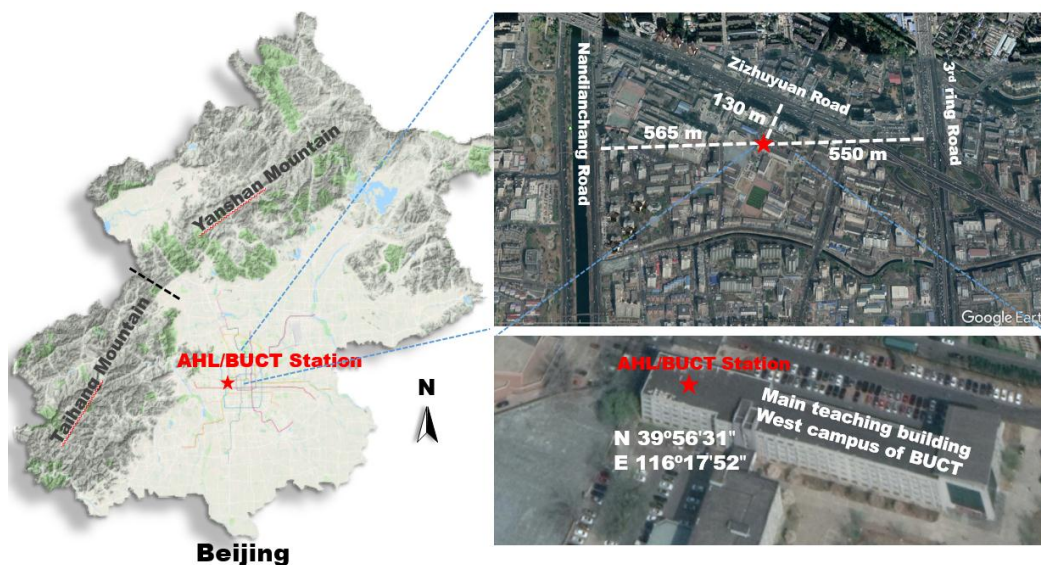
47 recorded with 3 min of time resolution, while hourly averaged concentration were  
48 reported in this work. Calibration was performed every week.

49 **HONO measurement.** HONO in ambient air directly sampled from the window of the  
50 laboratory was absorbed by a solution containing 0.06 mol L<sup>-1</sup> sulfnilamide in 1 mol L<sup>-1</sup>  
51 HCl, and then transformed into an azo dye by *N*-(1-naphthyl) ethylene-  
52 diaminedihydrochloride (0.8 mmol L<sup>-1</sup>). The azo dye was pumped into Teflon absorption  
53 cells (Liquid Core Waveguide, LCW) and detected by a mini-spectrometer with a diode  
54 array detector (Ocean Optics, SD2000). The HONO concentrations was obtained by  
55 subtracting the calibrated signal of the second coil from the first coil using external  
56 nitrile standard solutions. Zero point calibration was performed every day using  
57 scrubbed zero air (Tong et al., 2016).

58 **Photolysis rate constants of HONO and O<sub>3</sub>.** Photolysis rate constants of NO<sub>2</sub>( $J_{NO_2}$ ),  
59 HONO( $J_{HONO}$ ) and O<sub>3</sub>( $J_{O_3}$ ) under clear sky conditions were calculated according to the  
60 solar zenith angle and the location using a box model (FACSIMILE 4). NO<sub>2</sub> photolysis  
61 sensor ( $J_{NO_2}$ , Metcon) was unavailable, while UVB is always available during our  
62 observation study. However, it was available from Aug 17 to Sep 16, 2018. A  
63 calibration function between the measured UVB light intensity and  $J_{NO_2}$  was  
64 established to correct the influence the climatological O<sub>3</sub> column, aerosol optical depth  
65 and cloud cover on surface UV light intensity from Aug 17 to Sep 16, 2008. As shown  
66 in Figure S10, the model well predicted the  $J_{NO_2}$ . Then the  $J_{NO_2}$  during this campaign  
67 study was predicted using the model. We further confirmed the calculated  $J_{NO_2}$  by  
68 comprising the OH concentration estimated by the  $J_{OH}$  according to the equation

69 ( $C_{OH} = J_{OH} \times 2 \times 10^{11}$  molecules  $\text{cm}^{-3}$ ) (Tan et al., 2019) and the measured OH  
70 concentration at Huairou, which is 60 km northeast from BUCT, from Jan 11 to Mar 10,  
71 2016. As shown in Figure S10C, the estimated diurnal curve of OH is comparable with  
72 that measured at Huairou. **Fig. S7 shows the calculated photolysis rates.**  
73

74 **Supplementary figures**

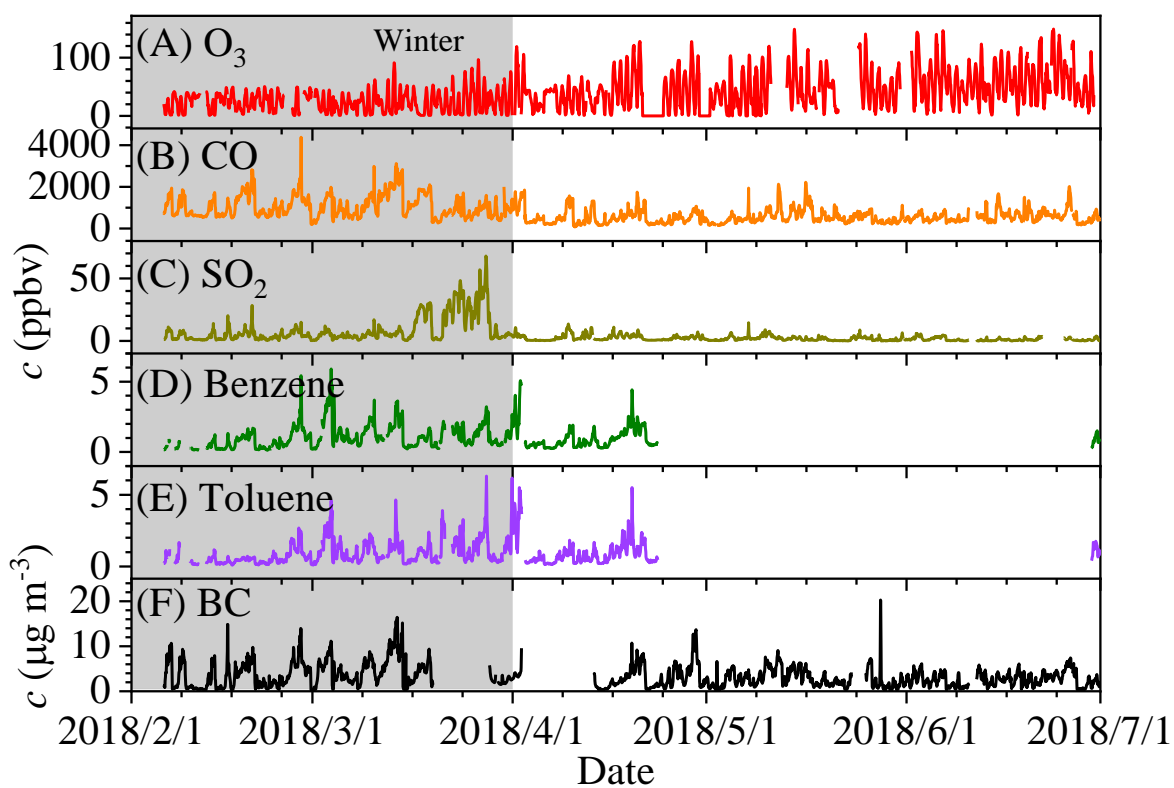


75

76 Figure S1. Location of AHL/BUCT observation station. The map was

77

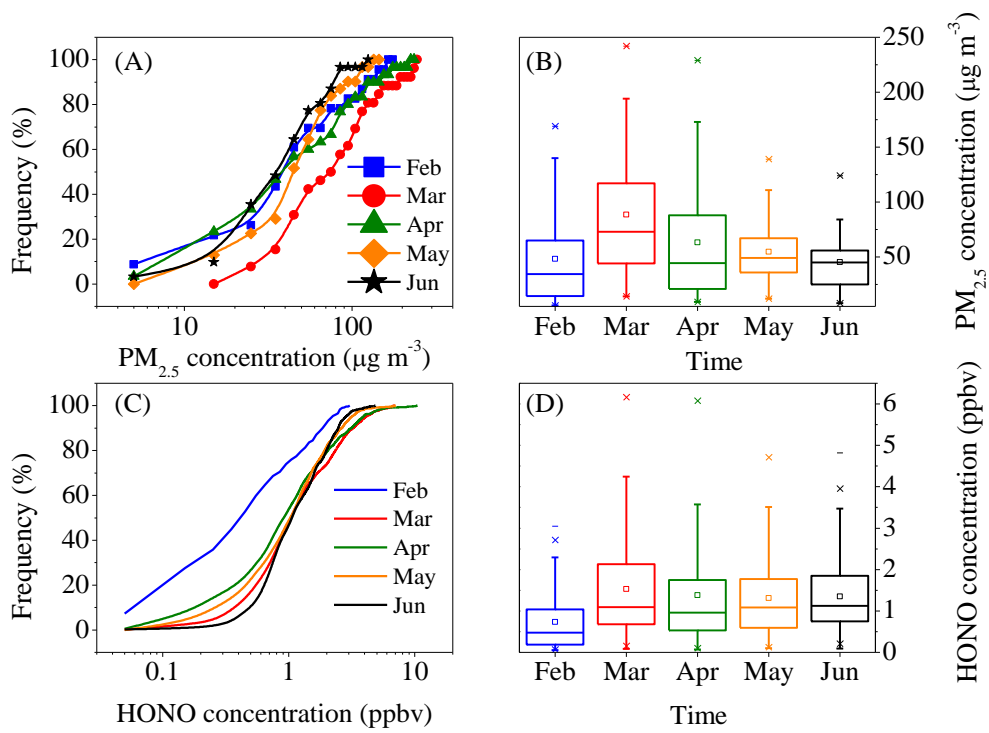
made from Wemap and Google Earth.



78

79 Figure S2. Hourly averaged (A)-(F) concentration of pollutants from Feb 1 to Jun 30,

80 2018.



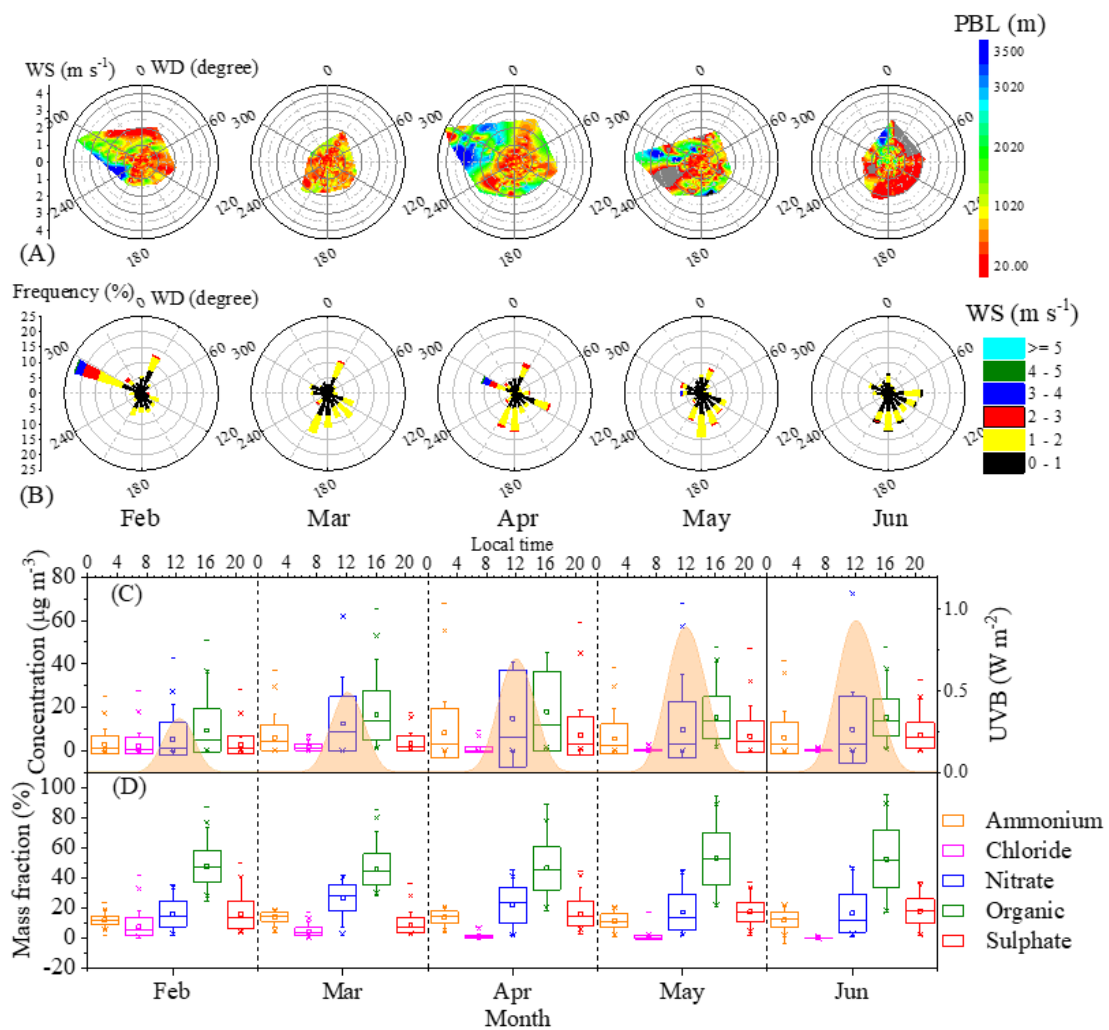
81

82

83 Figure S3. The monthly cumulative frequency of PM<sub>2.5</sub> and HONO and the monthly

84 mean concentration of PM<sub>2.5</sub> and HONO.

85



86

87 Figure S4. (A)-(B) monthly Windrose-PBL plots, and monthly averaged (C) UVB

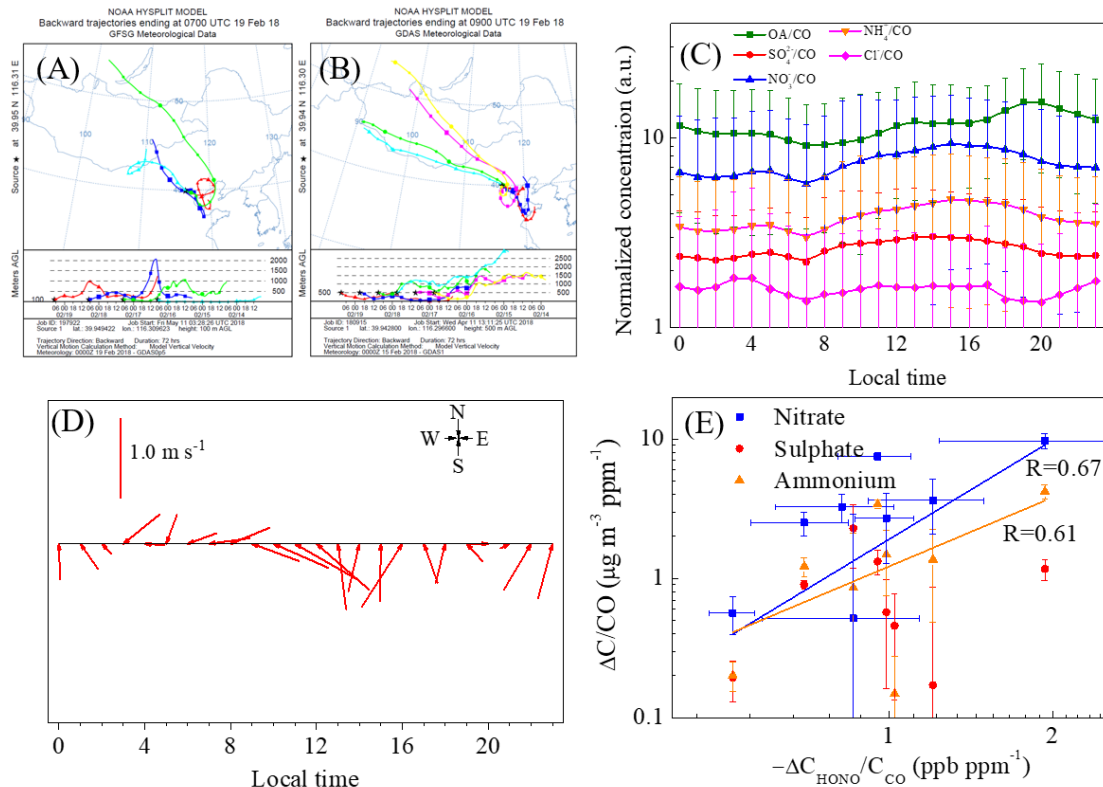
88 intensity, mass concentration and (D) fraction of individual component in NR-PM<sub>2.5</sub>

89 composition from Feb to Jun, 2018.

90

91

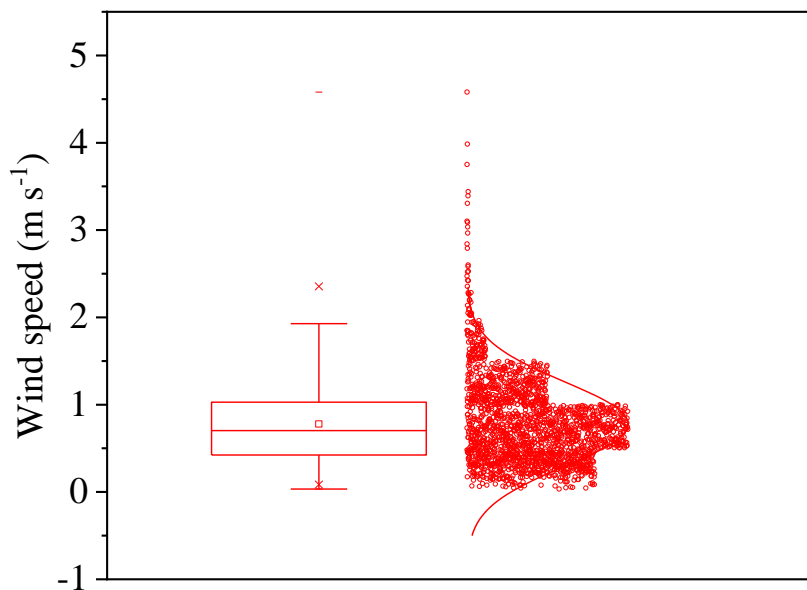




92

93 Figure S5. Transport of air mass during Chinese New Year based on back trajectory  
 94 analysis (A) at 100 and (B) 500 m height; (C) Diurnal variation of NR-PM<sub>2.5</sub> normalized  
 95 to CO concentration from Feb 1 to March 31; (D) Hourly averaged wind speed variation  
 96 in the 12<sup>th</sup> episode; (E) Correlation of the concentration increment of individual  
 97 component and consumed HONO normalized to CO in the daytime.

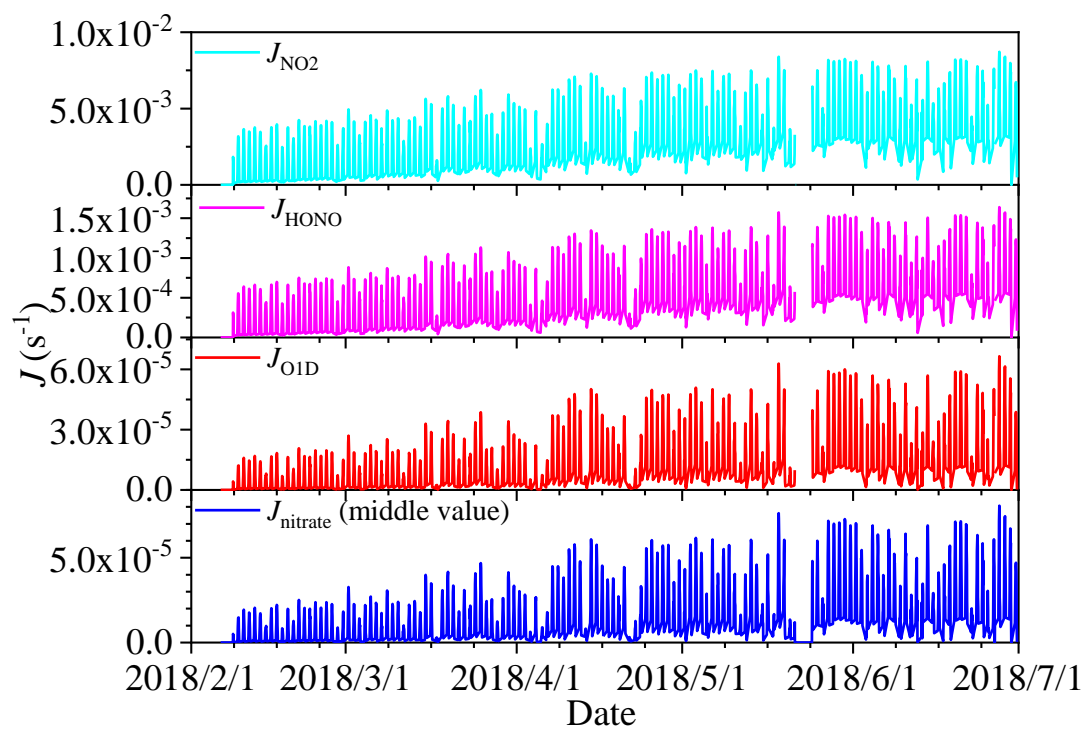
98



99

100 Figure S6. Distribution of wind speed when the  $\text{PM}_{2.5}$  concentration was larger than 50

101  $\mu\text{g m}^{-3}$  and the RH was less than 90 %.



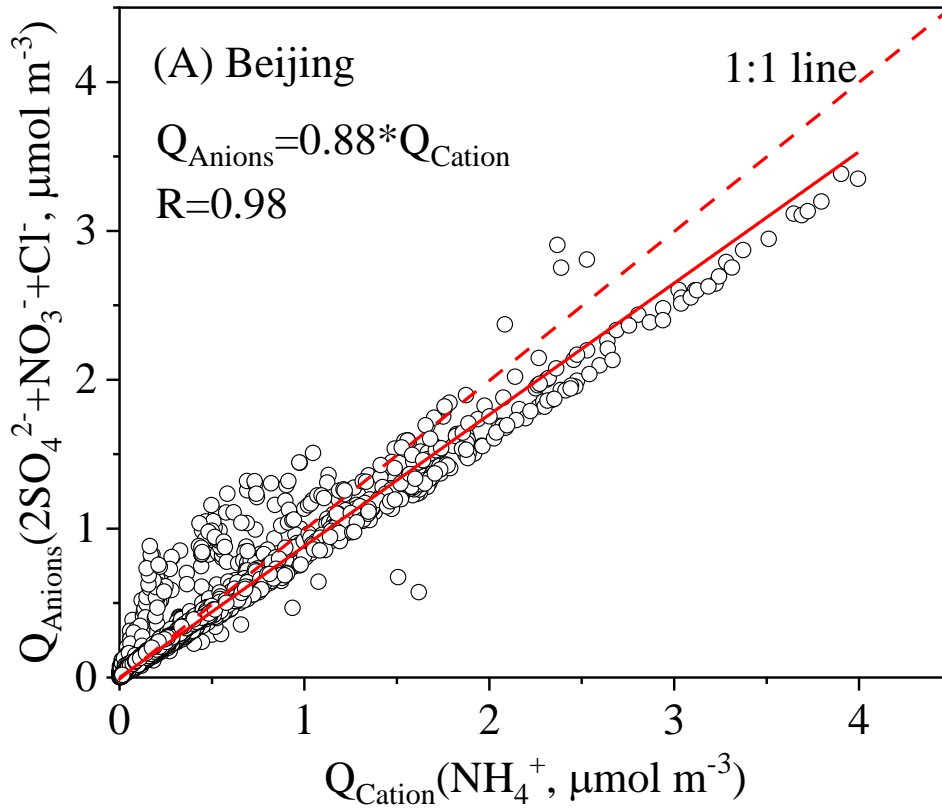
102

103 Fig. S7. The photolysis rate of  $\text{NO}_2$ , HONO,  $\text{O}_3$  (O1D) and nitrate (middle value)

104

from 8:00 am to 6:00 pm.

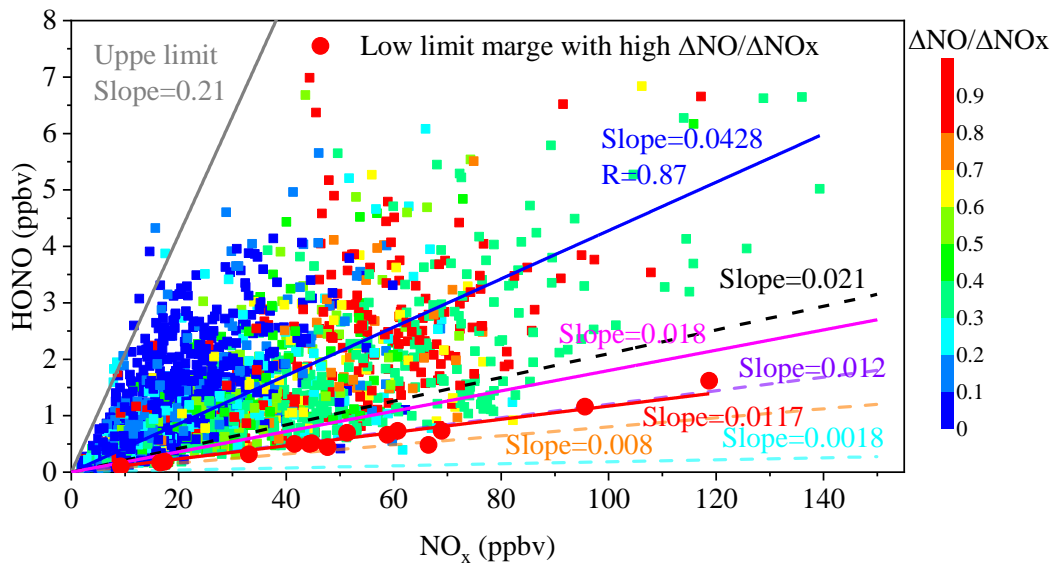
105



106

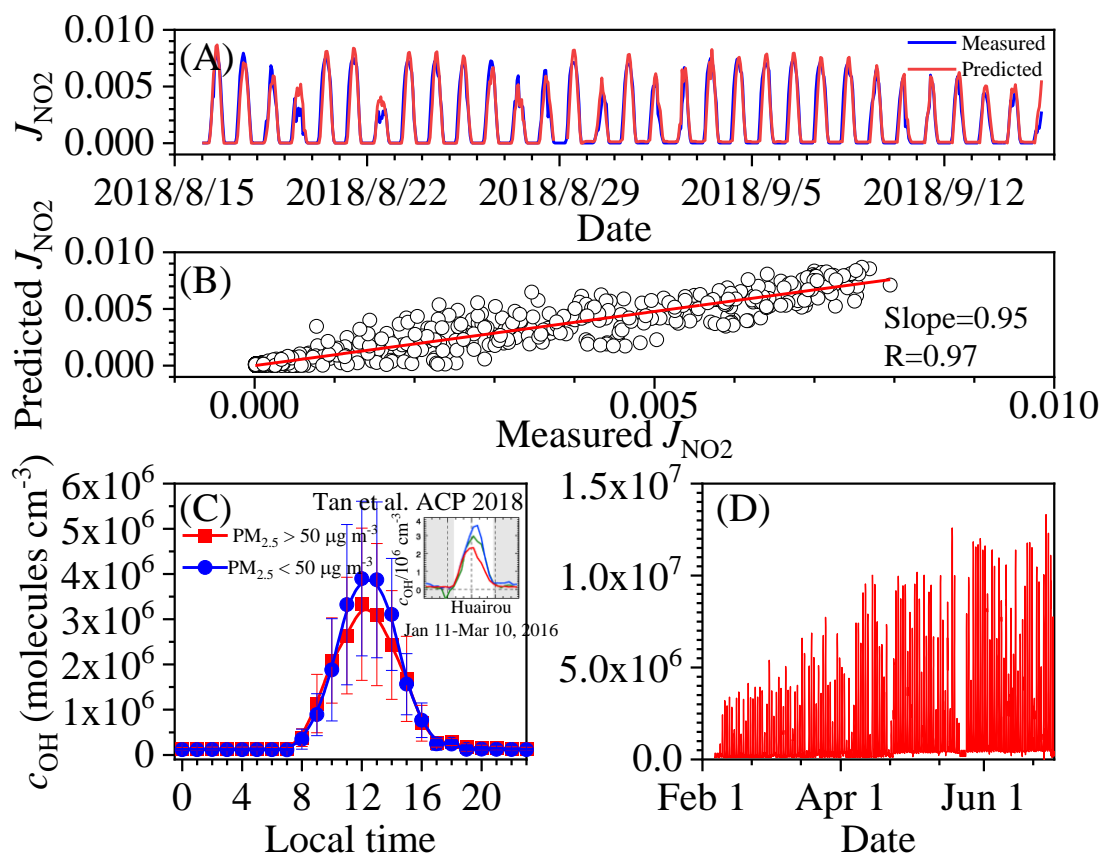
107 Figure S8. Correlation of the charge between inorganic anions and cations in non-  
 108 refractory  $\text{PM}_{2.5}$  in Beijing.

109



110

111 Figure S9. Correlation of measured HONO concentration with  $\text{NO}_x$  concentration.



112

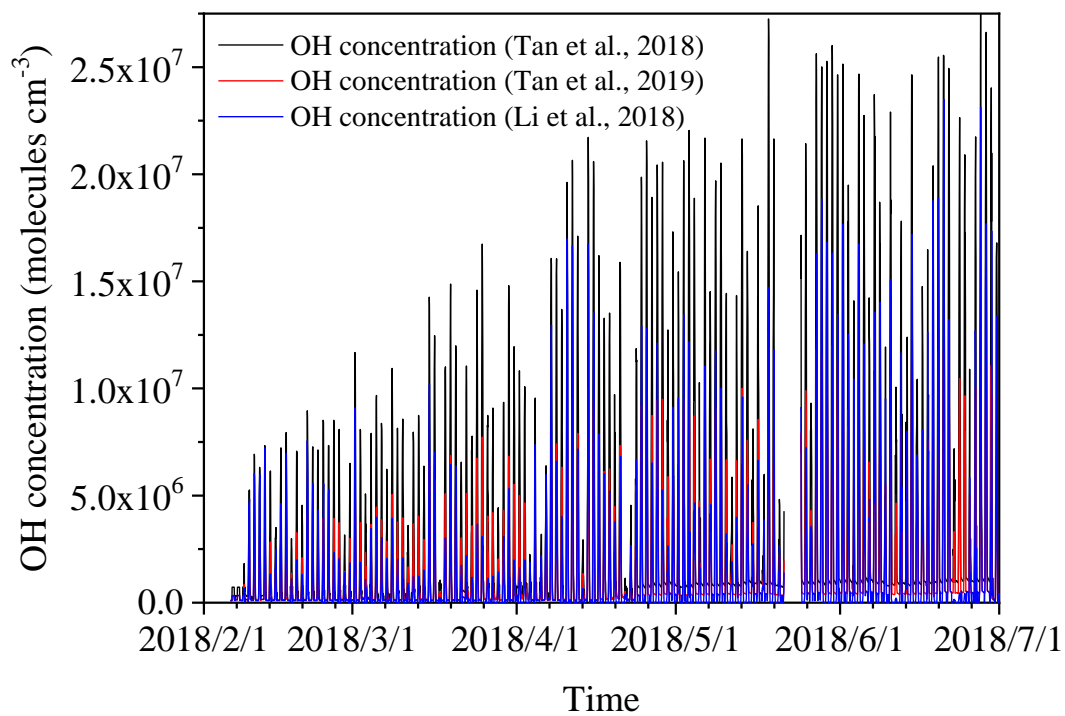
113 Figure S10. (A) Measured and predicted  $J_{\text{NO}_2}$  and (B) the correlation between measured

114 and predicted  $J_{\text{NO}_2}$  from Aug. 15 to Sep. 16; (C) calculated diurnal curve of OH

115 concentration based on  $J_{\text{O}_1\text{D}}$  compared with that measured at Huairou (60 km northeast

116 from BUCT) from Jan 11 to Mar 10, 2016; (D) OH concentrations estimated using

117  $c_{\text{OH}}=J_{\text{O}_1\text{D}} \times 2 \times 10^{11}$  (Tan et al., 2019).



118  
119  
120

Fig. S11. Estimated OH concentration using different methods.

## Supplementary tables

Table S1. ANOVA statistics analysis for the monthly mean fraction of the individual component in NR-PM<sub>2.5</sub> and HONO concentration.

Component	Fraction of NR-PM <sub>2.5</sub> (%)				
	or Concentration of gaseous pollutants (ppbv)	Feb	Mar	Apr	May
Ammonium	Feb (12.2±2.9)				
	Mar (14.2±2.8)	Significant			
	Apr (14.0±4.0)	Significant	Not significant		
	May (11.6±4.6)	Not significant	Significant	Significant	
	Jun (12.2±5.2)	Not significant	Significant	Significant	Not significant
Chloride	Feb (7.7±6.1)				
	Mar (4.4±2.6)	Significant			
	Apr (1.1±1.2)	Significant	Significant		
	May (0.7±1.1)	Significant	Significant	Not significant	
	Jun (0.3±0.2)	Significant	Significant	Significant	Not significant
Nitrate	Feb (16.2±8.5)				
	Mar (26.7±8.8)	Significant			
	Apr (22.0±11.7)	Significant	Significant		
	May (17.3±11.8)	Not significant	Significant	Significant	
	Jun (16.7±12.8)	Not significant	Significant	Significant	Not significant
Organic	Feb (47.9±10.7)				
	Mar (45.9±10.2)	Not significant			
	Apr (46.5±14.2)	Not significant	Significant		
	May (52.9±17.0)	Not significant	Significant	Significant	
	Jun (52.6±18.7)	Significant	Significant	Significant	Not significant

Sulfate	Feb (16.0±9.1)					
	Mar (8.8±5.4)	Significant				
	Apr (16.4±8.2)	Not significant	Significant			
	May (17.5±6.6)	Significant	Significant	Not significant		
	Jun (18.2±8.0)	Significant	Significant	Significant	Not significant	
BC	Feb (3.0±2.8)					
	Mar (4.6±3.1)	Significant				
	Apr (3.2±2.6)	Not significant	Significant			
	May (2.8±2.1)	Not significant	Significant	Not significant		
	Jun (2.6±1.5)	Significant	Significant	Significant	Not significant	
HONO	Feb (0.73±0.70)					
	Mar (1.53±1.25)	Significant				
	Apr (1.38±1.35)	Significant	Not significant			
	May (1.31±1.00)	Significant	Significant	Not significant		
	Jun (1.35±0.80)	Significant	Significant	Not significant	Not significant	
NO <sub>x</sub>	Feb (20.4±17.3)					
	Mar (40.5±24.0)	Significant				
	Apr (22.8±18.6)	Not significant	Significant			
	May (25.0±15.9)	Significant	Significant	Not significant		
	Jun (19.0±12.1)	Not significant	Significant	Significant	Significant	Significant
SO <sub>2</sub>	Feb (3.8±3.3)					
	Mar (12.1±13.0)	Significant				
	Apr (2.8±2.4)	Significant	Significant			
	May (1.8±1.7)	Significant	Significant	Not significant		
	Jun (1.3±1.2)	Significant	Significant	Significant	Not significant	
CO	Feb (959.6±554.6)					

	Mar (1075.0±571.8)	Significant				
	Apr (546.6±378.1)	Significant	Significant			
	May (554.1±336.9)	Significant	Significant	Not significant		
	Jun (583.4±286.2)	Significant	Significant	Not significant	Not significant	
O <sub>3</sub>	Feb (22.6±14.6)					
	Mar (23.8±19.2)	Not significant				
	Apr (43.5±29.0)	Significant	Significant			
	May (42.5±28.3)	Significant	Significant	Not significant		
	Jun (57.2±30.7)	Significant	Significant	Significant	Significant	

Note: “Significant” or “Not significant” denotes that the difference of the monthly mean fractions or concentrations is significant or not significant at the 0.05 level.



Tab. S2. Mean concentrations of HONO and PM<sub>2.5</sub> in selected episodes

Episode No.	Duration	HONO (ppb)	Average PM <sub>2.5</sub> concentration	NR-PM <sub>2.5</sub> Concentration (%)									
				Chloride		Nitrate		Organic		Sulphate		Ammonium	
				(%)	( $\mu\text{g m}^{-3}$ )	(%)	( $\mu\text{g m}^{-3}$ )	(%)	( $\mu\text{g m}^{-3}$ )	(%)	( $\mu\text{g m}^{-3}$ )	(%)	( $\mu\text{g m}^{-3}$ )
1	Feb 2-5	0.38±0.28	9.3±4.5	4.0±2.3	0.26±0.39	12.3±5.6	0.80±1.17	51.1±10.0	2.68±3.00	20.6±9.2	0.69±0.24	12.0±3.2	0.54±0.49
2	Feb 8-9	0.90±0.72	44.5±3.5	6.3±2.9	1.59±1.46	15.8±7.9	4.20±3.87	49.9±4.8	9.63±7.64	17.3±8.8	2.31±1.42	10.8±1.0	2.14±1.69
3	Feb 10-12	0.31±0.40	9.0±0.8	5.2±3.5	0.18±0.22	6.8±3.9	0.30±0.44	48.6±10.6	1.75±1.72	28.1±11.5	0.74±0.38	11.2±2.5	0.35±0.23
4	Feb 16-19	1.38±0.86	101.5±26.8	15.5±4.2	9.04±4.94	25.0±4.1	13.15±7.73	32.2±3.8	18.21±8.25	14.4±3.7	7.82±4.39	12.9±1.5	6.85±3.78
5	Feb 21-24	0.64±0.58	24.3±7.0	5.5±4.1	0.60±0.51	14.9±6.3	1.80±1.38	56.3±10.0	5.83±2.94	11.8±5.0	1.17±0.67	11.6±2.8	1.24±0.77
6	Feb 25-28	0.87±0.64	108.8±42.9	5.2±1.4	2.94±1.97	27.1±3.9	15.3±8.77	42.5±6.8	22.83±9.68	10.4±3.8	6.44±5.78	14.7±1.8	8.34±5.30
7	Mar 2-3	1.41±0.84	120.0±47.0	8.3±2.2	4.23±1.72	26.5±4.8	15.29±9.44	44.4±6.2	23.40±10.49	7.2±1.9	4.36±3.37	13.5±1.9	7.74±4.76
8	Mar 8-10	1.36±0.89	88.7±34.2	4.8±1.8	1.87±1.09	28.3±5.2	11.00±6.20	43.0±7.0	15.65±7.15	9.0±2.8	3.10±1.42	14.9±2.0	5.58±2.92
9	Mar 11-14	2.27±1.68	170.3±75.4	3.5±0.9	2.48±1.32	34.8±4.3	28.32±19.09	36.8±5.0	27.90±15.78	8.1±1.8	6.60±4.72	16.8±1.5	13.57±8.99
10	Mar 16-19	1.88±1.38	66.0±25.7	3.8±1.7	1.99±1.18	30.2±6.3	17.40±12.45	35.9±2.8	20.87±10.52	13.5±5.1	7.00±4.92	16.5±1.0	9.17±5.86
11	Mar 21-23	1.41±0.72	83.7±22.1	5.3±2.8	2.54±2.30	31.5±3.8	12.23±5.22	45.1±6.7	18.02±5.46	4.4±1.0	1.67±0.92	13.7±1.6	5.38±2.08
12	Mar 25-27	2.22±1.34	129.5±51.9	2.0±0.7	0.94±0.64	35.3±3.6	16.32±9.90	41.5±5.4	20.46±10.18	5.7±1.2	2.56±1.68	15.6±1.6	7.11±4.37

1 Table S3. The summary of the HONO/NO<sub>x</sub> ratio from vehicles in this study and the  
 2 reported emission ratio of HONO/NO<sub>x</sub> from vehicles in China.

No.	Time	$\Delta\text{NO}/\Delta\text{NO}_x$	$R_{\Delta\text{NO}/\Delta\text{NO}_x}$	$\Delta\text{HONO}/\Delta\text{NO}_x$	$R_{\Delta\text{HONO}/\Delta\text{NO}_x}$
1	2018/2/6 5:00-8:00	1.00	0.99	1.3%	0.92
2	2018/2/8 5:00-8:00	0.94	0.99	1.8%	0.96
3	2018/3/3 5:00-8:00	0.98	0.99	2.4%	0.96
4	2018/3/13 5:00-8:00	1.00	0.99	1.4%	0.86
5	2018/4/15 5:00-7:00	0.82	0.97	2.3%	0.99
Mean		0.95±0.08	-	1.8±0.5%	-
Time	Place	Methods	$\Delta\text{HONO}/\Delta\text{NO}_x$		Reference
			Range	Mean	
2015/9/1-2016/8/31	Ji'nan, Shandong	Empirical analysis of field data	0.19%-0.87%	0.53±0.20%	(Li et al., 2018)
2011/8/3-2012/5/31	Hongkong	Empirical analysis of field data	0.5%-1.6%	1.2±0.4%	(Xu et al., 2015)
2015/3/11-2015/3/21	Hongkong	Tunnel experiment	-	1.24±0.35%	(Liang et al., 2017)
2014	Beijing	Tunnel experiment	-	2.1%	(Yang et al., 2014)
2017	Beijing	Chassis dynamometer test	0.03%-0.42%	0.18%	(Liu et al., 2017)
2016/12/16-2016/12/24	Beijing	Empirical analysis of field data	-	1.3%	(Zhang et al., 2018)
2016/12/7-2016/12/13	Beijing	Low limit correlation of field data	-	1.41%	(Meng et al., 2019)
2018/2/1-2018/6/30	Beijing	Low limit correlation of field data	-	1.17%	This study
2018/2/1-2018/6/30	Beijing	Empirical analysis of field data	1.3-2.4%	1.8±0.5%	This study

3

#### 4 **References:**

- 5 Fröhlich, R., Cubison, M. J., Slowik, J. G., Bukowiecki, N., Prévôt, A. S. H., Baltensperger, U., Schneider,  
 6 J., Kimmel, J. R., Gonin, M., Rohner, U., Worsnop, D. R., and Jayne, J. T.: The ToF-ACSM: a portable  
 7 aerosol chemical speciation monitor with TOFMS detection, *Atmos. Meas. Tech.*, 6, 3225-3241,  
 8 10.5194/amt-6-3225-2013, 2013.
- 9 Li, D., Xue, L., Wen, L., Wang, X., Chen, T., Mellouki, A., Chen, J., and Wang, W.: Characteristics and  
 10 sources of nitrous acid in an urban atmosphere of northern China: Results from 1-yr continuous  
 11 observations, *Atmos. Environ.*, 182, 296-306, <https://doi.org/10.1016/j.atmosenv.2018.03.033>, 2018.
- 12 Liang, Y., Zha, Q., Wang, W., Cui, L., Lui, K. H., Ho, K. F., Wang, Z., Lee, S.-c., and Wang, T.: Revisiting

13 nitrous acid (HONO) emission from on-road vehicles: A tunnel study with a mixed fleet, *J. Air Waste*  
14 *Manage. Assoc.*, 67, 797-805, 10.1080/10962247.2017.1293573, 2017.

15 Liu, Y., Lu, K., Ma, Y., Yang, X., Zhang, W., Wu, Y., Peng, J., Shuai, S., Hu, M., and Zhang, Y.: Direct  
16 emission of nitrous acid (HONO) from gasoline cars in China determined by vehicle chassis  
17 dynamometer experiments, *Atmos. Environ.*, 169, 89-96, 10.1016/j.atmosenv.2017.07.019, 2017.

18 Meng, F., Qin, M., Tang, K., Duan, J., Fang, W., Liang, S., Ye, K., Xie, P., Sun, Y., Xie, C., Ye, C., Fu,  
19 P., Liu, J., and Liu, W.: High resolution vertical distribution and sources of HONO and NO<sub>2</sub> in the  
20 nocturnal boundary layer in urban Beijing, China, *Atmos. Chem. Phys. Discuss.*, 2019, 1-34,  
21 10.5194/acp-2019-613, 2019.

22 Tan, Z. F., Lu, K. D., Jiang, M. Q., Su, R., Wang, H. L., Lou, S. R., Fu, Q. Y., Zhai, C. Z., Tan, Q. W.,  
23 Yue, D. L., Chen, D. H., Wang, Z. S., Xie, S. D., Zeng, L. M., and Zhang, Y. H.: Daytime atmospheric  
24 oxidation capacity in four Chinese megacities during the photochemically polluted season: a case study  
25 based on box model simulation, *Atmos. Chem. Phys.*, 19, 3493-3513, 10.5194/acp-19-3493-2019, 2019.

26 Tong, S., Hou, S., Zhang, Y., Chu, B., Liu, Y., He, H., Zhao, P., and Ge, M.: Exploring the nitrous acid  
27 (HONO) formation mechanism in winter Beijing: direct emissions and heterogeneous production in  
28 urban and suburban areas, *Faraday Discuss.*, 189, 213-230, 10.1039/c5fd00163c, 2016.

29 Williams, L. R., Gonzalez, L. A., Peck, J., Trimborn, D., McInnis, J., Farrar, M. R., Moore, K. D., Jayne,  
30 J. T., Robinson, W. A., Lewis, D. K., Onasch, T. B., Canagaratna, M. R., Trimborn, A., Timko, M. T.,  
31 Magoon, G., Deng, R., Tang, D., de la Rosa Blanco, E., Prevot, A. S. H., and Worsnop, D. R.:  
32 Characterization of an aerodynamic lens for transmitting particles greater than 1 micrometer in diameter  
33 into the Aerodyne aerosol mass spectrometer, *Atmos. Meas. Tech.*, 6, 3271-3280, 10.5194/amt-6-3271-  
34 2013, 2013.

35 Xu, Z., Wang, T., Wu, J., Xue, L., Chan, J., Zha, Q., Zhou, S., Louie, P. K. K., and Luk, C. W. Y.: Nitrous  
36 acid (HONO) in a polluted subtropical atmosphere: Seasonal variability, direct vehicle emissions and  
37 heterogeneous production at ground surface, *Atmos. Environ.*, 106, 100-109,  
38 10.1016/j.atmosenv.2015.01.061, 2015.

39 Yang, Q., Su, H., Li, X., Cheng, Y., Lu, K., Cheng, P., Gu, J., Guo, S., Hu, M., Zeng, L., Zhu, T., and  
40 Zhang, Y.: Daytime HONO formation in the suburban area of the megacity Beijing, China, *Science*  
41 *China-Chemistry*, 57, 1032-1042, 10.1007/s11426-013-5044-0, 2014.

42 Zhang, W., Tong, S., Ge, M., An, J., Shi, Z., Hou, S., Xia, K., Qu, Y., Zhang, H., Chu, B., Sun, Y., and  
43 He, H.: Variations and sources of nitrous acid (HONO) during a severe pollution episode in Beijing in  
44 winter 2016, *The Science of the total environment*, 648, 253-262, 10.1016/j.scitotenv.2018.08.133, 2018.

45